AD-A052 131 ROCKWELL INTERNATIONAL COLUMBUS OHIO COLUMBUS AIRCRA--ETC F/G 20/4
AN INVESTIGATION OF CORNER SEPARATION WITHIN A THRUST AUGMENTER--ETC(U)
DEC 77 M R SEILER N62269-76-C-0402
UNCLASSIFIED NR77H-18 NADC-76153-30 NL

| OF |
AD
A052131

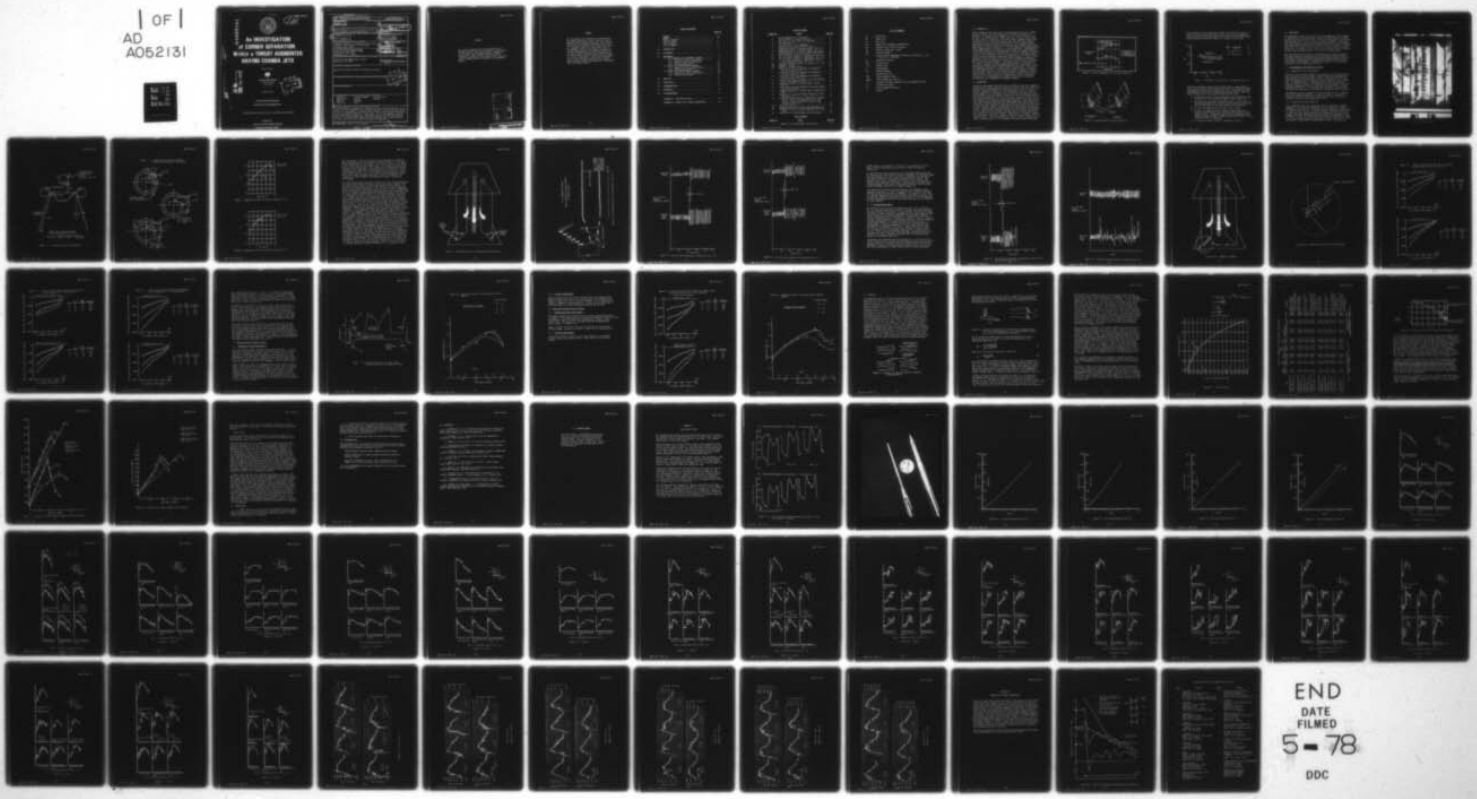

END
DATE FILMED
5-78
DDC

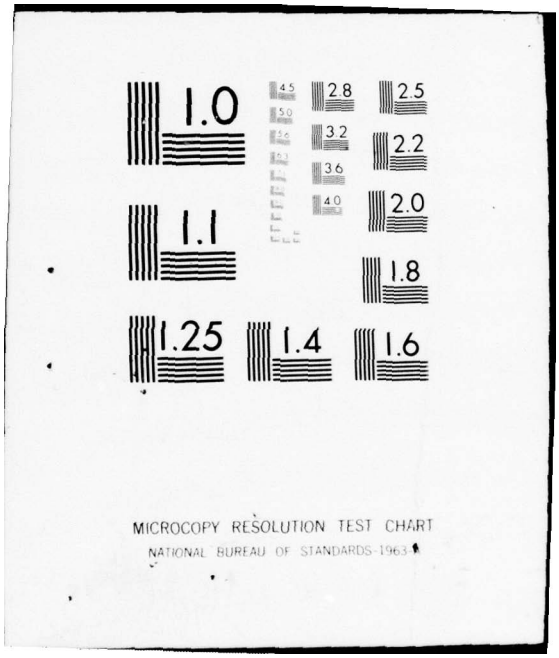
1.0
1.1
1.25
1.4
1.6
1.8
2.0
2.2
2.5
2.8
3.2
3.6
4.0
4.5
5.0
5.6
6.3
7.1
8.0
9.0
10.0
MICROCOPY RESOLUTION TEST CHART
NATIONAL BUREAU OF STANDARDS-1963-A

NADC 76153-30

An INVESTIGATION of CORNER SEPARATION Within a THRUST AUGMENTER HAVING COANDA JETS

Milton R. Seiler

Rockwell International
Columbus Aircraft Division
4300 East Fifth Avenue
PO Box 1259
Columbus, Ohio 43216

December 1977

FINAL REPORT FOR PERIOD

30 JUNE 1976–23 DECEMBER 1977

APPROVED FOR PUBLIC RELEASE: DISTRIBUTION UNLIMITED

Prepared for:

NAVAL AIR DEVELOPMENT CENTER

Warminster, Pennsylvania 18974

Unclassified

SECURITY CLASSIFICATION OF THIS PAGE *(When Data Entered)*

REPORT DOCUMENTATION PAGE

READ INSTRUCTIONS BEFORE COMPLETING FORM

1. REPORT NUMBER: NADC 76153-30	2. GOVT ACCESSION NO.
3. RECIPIENT'S CATALOG NUMBER	
4. TITLE *(and Subtitle)*: An Investigation of Corner Separation within a Thrust Augmenter Having Coanda Jets.	5. TYPE OF REPORT & PERIOD COVERED: Final Report, 30 Jun 76 - 23 Dec 77
6. PERFORMING ORG. REPORT NUMBER: NR77H-18	
7. AUTHOR(s): Milton R. Seiler	8. CONTRACT OR GRANT NUMBER(s): N62269-76-C-0402 New
9. PERFORMING ORGANIZATION NAME AND ADDRESS: Rockwell International Columbus Aircraft Division, 4300 East Fifth Avenue, P. O. Box 1259, Columbus, Ohio 43216	10. PROGRAM ELEMENT, PROJECT, TASK AREA & WORK UNIT NUMBERS: 61153N WR02302 WR0230201 NN701
11. CONTROLLING OFFICE NAME AND ADDRESS: Naval Air Systems Command (320D), Department of the Navy, Washington, D. C. 20361	12. REPORT DATE: Dec 77
	13. NUMBER OF PAGES: 49 Pg.
14. MONITORING AGENCY NAME & ADDRESS *(if different from Controlling Office)*: Naval Air Development Center (3014), Warminster, PA 18974	15. SECURITY CLASS. *(of this report)*: Unclassified
	15a. DECLASSIFICATION/DOWNGRADING SCHEDULE

16. DISTRIBUTION STATEMENT *(of this Report)*

Approved for public release; distribution unlimited

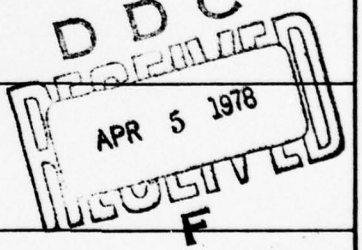

17. DISTRIBUTION STATEMENT *(of the abstract entered in Block 20, if different from Report)*

18. SUPPLEMENTARY NOTES

19. KEY WORDS *(Continue on reverse side if necessary and identify by block number)*

Augmenters	Stratford Number	Boundary Layer
Augmentation	Surveys	Diffuser
Ejectors	Hot-film	
Separation	Thrust	

20. ABSTRACT *(Continue on reverse side if necessary and identify by block number)*

An investigation was conducted to determine the way separation develops in the corners of thrust augmenter wings having Coanda jets. Hot film surface sensors and pressure transducers were used, and the results indicated that separation on the test augmenter began at a corner very close to the augmenter exit and then rapidly proceeded upstream. Measurements of the velocity and pressure fields in the corner region indicated that a modified form of the Stratford criterion could be used to predict the onset of separation.

DD FORM 1 JAN 73 1473 EDITION OF 1 NOV 65 IS OBSOLETE

Unclassified

SECURITY CLASSIFICATION OF THIS PAGE *(When Data Entered)*

407 390

PREFACE

This report documents the work performed by the Columbus Aircraft Division of Rockwell International for the Naval Air Development Center, Warminster, Pennsylvania, under Contract N62269-76-C-0402. Technical coordination was provided by Mr. John Cyrus and Dr. Kenneth Green of the Naval Air Development Center.

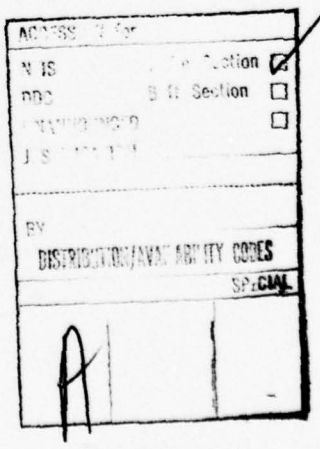

SUMMARY

An investigation was conducted to determine the way separation develops in the corners of thrust augmenter wings having Coanda jets. Hot film surface sensors and pressure transducers were used, and the results indicated that separation on the test augmenter began at a corner very close to the augmenter exit and then rapidly proceeded upstream. Measurements of the pressure fields in the corner region indicated that a modified form of the Stratford criterion could be used to predict the onset of separation. Testing was conducted over a range of nozzle pressure ratios, aspect ratios, diffuser angles and designs of the boundary layer and Coanda nozzles.

TABLE OF CONTENTS

LIST OF FIGURES

LIST OF TABLES

LIST OF SYMBOLS

A_0	Nozzle Area
A_2	Throat Area
A_3	Exit Area
AR	Aspect Ratio (Augmenter Span/Throat)
BLC	Boundary Layer Control (Blowing)
C_P	Pressure Coefficient ($=\Delta P/q$)
N_{ST}	Stratford Number
P	Static Pressure (Measured in Pascals, P_a; 6895 P_a = 1 psi, 249.1 P_a = 1 inch H_2O)
P_∞	Barometric Pressure
P_R	Pressure Ratio
q, Q	Dynamic Head
R	Coanda Radius
R_N	Reynolds Number
t	Coanda Nozzle Gap
TAW	Thrust Augmenter Wing
U_{MAX}	Local Maximum Jet Velocity
x	Streamwise Distance Measured from the Augmenter Throat
δ_D	Diffuser Half Angle
Ø	Thrust Augmentation Ratio
ρ	Density

1.0 INTRODUCTION

Thrust augmenters have been used in aircraft applications for a number of years. One of the first application attempts was reported in Reference (1), where the main impetus was to use them to draw cooling air over a jet engine nozzle. Modest increases in static thrusts were observed as well. During the early 1960's thrust augmenters were used to provide lift for the XV-4A research VTOL aircraft. More recently they have been used in the design concept of thrust augmenter wings (TAW) which provide the direct lift mechanism for the Navy XFV-12A VTOL demonstrator aircraft (Reference 2). In such applications maximization of thrust augmentation is, obviously, of prime importance. Experimentally it has been observed that flow separation within the augmenter diffuser section is very often the limiting factor. Classical diffuser separation criteria such as Reference (3) are not applicable to most TAW designs since the latter experience imperfectly mixed primary jet flows in their diffuser sections because of aircraft-related packaging requirements. Therefore, realistic separation criteria is a necessity in the development of efficient TAW hardware. The purpose, then, of this study was to conduct a suitable testing program and analysis of an unswept, untapered (rectangular) model TAW-Type augmenter with Coanda jets so that a preliminary separation criterion could be established. A desirable criterion would involve a two-dimensional computer program to predict pressure and/or velocity on the diffuser flap as a function of streamwise distance. When the pressure distributions reached some critical value or pattern, based upon a pre-determined criterion, separation would occur. Any two-dimensional program assumes that the pressure distributions are independent of spanwise location.

2.0 BACKGROUND

Testing at the Columbus Aircraft Division (CAD) has shown that augmenter thrust ratio $\emptyset$ (actual measured thrust/ideal thrust from all primary jets and BLC) rises monotonically with diffuser angle δ_D until the onset of diffuser separation (Figure 1). This separation occurs at or near a corner formed by the intersection of the diffuser surfaces, which form flow boundaries for the augmenter Coanda jets, and the diffuser endwall. This was also identified as a critical area of the flow in Reference (4). When separation develops, it does so with such rapidity that the separation initiation point cannot be determined visually. There were two possible modes through which separation development might pass (Figure 2). In the first mode, separation would initially occur at or near the corner trailing edge and, because of the adverse pressure gradient within the diffuser, rapidly progress upstream until it stabilized at the augmenter throat. Alternatively, separation might begin on a Coanda corner intersection, where the flow stresses are high, and then proceed downstream until the entire corner was involved. Regardless of the mode of separation development, there are a number of factors which influence the δ_D at which it occurs. The most important of these is endwall boundary layer control (BLC) because it is not uncommon to achieve large δ_D increases

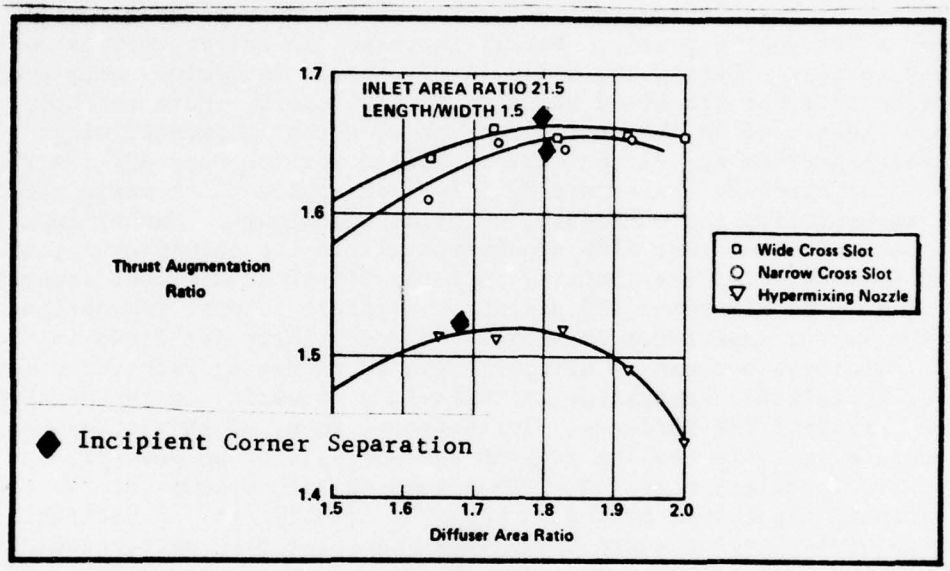

Figure 1. Thrust Augmentation vs. Diffusion (Ref. 4)

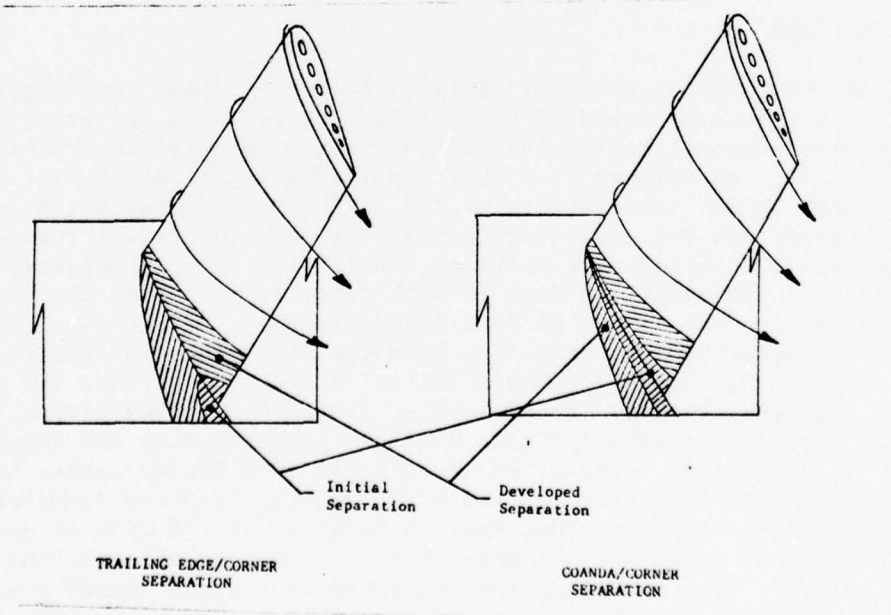

Figure 2. Possible Modes of Corner Separation

with attached flow with proper BLC blowing in the diffuser corners. In addition, recent results (Reference 5) have indicated that augmenter aspect ratio AR (span/throat width) has an effect on the diffuser angle at which separation occurred (Figure 3). Finally, because most

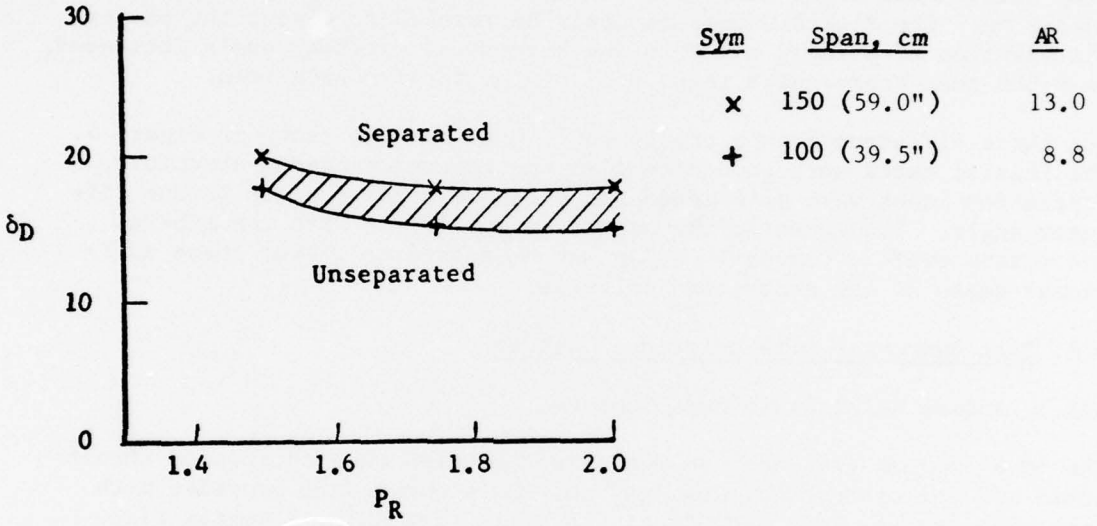

Figure 3. The Effect of Aspect Ratio on Separation (Ref. 5)

successful separation criteria in use today rely on some boundary layer or free stream velocity and pressure conditions being met (which any augmenter criteria will probably also use), a reasonable data base should include testing over a considerable pressure range. Thus, the detailed objectives of this project involved five tasks:

a) To determine which of the two possible corner separation modes actually occur in an operating augmenter with Coanda jets.

b) To measure the pressure and velocity fields in the vicinity of the separation point for a range of nozzle pressure ratios (P_R) and BLC conditions at and near separated flow conditions.

c) To alter the augmenter AR and repeat task b, above.

d) To alter the Coanda design to provide comparative data on Coandas of smaller R/t. This provides a more highly stressed Coanda surface. In addition, the internal Coanda nozzle configurations were altered to examine the possible effects of exit velocity profile on separation.

e) To analyze the data to derive a separation criteria.

3.0 EXPERIMENTS

The experimental effort was conducted with the augmenter shown in Figure 4. Primary air was delivered from a cross-slot centerbody, two Coanda nozzles, and four corner BLC tubes. Ratio of throat area to total nozzle area was $A_2/A_0 \cong 20$. A cross section is shown in Figure 5. Diffuser flaps were rigidly attached to the Coanda surfaces and the entire Coanda-flap combination could be rotated by hand to achieve a change in diffuser angle, δ_D. The four BLC nozzles could be rotated to direct the proper distribution of primary air into the corners as diffuser angle increased. Each BLC tube represented about 0.5% of the total nozzle area.

The three different Coanda nozzle configurations are shown in Figure 6. The initial tests were conducted with the reference Coanda structure. Separation modes were determined and pressure data recorded versus diffuser angle. Subsequently the augmenter was fitted with the top-hat and vortex profile Coandas. A_2/A_0 was decreased to 17 for these additional tests of the separation criteria.

3.1 Test Augmenter with Reference Coandas

3.1.1 Augmentation Ratio Measurements

The 50.8 cm span (20 inch) augmenter was mounted on a calibrated thrust stand and the centerbody, Coandas, and BLC blowers were provided with high pressure air from individual venturis. Initially ϕ versus flap angle was measured with all nozzles at pressure ratios of 1.5, 2.0 and 2.5. Also measured was the augmentation ratio with BLC turned off. Figure 7 shows the results. No significant pressure ratio effects were observed, although the effect of the BLC is most pronounced. Corner separation occurred at .21 radian with BLC off and at .35 radian with the BLC pressure matched to the Coanda and centerbody nozzle pressures.

The augmenter span was changed to 31 cm to provide AR = 2.5. Again ϕ versus flap angle was measured, as shown in Figure 8. Separation occurred at slightly smaller flap angles but the overall ϕ levels are similar to those with the higher aspect ratio.

3.1.2 Separation Mode Determination

It was imperative that the separation tests be conducted on a high ϕ augmenter; a low performance augmenter does not represent a highly stressed flow of interest. The corner in which separation occurred could be varied by minor rotation of the BLC blowers, although the fact that at least one corner would separate at the appropriate δ_D could not be changed. This was especially convenient in that the separation could be insured to occur in a particular (instrumented) corner without changing the δ_D at which separation took place. Visual inspection of tufts at the exit is sufficient to determine which corner is separating.

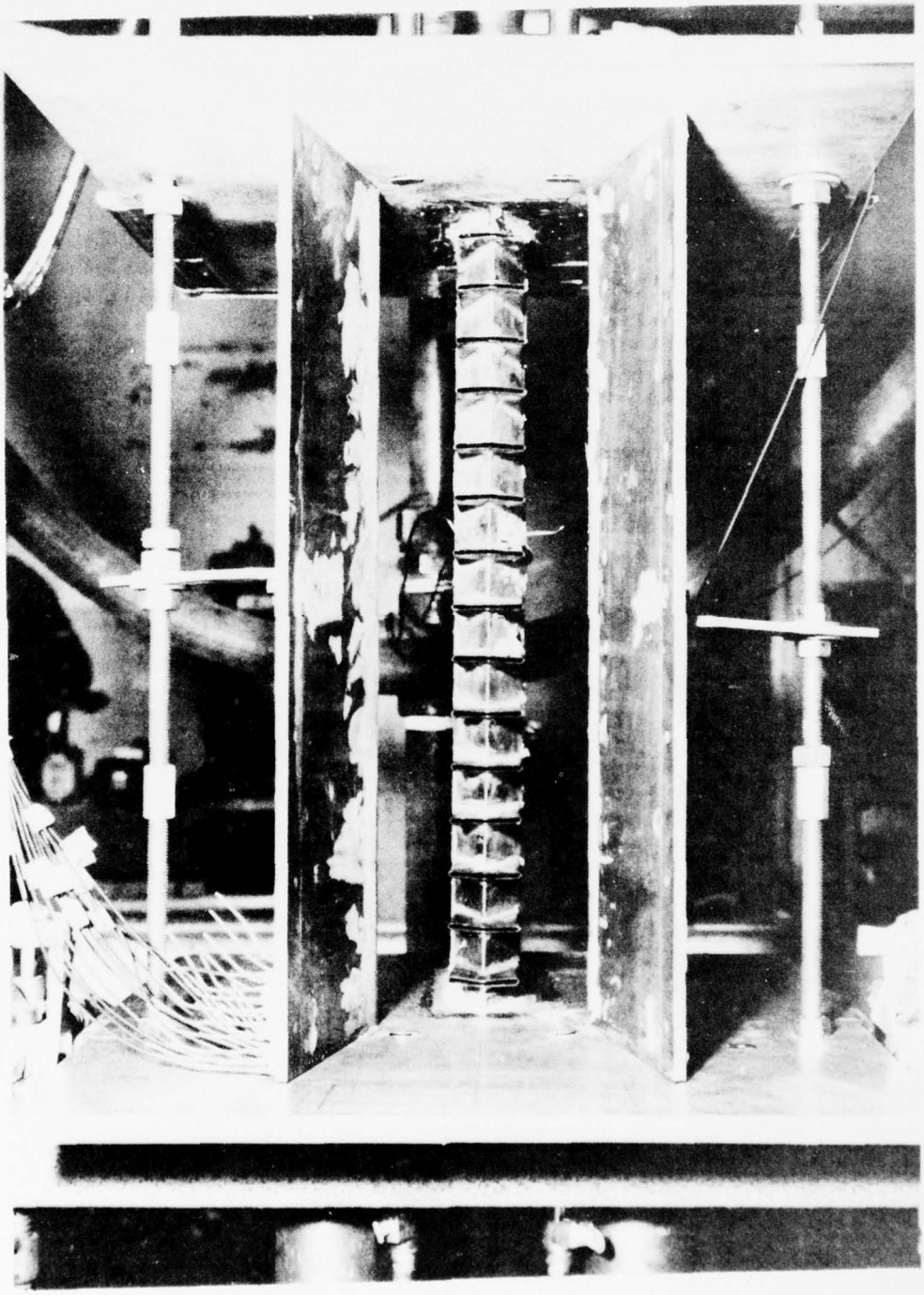

Figure 4. Test Augmenter

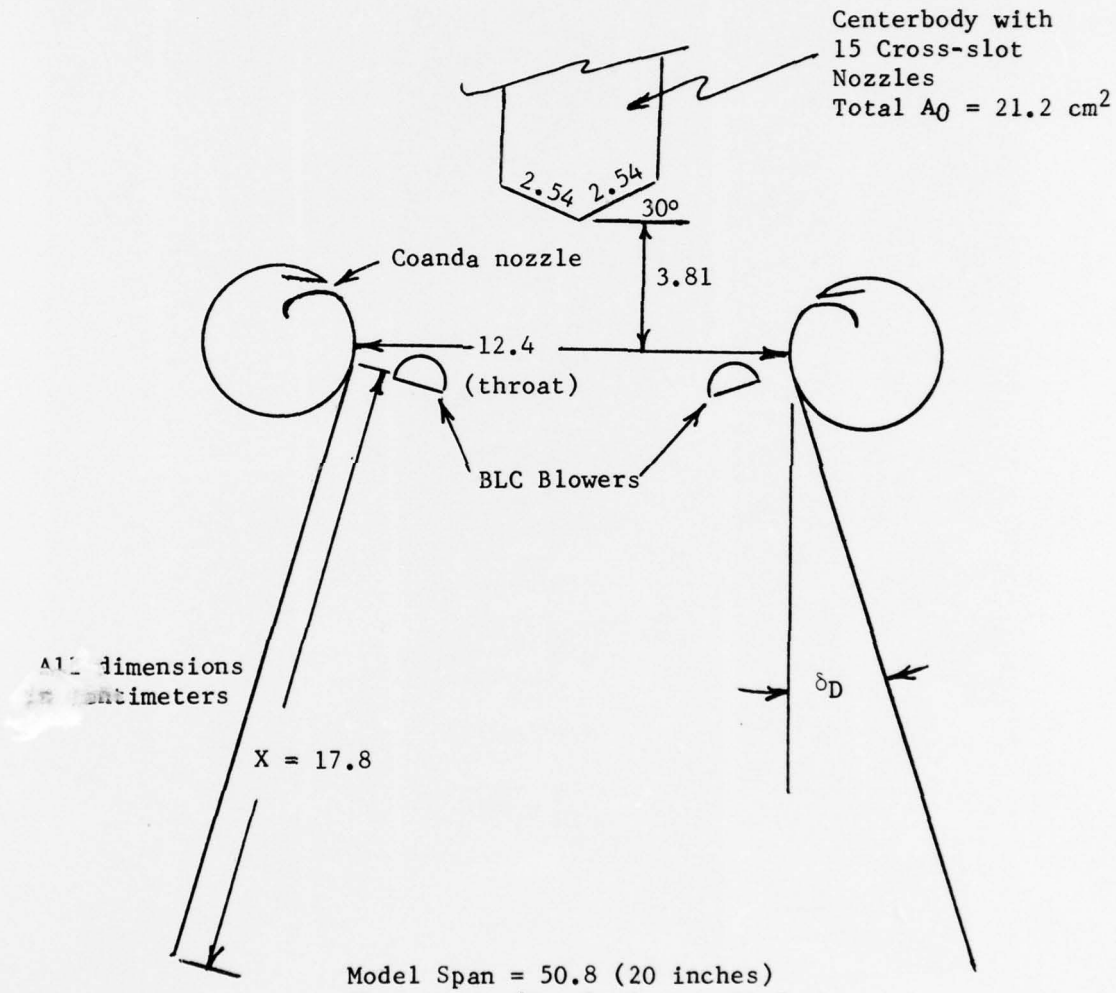

Figure 5 . Sectional View of Test Augmenter

Figure 6 . Coanda Nozzles Tested in Present Study (All dimensions in Centimeters)

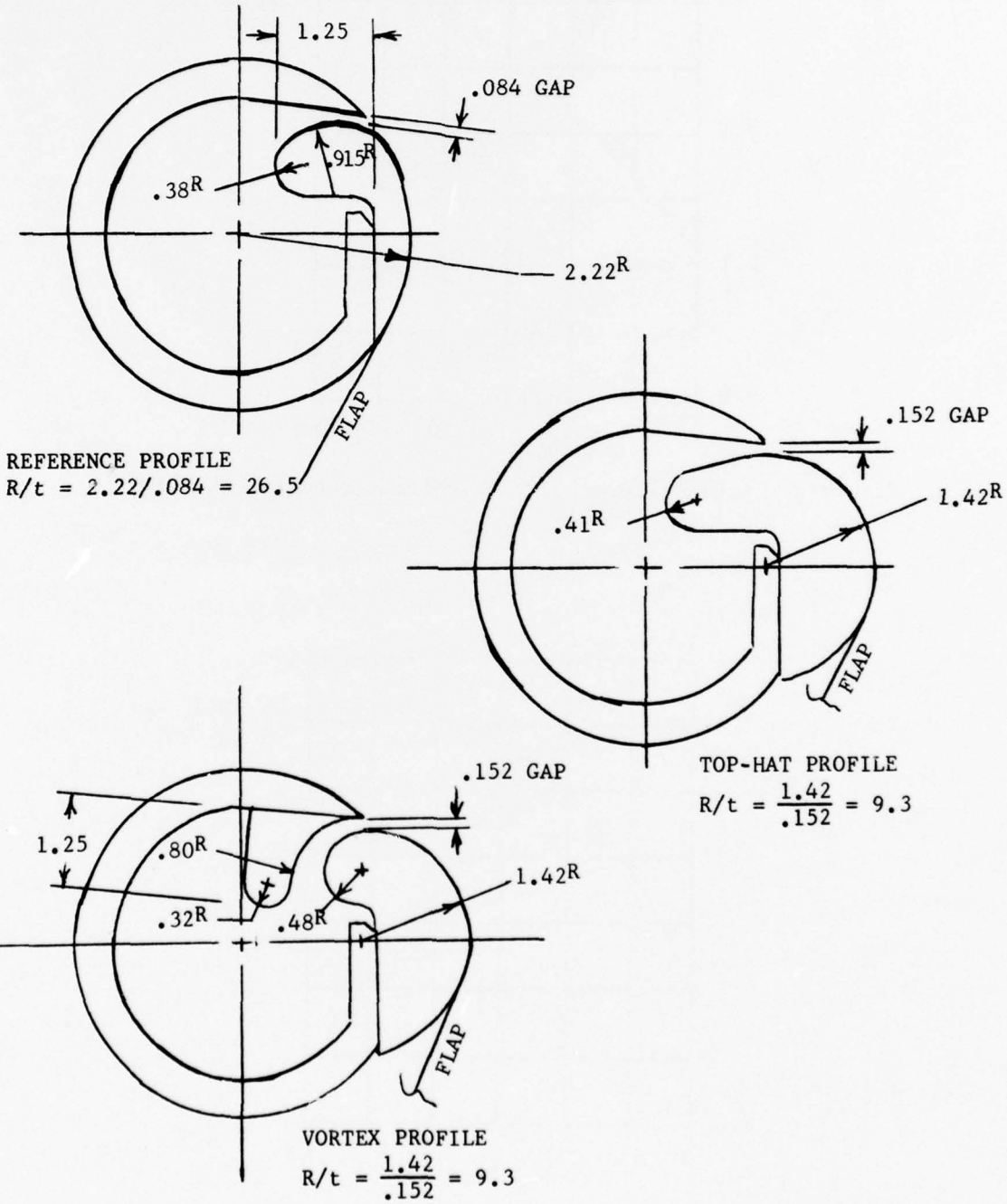

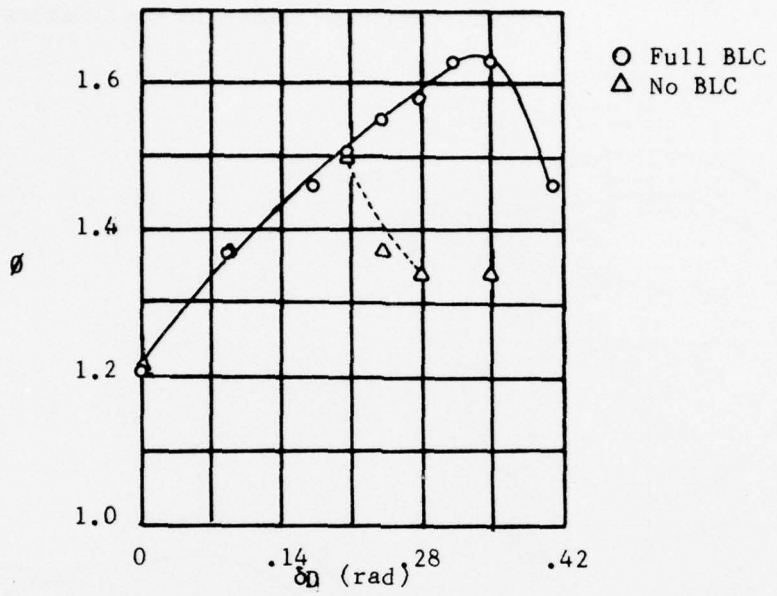

Figure 7. Augmentation Ratio vs. Diffuser Angle: AR = 4.1

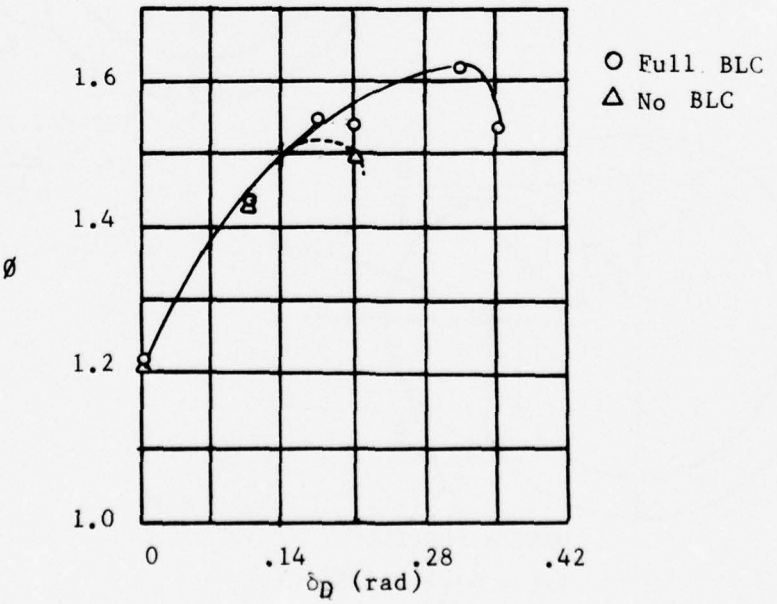

Figure 8. Augmentation Ratio vs. Diffuser Angle: AR = 2.5

For the portion of testing concerned with determining the separation mode, the augmenter was instrumented as shown in Figure 9. Two flush-mounted Thermo-Systems, Inc., Model 1237 hot film sensors were mounted on one flap surface at the endwall corner .032 cm and 5.01 cm upstream from the flap trailing edge. Two Statham ±2 psi differential pressure transducers were connected to surface pressure taps similarly located on the opposite flap. The hot film sensors were connected to a model 1050-2C Thermo-Systems, Inc., dual channel constant temperature anemometer whose output, together with that of the two transducers, was connected to a multi-channel Consolidated Electronics Corporation oscillograph.

Hot film surface sensors are able to detect the onset of flow separation over them by sensing the difference in the rate of heat transfer from the sensor surface between attached and separated flow (Reference 6). Further, their response rates (5×10^{-6} sec) are an order of magnitude faster than any mean flow changes likely to occur on the test augmenter. The test strategy for separation mode determination was to observe which of the two sensors changed output first when the augmenter was driven to separation by either raising δ_D or by lowering the BLC nozzle pressure. (Additional sensors and anemometers were available to provide more extensive sampling points should the results with two be indeterminant, but they were not needed.) First attempts were made by following the total (A. C. + D. C.) output signals, but the turbulent fluctuations (the A.C. signal) were so high in the diffuser that they almost masked the changes in the mean flow (the D.C. signal) associated with separation. Fortunately, separation also induces large changes in local turbulence, so the anemometer output was shifted to amplify the A. C. signals. The augmenter δ_D was then gradually increased to the point where a slight buffeting could be detected audibly (incipient separation), and the results recorded (Figure 10). For this case the BLC tubes were also gradually rotated so as to be blowing parallel to the flap (see Appendix B). It can be easily seen that the turbulence level increased markedly and suddenly at the downstream sensor but not at the upstream sensor, which is indicative of the fact that the separation was initiating downstream. Next, the augmenter δ_D, again initially with the flow attached, was rapidly raised without changing the BLC tube blowing angle. The signals (Figure 11) show that the downstream sensor responded to separation prior to the upstream. The time between the two changes was approximately equal to the distance between the two sensors divided by the speed of sound (335 m/sec) minus the average mean flow speed over the sensors (120 m/sec), which is approximately the speed at which the separation should propagate in an upstream direction. The above testing was done at $P_R = 2.0$. The test was repeated at $P_R = 1.5$ (Figure 12) where a similar result was observed. Finally the flow was forced to separate upstream by suddenly blocking off a 1 cm portion of the

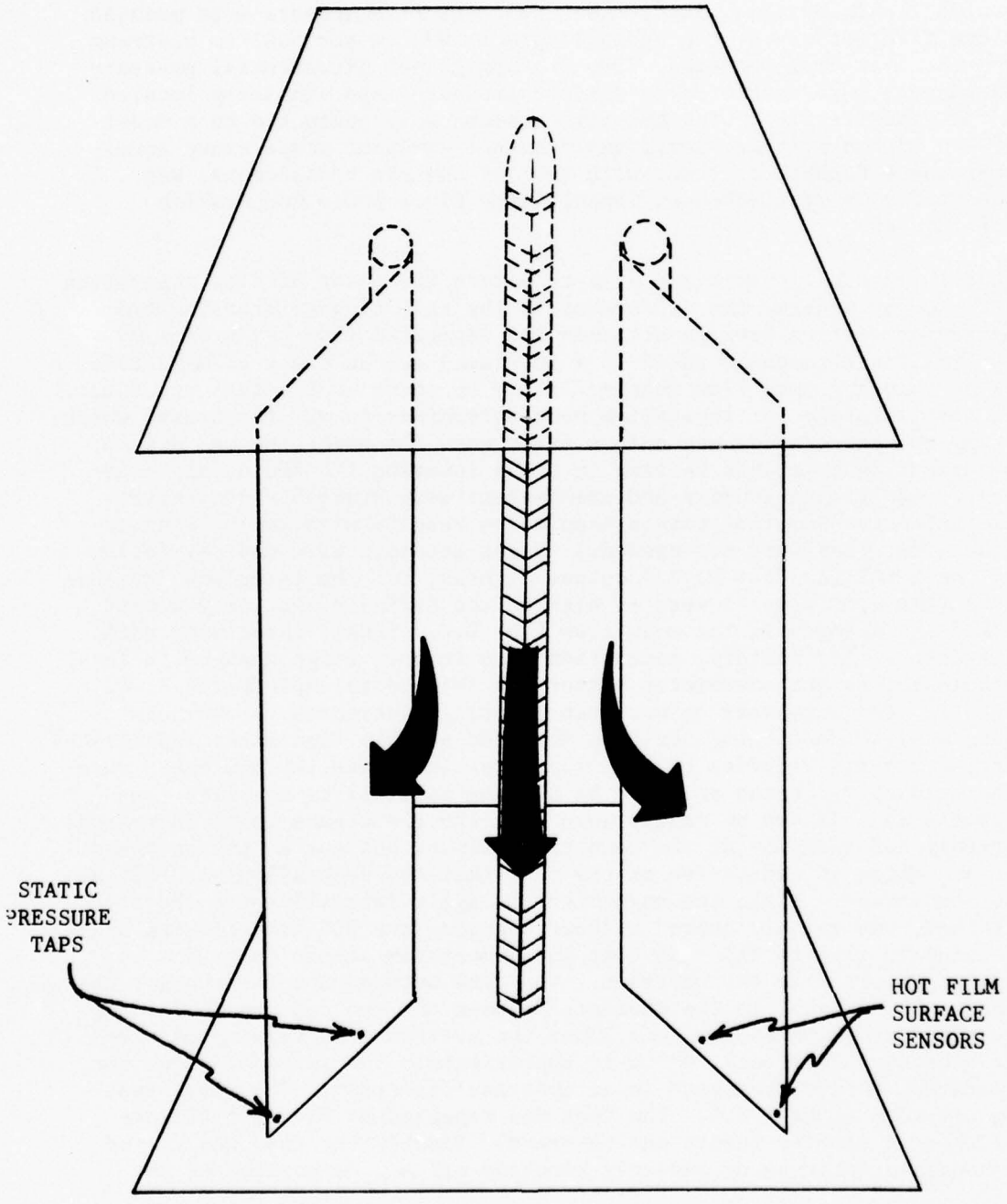

Figure 9. Instrumentation for Separation Mode Determination

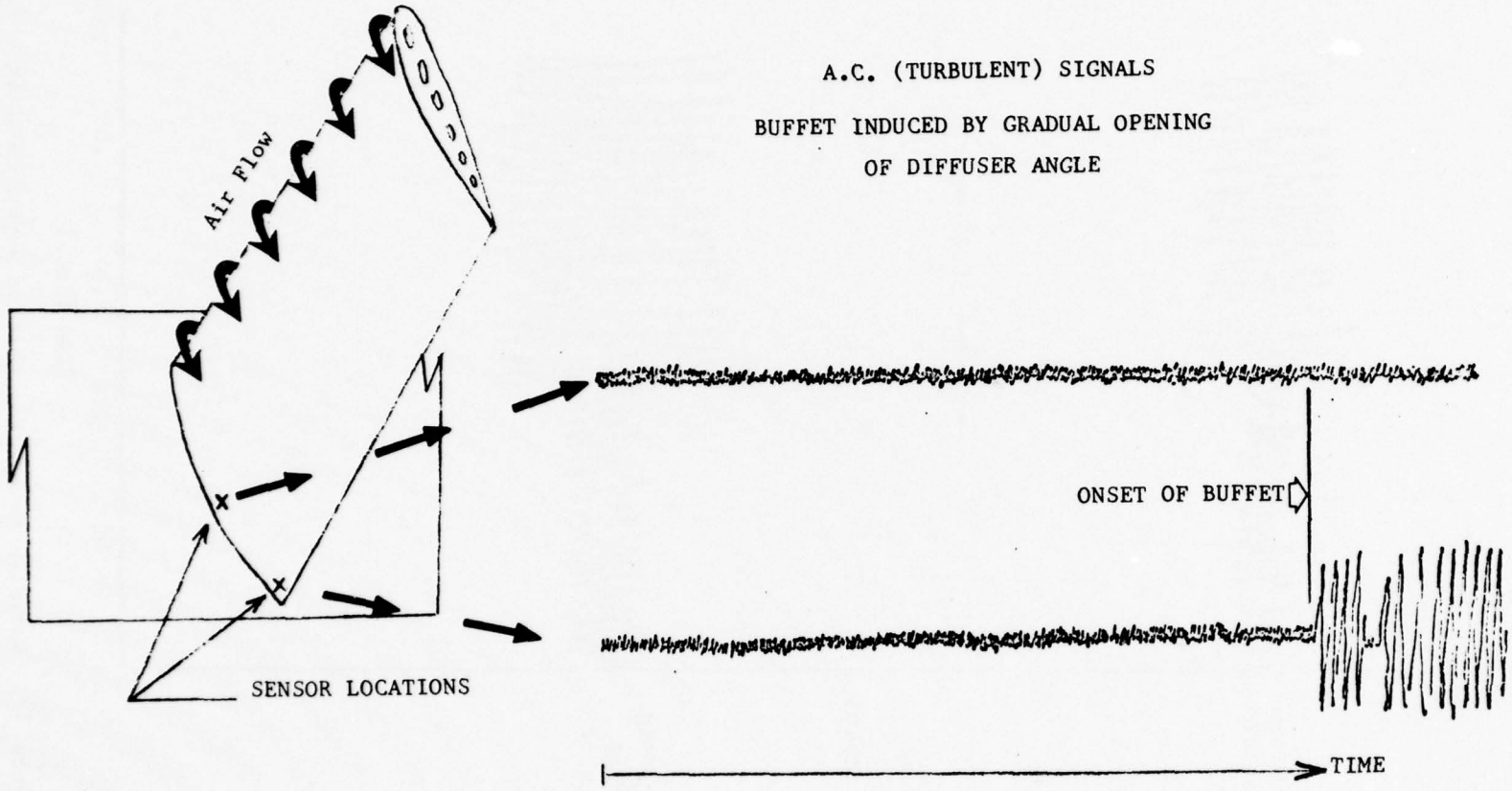

Figure 10. Buffet Response of Hot Film Sensors: P_R = 2.0

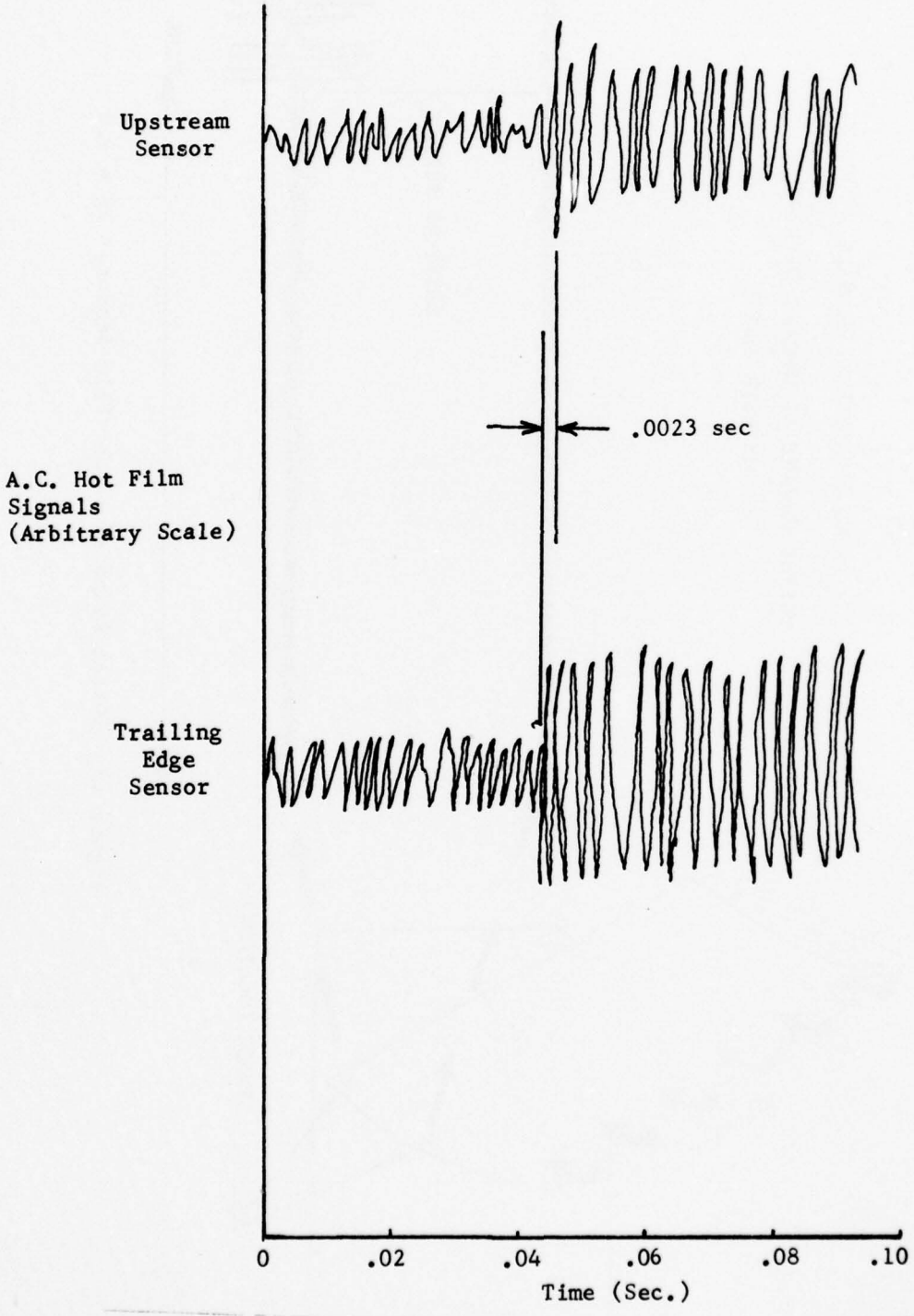

Figure 11. Hot-Film Sensor Response to Separation: $P_R = 2.0$

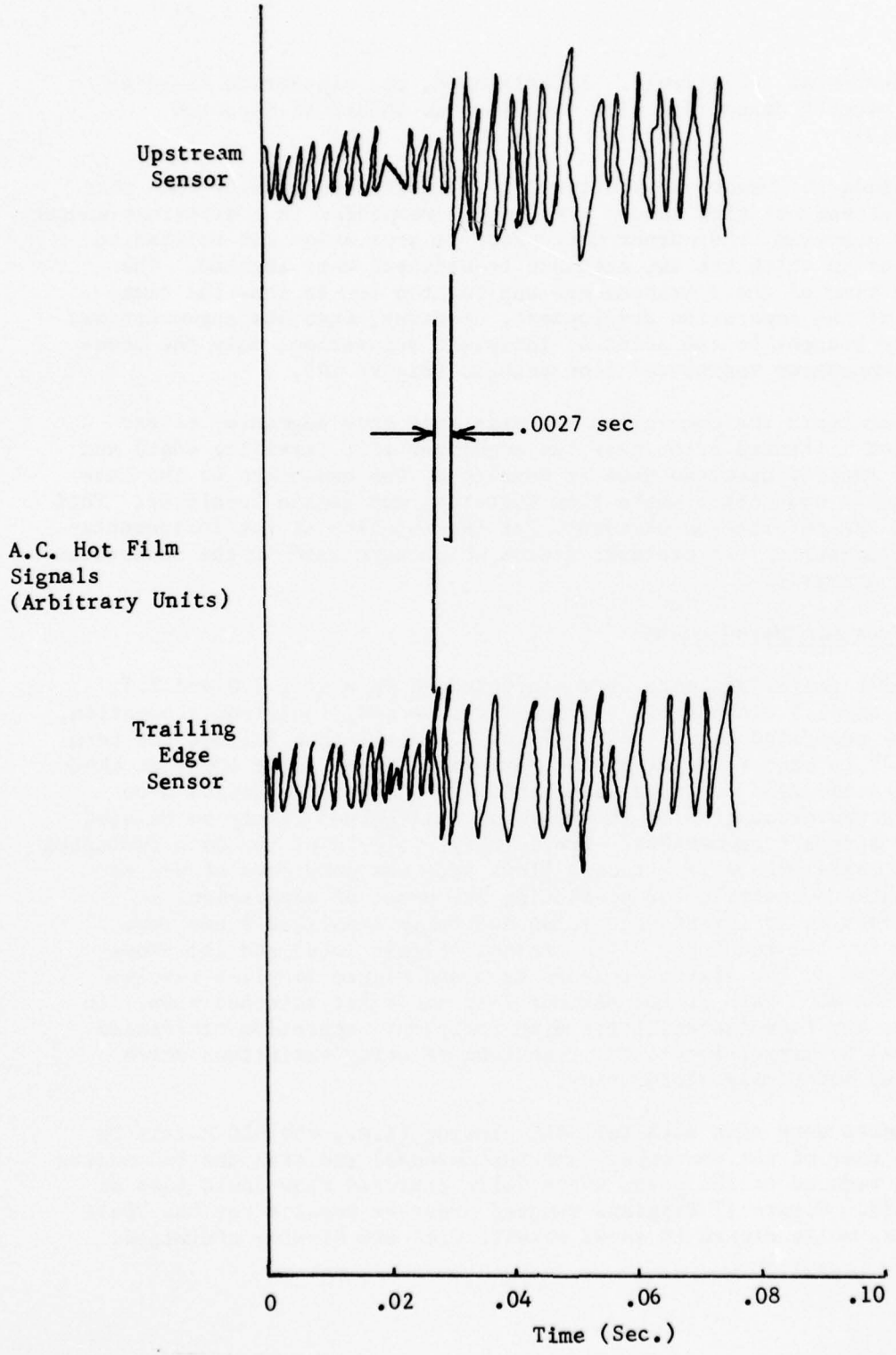

Figure 12. Hot-Film Sensor Response to Separation: P_R = 1.5

Coanda nozzle at the endwall. In this case, the separation could be seen to proceed downstream with the flow, as should be expected (Figure 13).

To preclude the remote possibility of an instrument anamoly such that the downstream hot film sensor artifically responded in a different manner than the upstream, the corner most prone to separation was shifted to the corner in which the two pressure transducers were located. The response time of these transducers was far too low to show the time history of the separation development. However, when the augmenter was carefully brought to the point of incipient separation, only the downstream transducer registered flow changes (Figure 14).

From these tests the conclusion was made that this augmenter corner separation initiates at or near the augmenter exit (trailing edge) and proceeds rapidly upstream when it develops. One exception is the case of incipient separation where flow buffeting may remain localized. This provided the information necessary for the location of the instrumentation for measuring the pressure fields which were used in the separation criteria analysis.

3.1.3 Pressure Measurements

The initial series of tests were conducted at P_R = 1.5, 2.0 and 2.5, AR = 4.1 and 2.5 without BLC blowing for attached, incipient separation, and fully separated conditions. (In this and all that follows the term "attached" is used to identify the maximum diffuser angle δ_{DMAX} at which fully attached flow could be maintained.) The pressure ratios were picked as representative of the range of jet engines likely to be used to power aircraft augmenters. Preliminary analysis of the data indicated that the measurements of attached flows were the only ones of use in establishing a criteria for predicting the onset of separation, so measurements at incipient separation and fully separated flows were not made for the remainder of the tests. Figure 15(a) and (b) shows the location of the static pressure taps and Figure 16 gives results for the "No BLC" case at the maximum flap angle for attached flow. In any case, the flow instabilities with incipient separation manifested themselves by large, localized, transient velocity variations which masked any underlying steady flow.

Measurements were made with full BLC blowing (i.e., the BLC nozzle P_R equal to that of the centerbody and the Coandas) and with the BLC nozzle pressure reduced to the point where fully attached flow could just be maintained. Figure 17 displays reduced pressure results for the "Full BLC" case, while Figure 18 shows results with BLC blowing minimized.

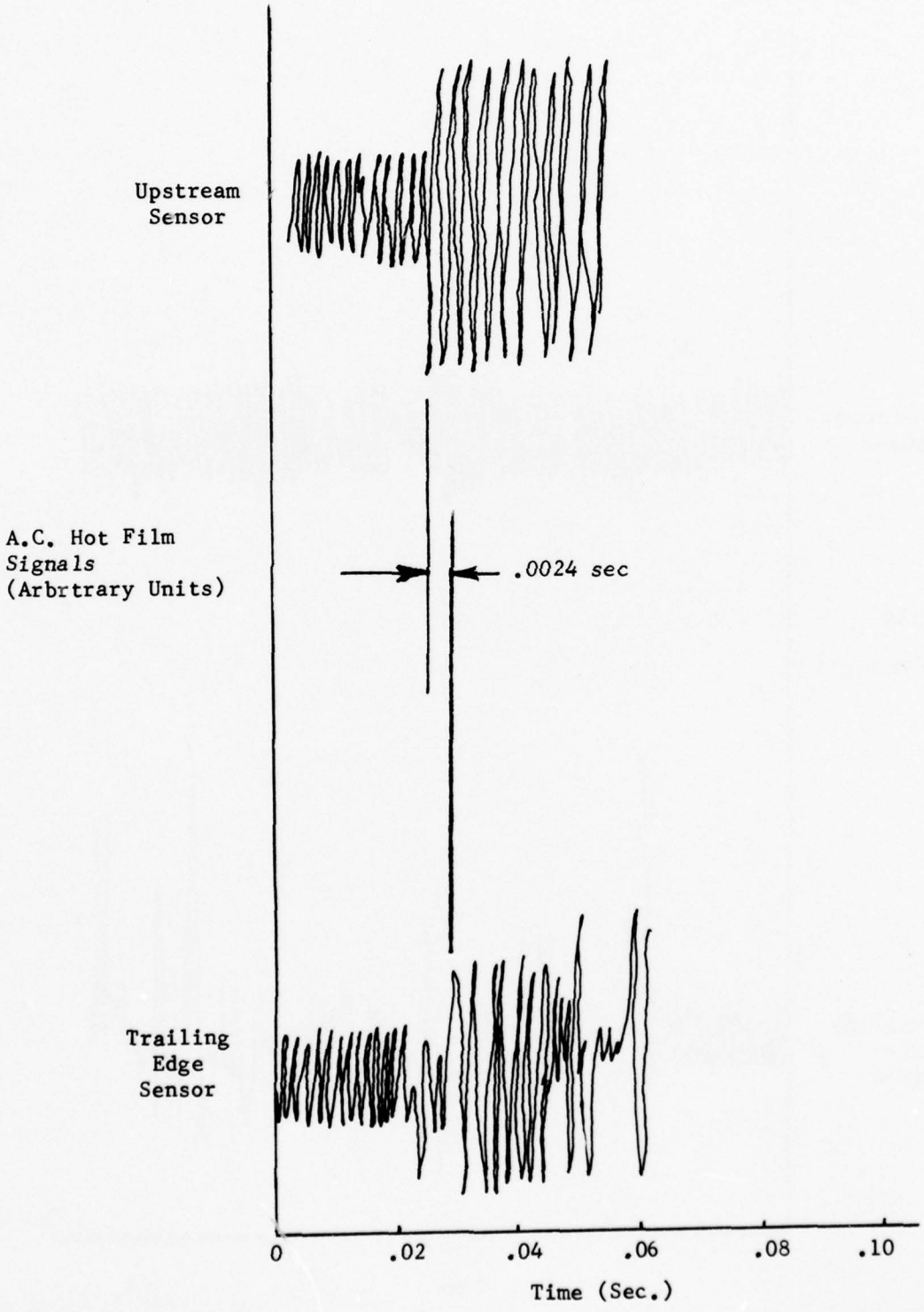

Figure 13. Hot-Film Sensor Response to Separation Forced at the Coanda Nozzle Exit: P_R = 2.0

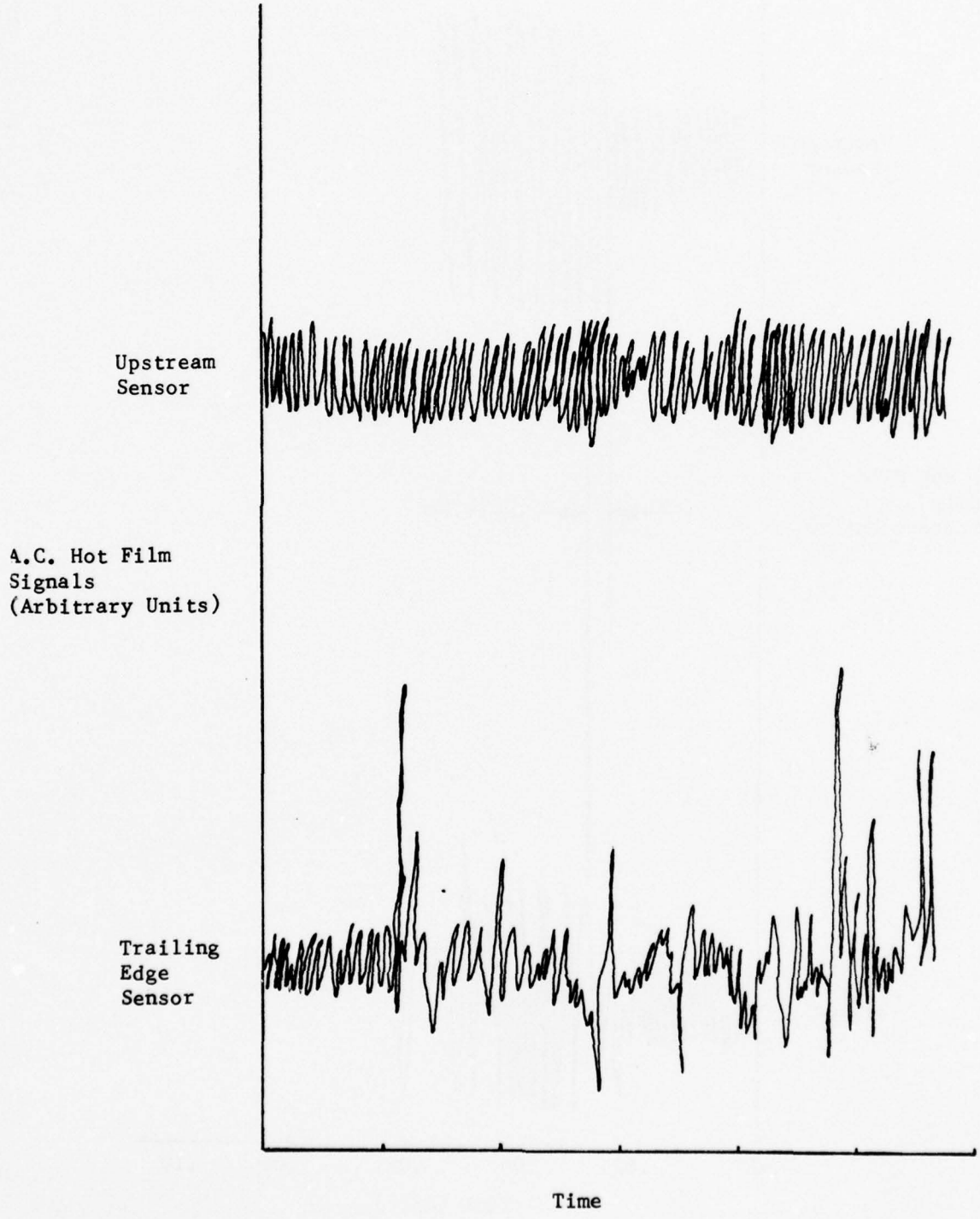

Figure 14. Pressure Transducer Response to Buffet: $P_R = 2.0$

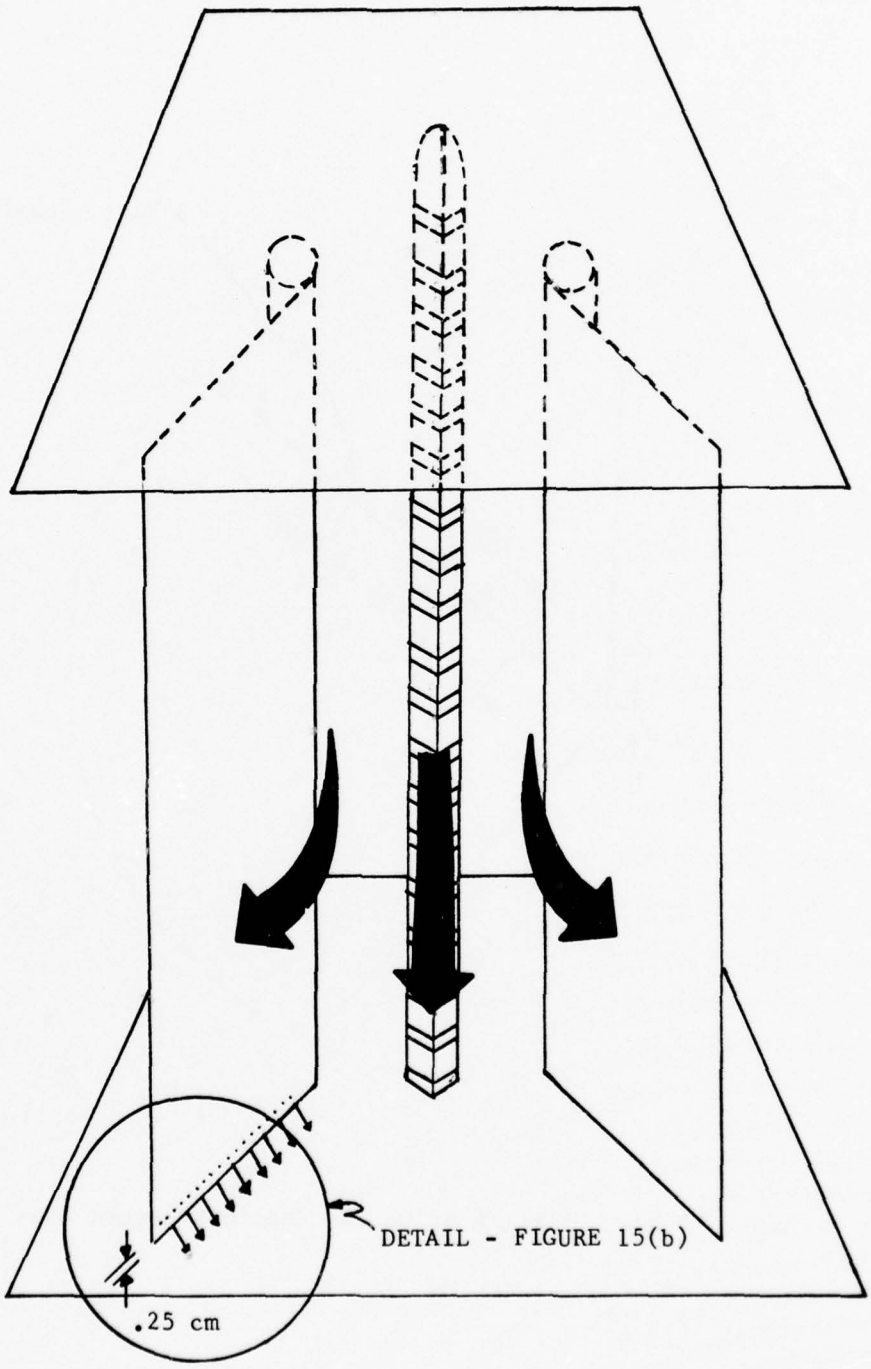

Figure 15(a). Augmenter Schematic

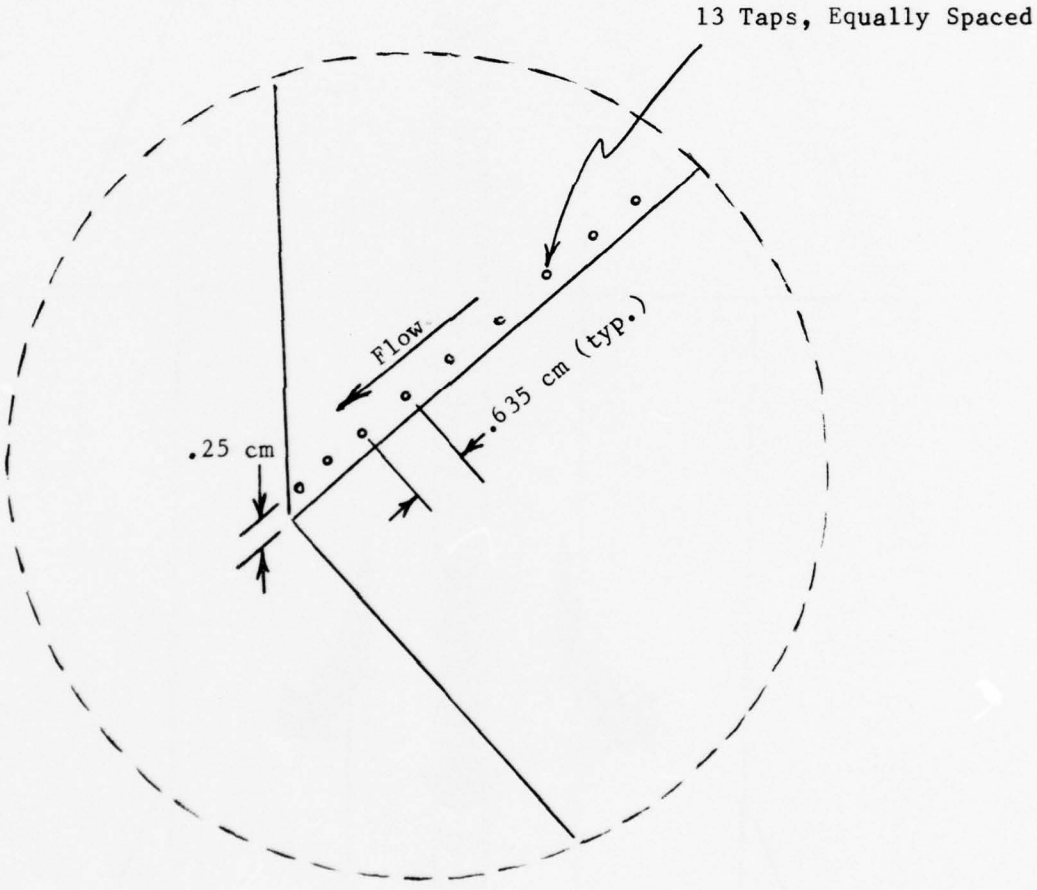

Figure 15(b). Location of Corner Static Pressure Taps

Figure 16 . Corner Static Pressure Readings for Reference Profile Coandas, R/t = 26.5, No BLC

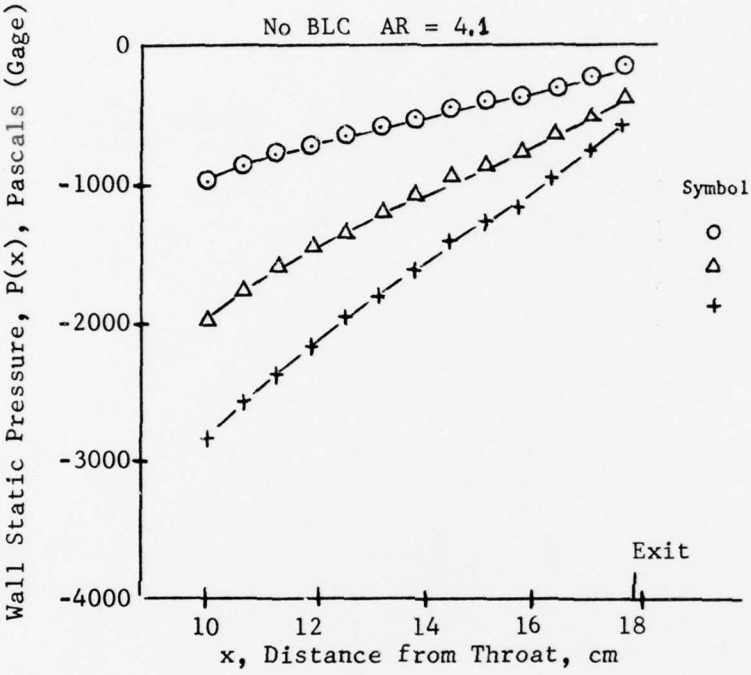

Symbol	Pressure Ratio	Flap Angle Radians	$[xdP/dx]_{exit}$ Pascals
○	1.5	.21	1860
△	2.0	.21	3950
+	2.5	.21	5600

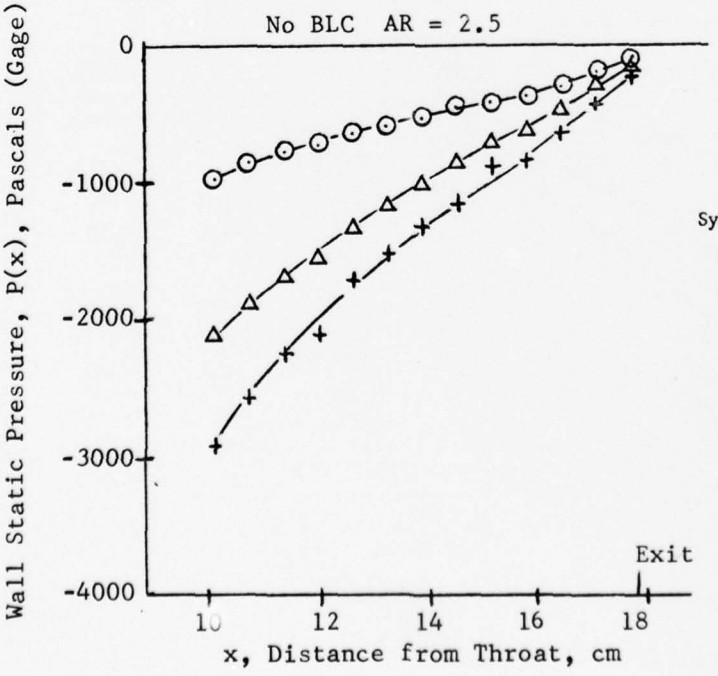

Symbol	Pressure Ratio	Flap Angle Radians	$[xdP/dx]_{exit}$ Pascals
○	1.5	.175	2190
△	2.0	.175	4400
+	2.5	.175	6050

Figure 17 . Corner Static Pressure Readings for Reference Profile Coandas, R/t = 26.5, Full BLC

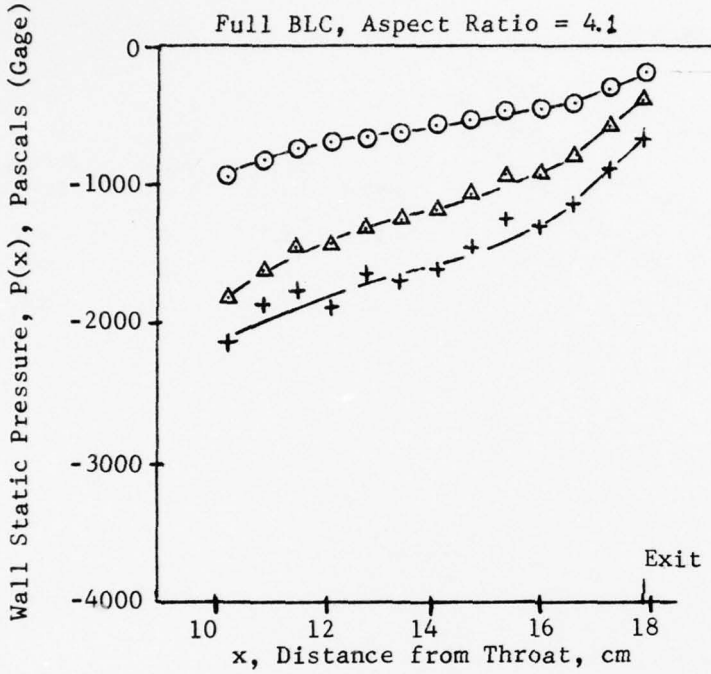

Symbol	Pressure Ratio	Flap Angle Radians	$[xdP/dx]_{exit}$ Pascals
○	1.5	.33	2320
△	2.0	.33	4600
+	2.5	.33	6950

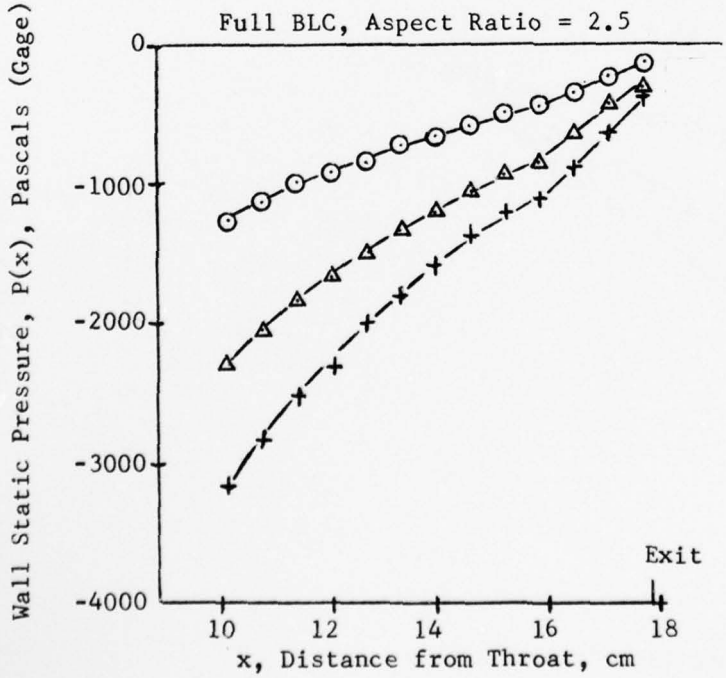

Symbol	Pressure Ratio	Flap Angle Radians	$[xdP/dx]_{exit}$ Pascals
○	1.5	.30	2890
△	2.0	.30	5120
+	2.5	.30	6850

Figure 18 . Corner Static Pressure Readings for Reference Profile Coandas, R/t = 26.5, Minimum BLC

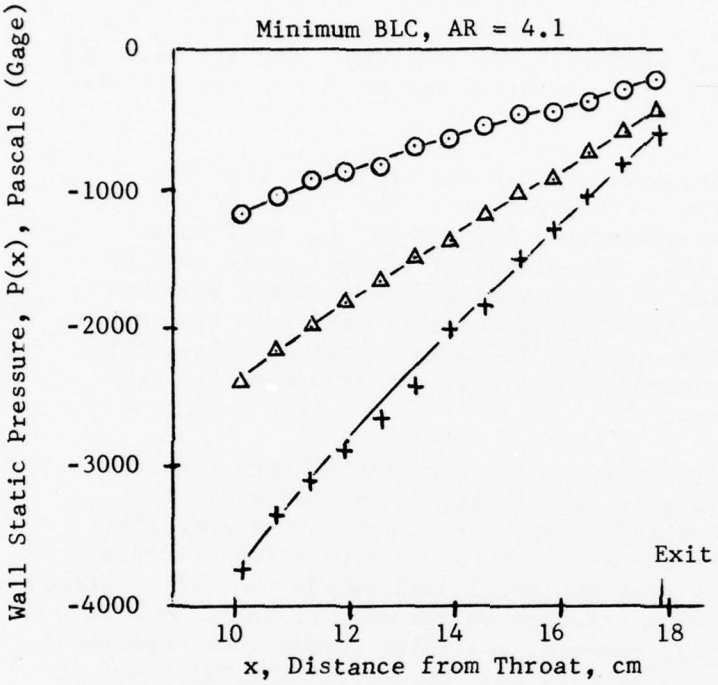

Symbol	Pressure Ratio	Flap Angle Radians	$[xdP/dx]_{exit}$ Pascals
○	1.5	.33	2320
△	2.0	.33	4650
+	2.5	.33	6500

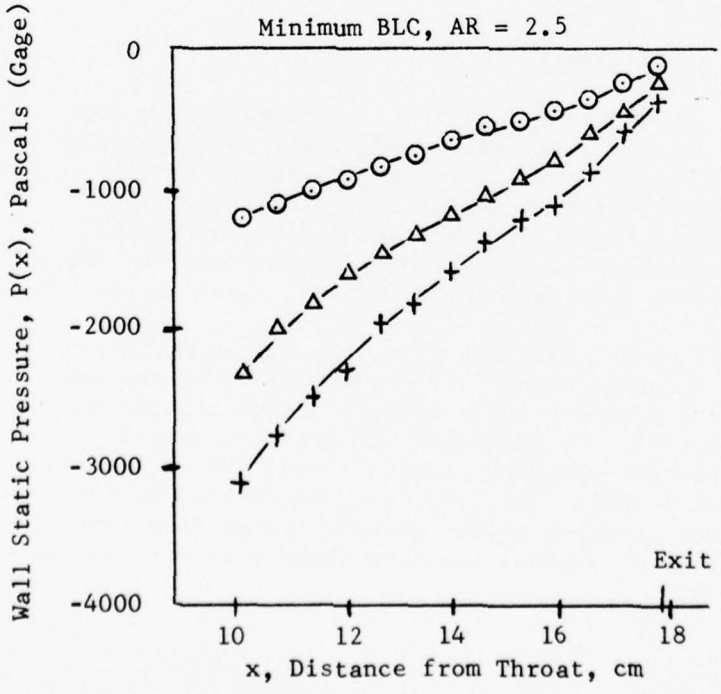

Symbol	Pressure Ratio	Flap Angle Radians	$[xdP/dx]_{exit}$ Pascals
○	1.5	.30	3020
△	2.0	.30	5330
+	2.5	.30	7000

Also indicated on Figures 16, 17 and 18 is the quantity $[xdP/dx]_{exit}$. This is the derived gradient of static pressure at the trailing edge multiplied by the distance, x, from the throat. Generally, it is the last three or four taps which establish the gradient. For all measurements x = 17.8 cm (7 inches). This quantity was needed in the calculation of the separation criterion.

In addition to the static pressure taps in the corner of the flap, a static tap was mounted in the secondary flow at the throat of the augmenter. Its location was approximately midspan and 1.6 cm from a Coanda surface (see Figure 19). The placement of this probe must be such that it is in the region of relatively constant static pressure which occurs in the uniform secondary flow. This region is also where the total pressure is ambient. Figure 19 shows a typical total, ΔP_T, and static pressure, ΔP_S, distribution across the throat of the augmenter and the probe location.

This throat static tap was recorded at all flap angles with the augmentation ratio and corner static distributions. It was hoped that this throat static pressure would serve as a suitable reference pressure for subsequent application of the Stratford separation criteria. This reading is particularly easy to record, and avoids the difficulties of attempting to measure static pressure on the wall of the Coanda at the throat. These latter measurements, according to previous experience, are subject to much uncertainty due to the shock pattern established on the Coanda surface downstream of the nozzle.

3.2 Tests with Vortex Profile Coandas

3.2.1 Augmentation Ratio Measurements

The vortex profile Coandas of Figure 6 were next installed. This configuration is designed to achieve a velocity profile across the nozzle that shows a maximum on the inner radius. The nozzle is too small, however, to allow experimental verification of this profile by probe measurements. In any event, a highly stressed Coanda flow with small R/t (9.3) is achieved. The nozzle gap was .152 cm (.060 inch) but the remaining augmenter dimensions were unchanged. Overall A_2/A_0 became 17.

Figure 20 shows the results of augmentation ratio, Ø, versus diffuser angle. Corner separation occurred beyond .175 radian (10°) at pressure ratios of 1.5 and 2.0. At a pressure ratio of 2.5, corner separation occurred beyond .14 radian (8°). No amount of BLC nozzle rotation toward the corners could improve upon the results shown. At angles slightly beyond the maximum Ø angle, the flow is characterized by increased buffeting and random movement of the weakest corner from side to side. Finally, at very large angles, the flow shows a steady separation in one or more corners.

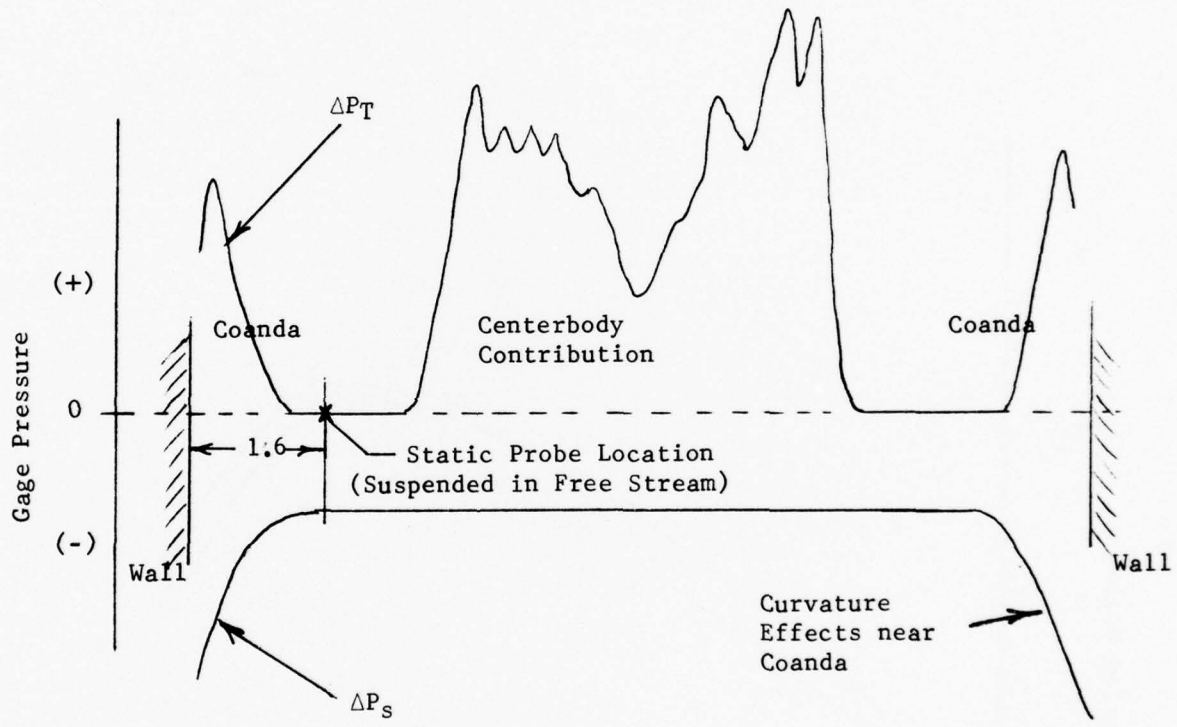

Figure 19. Typical Total, ΔP_T, and Static, ΔP_S Distribution Across the Augmenter Throat

Figure 20. Augmentation Ratio vs Diffuser Angle, Vortex Profile

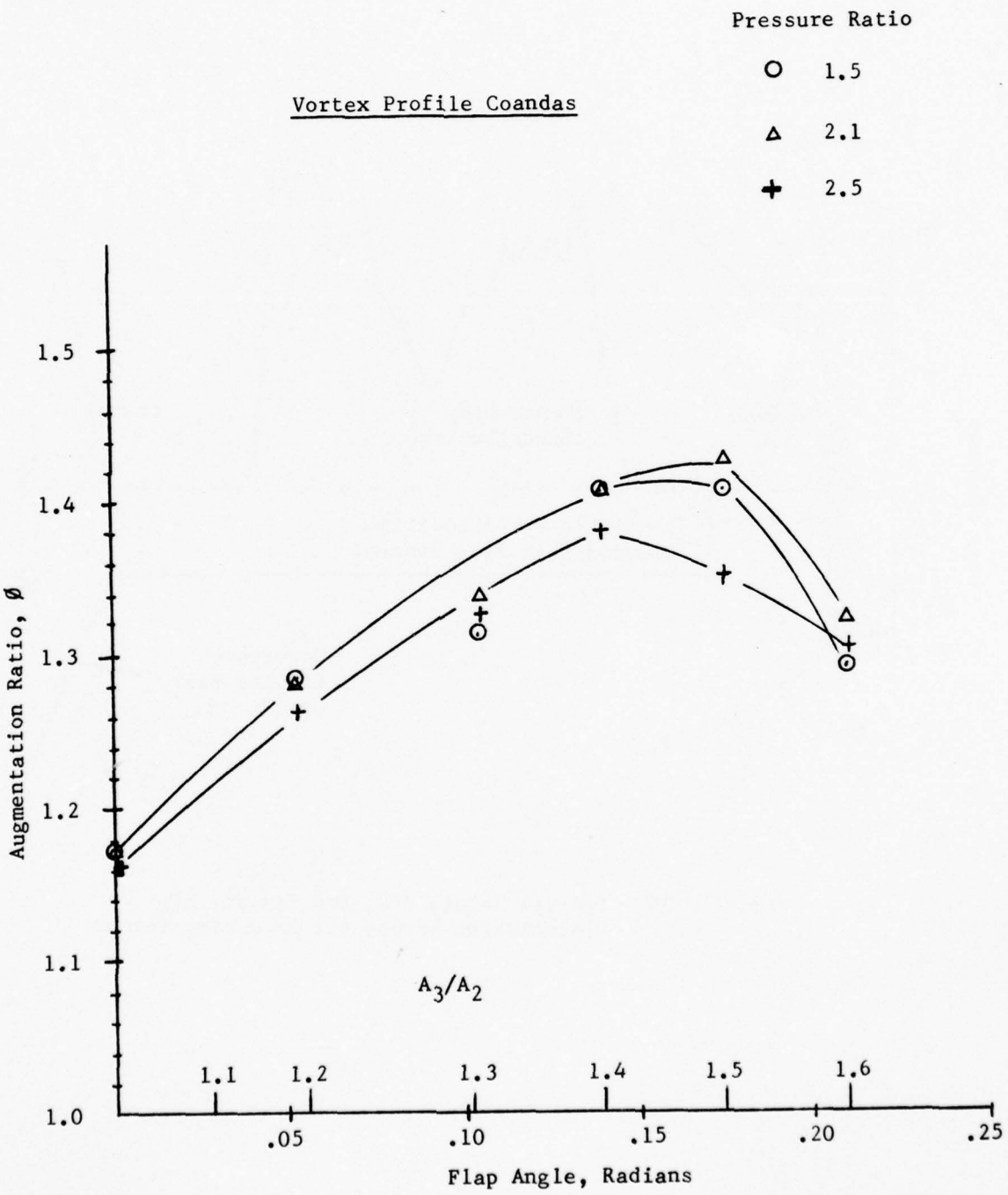

3.2.2 Pressure Measurements

Figure 21 gives the corner static pressure data at the maximum angles giving attached flow. Notice that the magnitude of the gradient term xdP/dx is larger than for the reference Coandas. This is caused by the changes in augmenter configuration; i.e., nozzle gap and A2/A0, which affect the wall jet rate-of-entrainment and dP/dx at the exit.

3.3 Tests with Top-Hat Profile Coandas

3.3.1 Augmentation Ratio Measurements

The Coanda surfaces were replaced with the top-hat configuration shown in Figure 6. This Coanda design was intended to produce a "uniform" velocity distribution across the nozzle and, simultaneously, produce a small value of R/t. The nozzle has a straight upstream convergence half-angle of about .25 radian (15°).

Figure 22 shows the results of Ø versus flap angle for the top-hat profile Coandas. Results are similar to those for the vortex profile.

3.3.2 Pressure Measurements

Also shown in Figure 21 are the static tap readings for the top-hat profile. Again, the gradient term is larger than for the reference profile.

Figure 21. Corner Static Pressure Readings for Vortex Profile and Top-Hat Profile, R/t = 9.3, Full BLC

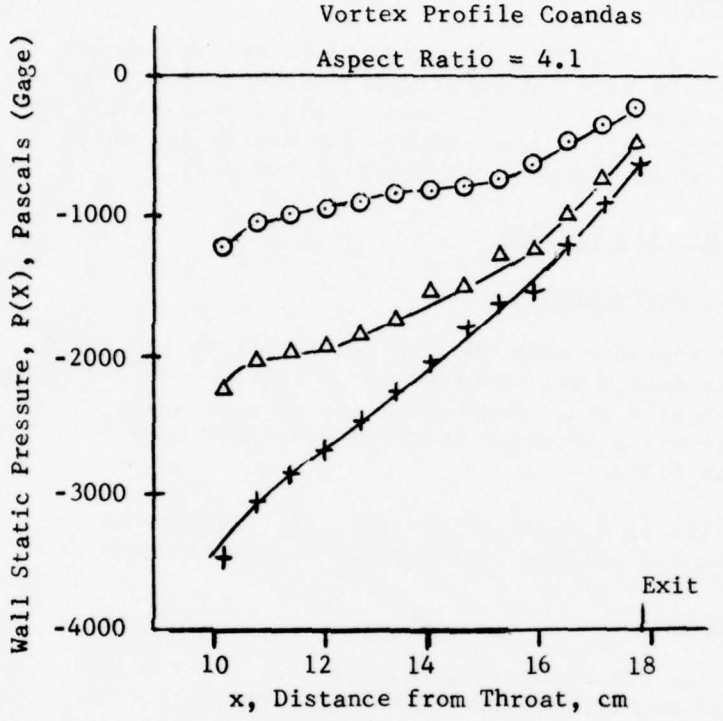

Symbol	Pressure Ratio	Flap Angle Radians	$[xdP/dx]_{exit}$ Pascals
○	1.5	.175	3480
△	2.1	.175	7000
+	2.5	.140	8850

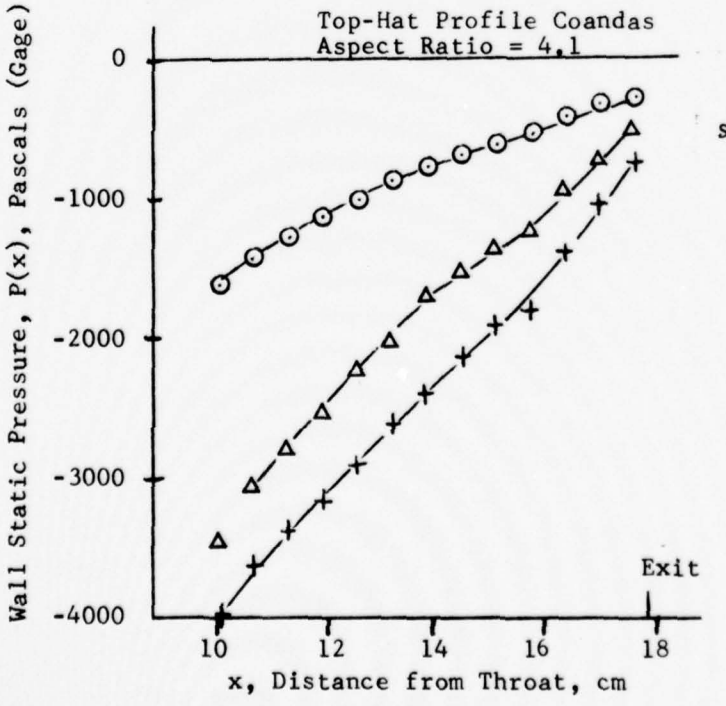

Symbol	Pressure Ratio	Flap Angle Radians	$[xdP/dx]_{exit}$ Pascals
○	1.5	.175	2440
△	2.0	.175	6500
+	2.5	.140	9750

Figure 22. Augmentation Ratio vs Diffuser Angle, Top-Hat Profile

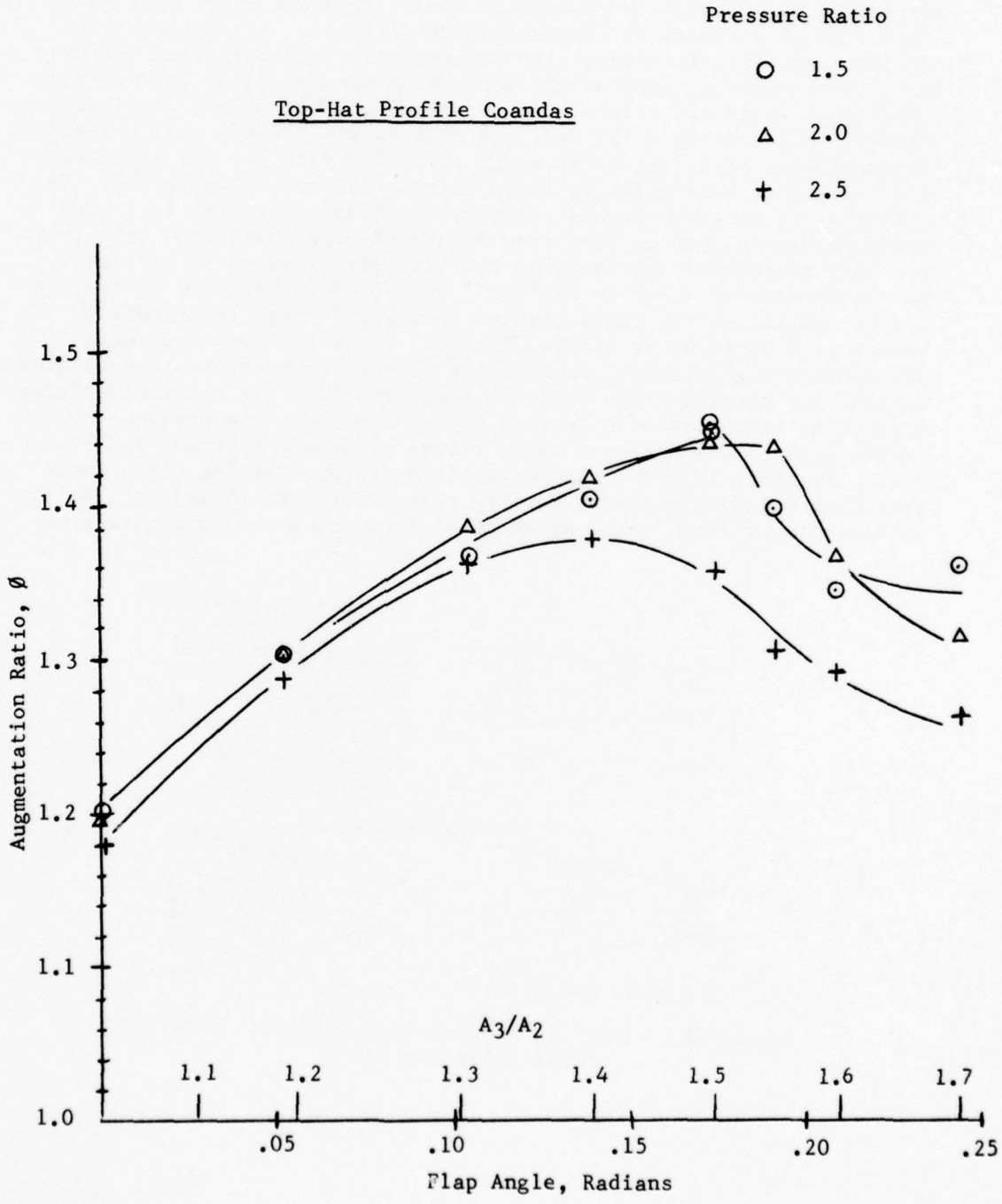

4.0 ANALYSIS

In a number of respects the separation phenomena observed in TAW-type augmenter diffusers more closely resembles subsonic wing separation than that of a classical straight-sided diffuser. A straight-sided diffuser normally is rather slow in developing separation as diffuser angle is increased, and, as the separation does develop, the diffuser efficiency falls off slowly. As an example, intermittent stall will normally occur by δ_D = .13 rad. and will slowly develop into a steady separation as δ_D is raised to about .17 rad. Finally, the separation will spread to both diffuser sides at $\delta_D \approx .21$ rad. (Figure 23). The diffusers of interest herein, however, develop separation in a very rapid fashion as can be seen from Figure 12, and associated with this are very pronounced decreases in diffuser efficiencies as reflected in the $\emptyset$ behavior shown in Figures 7 and 8. This behavior is qualitatively similar to the rapid changes in the lift-drag relationships common with airfoils at stall. Further, these diffusers are able to accommodate significantly higher δ_D's without separation--even without endwall BLC blowing--than would be predicted from the classic diffuser separation criterion of Reference (8). Undoubtedly the presence of the Coanda jets on the diffuser walls serves by itself a strong BLC function. Further, in the region near the diffuser trailing edge, these jets have relatively slowly varying peak velocities (U_{MAX}) so that the boundary layer flow "sees" an external flow and a pressure gradient

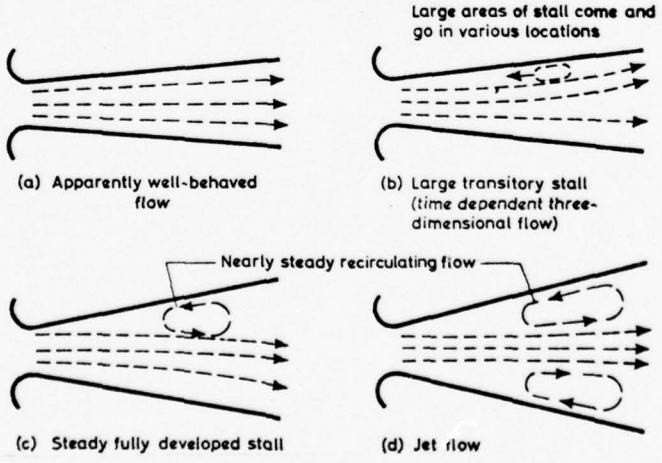

Figure 23. Schematic of Classical Diffuser Separation (from Reference 7)

qualitatively similar to that of an airfoil (Figure 24); i.e., both the TAW diffuser and the wing boundary layers are thin and embedded within strong outer flows. Thus, it appeared logical to attempt to use an airfoil separation criterion.

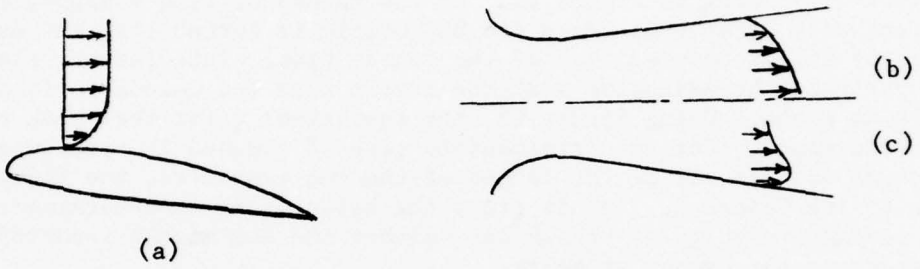

Figure 24. Similarity Between Wing and TAW Diffuser Boundary Layers: (a) Over a Wing (thin B.L.), (b) Classic Diffuser (thick B.L.), and (c) TAW Diffuser (thin B.L.)

One of the more successful and the one considered herein is that of Stratford (Reference 9) where the criteria is expressed as a non-dimensional number N_{ST}, viz,

$$N_{ST} = \frac{C_p \ (x dC_p/dx)^{1/2}}{(R_N \times 10^{-6})^{1/10}} \tag{1}$$

where C_p is the pressure coefficient, defined by

$$C_p = \frac{P(x) - P(0)}{q(0)} \tag{2}$$

C_p is based upon the difference between local wall static pressure $P(x)$ and that pressure occurring at the start of the interaction region, $P(0)$, at $x = 0$. $q(0)$ is the dynamic pressure $1/2\rho U_{max}^2$, where U_{max} is the maximum velocity at $x = 0$. R_N is the Reynolds number based upon U_{max} and x. Stratford's method involves an approximate solution of the equations of motion, and matching the solutions at the junction of the "inner" and "outer" boundary layer. A subsonic airfoil will not separate if $N_{ST} \leq .37$.

Although Stratford used $P(0)$ as the wall pressure at $x = 0$, there are experimental difficulties in determining its value (see discussion in Section 3.1.3). Furthermore, because of the highly curved flow near the Coanda, the value of $P(0)$ at the wall is also difficult to predict analytically. For these reasons, $P(0)$ was chosen for the ejector diffuser to be the value of the static pressure in the uniform secondary stream (see Figure 19).

q(0) is merely a normalizing factor for the various pressure terms. In addition, q(0) cannot be taken simply as $1/2\rho_{\infty}U_{max}^2$, where ρ_{∞} is the density of air at some standard temperature and pressure. In the high Mach-number flows in an ejector, it seems correct to define q as $P_T - P_{\infty}$ and use the isentropic flow equations. Near the throat, the maximum value of q is $Q(0) = P_T - P_{\infty}$, where P_T is the total pressure set on the BLC nozzle just outside the Coanda radius. The resulting isentropic velocity for a given q is shown in Figure 25. At low values of U, $q \cong 1/2\rho U^2$, consistent with Stratford. When the BLC nozzle is turned off, the maximum q at the throat becomes that of the Coanda flow. This latter value of q was estimated by measuring U at the throat near the Coanda surface with a hot-film probe. Using Figure 25, the equivalent q for that peak velocity was determined. For the intermediate case of reduced BLC pressure, the value of q(0) is set by the larger of the two pressures, the BLC pressure or the Coanda q. In all cases the value of R_N is determined by the maximum velocity at the throat--either the BLC nozzle isentropic velocity or the Coanda velocity.

Table I presents a summary of the Stratford Number calculations for the augmenters constructed under the present study. There are three BLC conditions--full, minimum, and no BLC, for aspect ratios of 4.1 and 2.5, using the reference Coandas. Also included are the top-hat and vortex profile Coanda results. The table gives the nominal pressure ratio and the flap angle where the measurements and calculations were made. This flap angle is the maximum angle for attached flow and is also the angle giving maximum Ø. The values of P(x) are the exit static pressures recorded in Figures 16, 17, 18 and 21. P(0) is the throat secondary static pressure. Q(0) is the highest value of q at the throat in the vicinity of the corner; i.e., the BLC nozzle pressure or the Coanda q. The term xdP/dx has also been previously given in Figures 16, 17, 18 and 21. The values of the calculated N_{ST} are indicated and the overall mean is $N_{ST} = .0196$ with a standard deviation of .0022, which is 11% of the mean.

The scatter in the magnitude is not uncommon in separation studies. As an example, Figure 26 shows the scatter reported in Stratford's own work; it is approximately of the same magnitude as that in the present study.

Returning to Table I, the results of the reduced BLC are particularly interesting. The effect of proceeding from Case 1, with full BLC, to Case 2, with minimum BLC, and finally Case 3, with no BLC, is to reduce gage pressure P(0), in proportion to Q(0). (Actually more in proportion to $[Q(0)]^{3/2}$.) The same trend is noted in Cases 4, 5 and 6. It is this effect that tends to maintain the constant upper limit on N_{ST}. All other quantities, such as P(x) or xdP/dx, are not changing as markedly or with the same trend.

$$U = \left(2RT \frac{\gamma}{\gamma-1} \left(1 - P_R^{-\frac{\gamma-1}{\gamma}}\right)\right)^{1/2} \text{ meters/sec}$$

$$R = 287 \frac{\text{Joules}}{^\circ\text{K kg}}$$

$$\gamma = 1.4$$

$$T = 289^\circ\text{K}$$

$$P_R = \frac{q + P_\infty}{P_\infty}$$

P_∞ = 99 Kilopascals

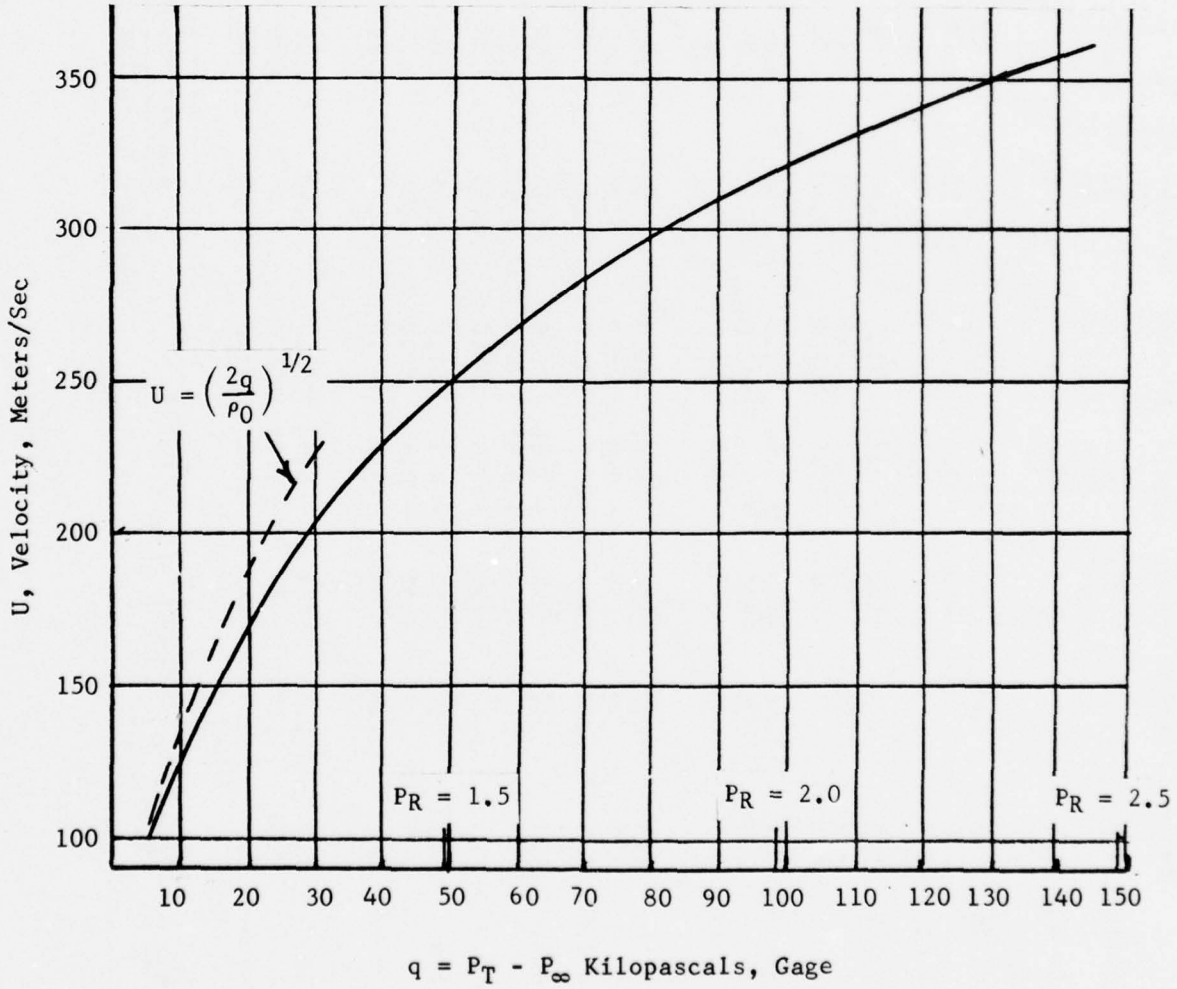

Figure 25. Velocity Versus q

Table I. Summary of Stratford Number Calculations

Case	Nom. Pressure Ratio	Flap Angle, Radians	P(x) Pascals (Gage)	P(0) Kilo-pascals (Gage)	Q(0) Kilo-pascals	$[xdP/dx]_{exit}$ Kilopascals	$R_N \times 10^{-6}$	N_{ST}*	Remarks
Reference Profile	1.5	.33	-200	- 6.0	51.0	2.32	2.99	.0217	Q(0) set by BLC
1. R/t = 26.5	2.0	.33	-400	-11.5	102.0	4.60	3.81	.0202	nozzle pressure
Full BLC, AR = 4.1	2.5	.33	-650	-15.0	147.0	6.95	4.25	.0184	which is identical to all other nozzles.
Reference Profile	1.5	.33	-200	- 5.0	47.4	2.32	2.92	.0201	Q(0) set by BLC
2. R/t = 26.5	2.0	.33	-450	- 9.7	91.5	4.65	3.68	.0200	nozzle pressure.
Min. BLC, AR = 4.1	2.5	.33	-600	-14.0	136.0	6.50	4.17	.0187	
Reference Profile	1.5	.21	-150	- 4.2	35.2	1.86	2.58	.0241	Q(0) set by Coanda
3. R/t = 26.5	2.0	.21	-375	- 8.1	70.5	3.95	3.28	.0230	flow at throat.
No BLC, AR = 4.1	2.5	.21	-550	-11.5	101.0	5.60	3.56	.0225	
Reference Profile	1.5	.30	-150	- 5.1	51.0	2.89	2.99	.0207	Q(0) set by BLC noz-
4. R/t = 26.5	2.0	.30	-300	- 9.4	102.0	5.12	3.81	.0175	zle pressure which
Full BLC, AR = 2.5	2.5	.30	-375	-13.2	147.0	6.85	4.25	.0163	is identical to all other nozzles.
Reference Profile	1.5	.30	-125	- 4.85	48.0	3.02	2.92	.0222	Q(0) set by BLC
5. R/t = 26.5	2.0	.30	-250	- 9.0	88.0	5.33	3.63	.0215	nozzle pressure.
Min. BLC, AR = 2.5	2.5	.30	-375	-12.7	135.0	7.0	4.17	.0180	
Reference Profile	1.5	.175	-125	- 3.66	38.0	2.19	2.65	.0203	Q(0) set by Coanda
6. R/t = 26.5	2.0	.175	-200	- 6.92	76.0	4.4	3.22	.0189	flow at throat.
No BLC, AR = 2.5	2.5	.175	-250	- 9.2	109.0	6.05	3.56	.0170	
Top Hat Profile	1.5	.175	-250	- 4.73	51.0	2.44	2.99	.0172	Q(0) set by BLC noz-
7. R/t = 9.3	2.0	.175	-450	- 8.7	98.0	6.5	3.77	.0190	zle pressure which
Full BLC, AR = 4.1	2.5	.14	-700	-12.3	145.0	9.75	4.24	.0180	is identical to all other nozzles.
Vortex Profile	1.5	.175	-225	- 4.93	51.0	3.48	2.99	.0216	Q(0) set by BLC noz-
8. R/t = 9.3	2.06	.175	-520	- 9.25	108.0	7.0	3.90	.0180	zle pressure which
Full BLC, AR = 4.1	2.5	.14	-575	-11.2	145.0	8.85	4.24	.0157	is identical to all other nozzles.

$$*N_{ST} = \frac{P(x) - P(0)}{Q(0)} \left[\frac{xdP/dx}{Q(0)}\right]^{1/2} \left(R_N \times 10^{-6}\right)^{-.1}$$

Average N_{ST} = .0196

Standard Deviation = .0022 (11%)

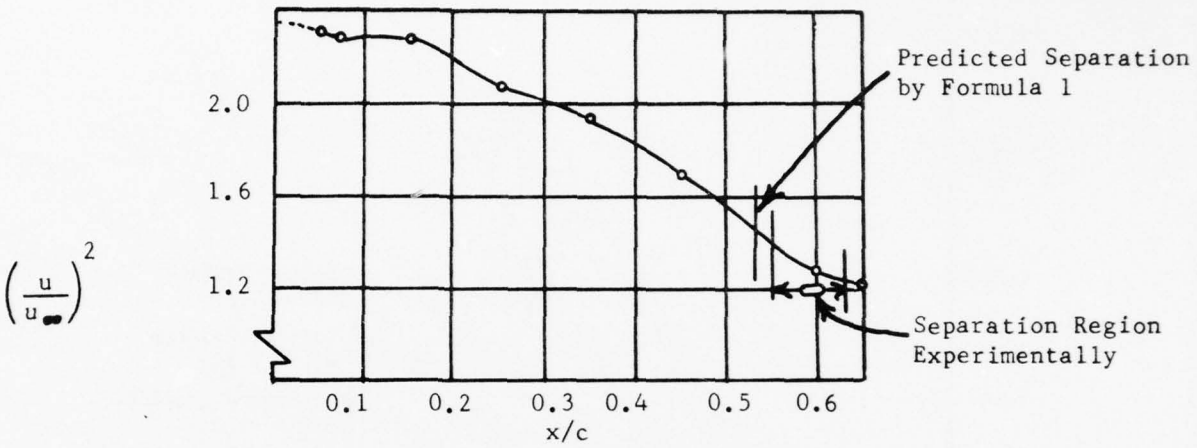

Figure 26. Separation Point Over a Wing (from Reference 9)

It is instructive to consider the difference in the three augmenters and to try to visualize what mechanism is setting $N_{ST} \approx .02$ as a common upper limit. Figure 27 shows a plot of the term $P_\infty - P(0) \approx P(x) - P(0)$ and the term xdP/dx versus diffuser angle for the three augmenters. The conditions are full BLC and PR $\approx$ 2.0. Notice that the vortex and top-hat profiles produce larger values of xdP/dx than does the reference profile. This, as mentioned earlier, is related to the larger nozzle gap and decreased A_2/A_0. The throat static gage pressure, or its negative, $P_\infty - P(0)$, is also greater for the vortex and top-hat at small diffuser angles. This is due to the reduced overall A_2/A_0. Finally near .175 to .2 radian, the reference profile produces the largest values of xdP/dx and $P_\infty - P(0)$. The reference profile also produces the greatest $\emptyset$.

A lesson to be learned from Figure 27 is that a high $\emptyset$ augmenter should produce a large drop in throat static pressure (as is well known) but simultaneously must not produce a large value of xdP/dx at the exit. This implies that small primary nozzles should be used to achieve well-mixed flows and nearly ambient static pressures at the exit. In other words, the exit static pressure should be nearly recovered to ambient. These facts are entirely consistent with the experience of many workers in the area of thrust augmentation.

Figure 28 shows the calculated values of N_{ST} for these augmenters under the same operating conditions; i.e., full BLC and PR = 2.0. The Stratford number rises to a maximum as flap angle is increased and does provide a useful separation criteria.

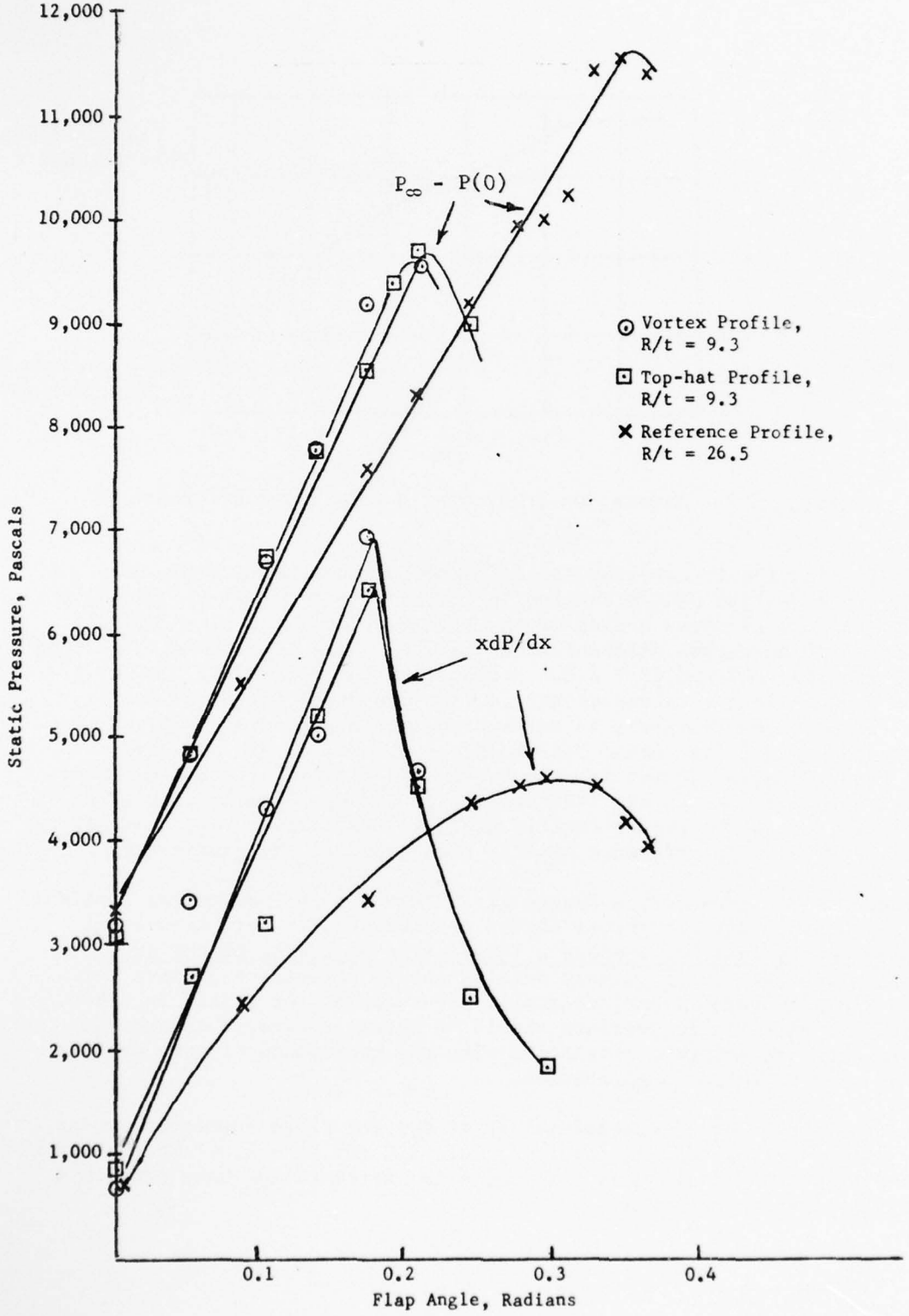

Figure 27. Variation of Static Pressure Components with Flap Angle

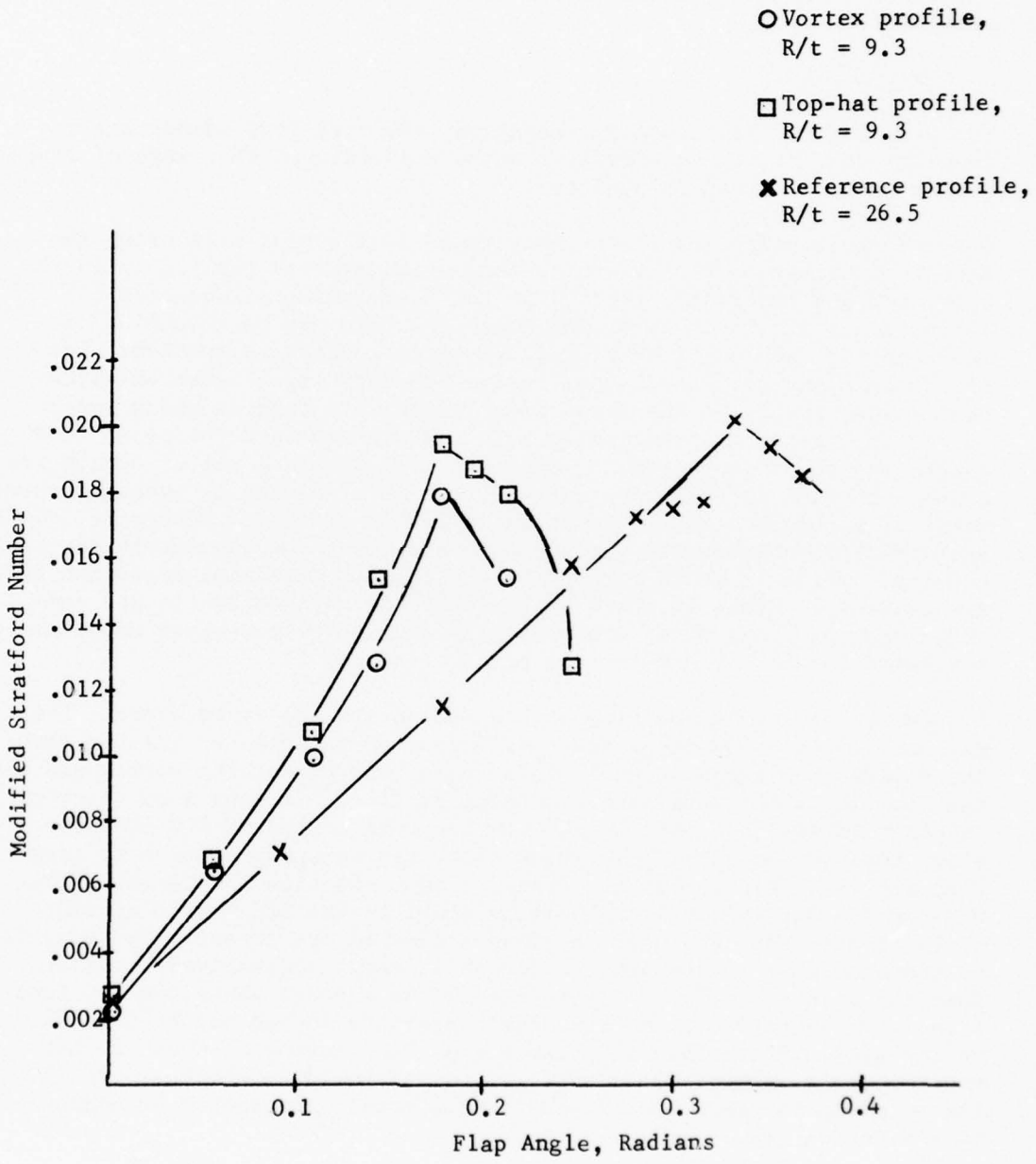

Figure 28. Variation of Stratford Number with Flap Angle

These plots indicate that we have not mistakenly selected a criteria this is insensitive to flap angle. The flow will be stable and attached provided

$$N_{ST} \leq .0196.$$

For flap angles that produce separation, the Stratford number has no meaning; that is, the criteria is to be used only in the range of flap angles where $d N_{ST}/d\delta$ is positive.

One difficulty which has been experienced in the past with using the Stratford criterion lies in the x term which appears explicitly in the numerator and implicitly (in R_N) in the denominator of Equation (1) (Reference 11). Physically, the numerator term may be thought of as representing the length of flow in an adverse pressure gradient, but the denominator is proportional to the boundary layer momentum thickness which depends on the local flow length in a fashion which can be quite complicated mathematically. In the present work the total flow length and the throat-trailing edge (adverse pressure ratio) length are almost the same so that apparently little harm is done by equating them. However, augmenters can be built wherein they are quite desparate. Under such conditions Reference (11) demonstrates that the two should not be equated. While it would perhaps be possible to determine experimentally the correct lengths, it would be somewhat more attractive to use computational programs which are presently available to compute momentum thickness for direct use in separation criteria.

A comment concerning the size of the BLC nozzle gap is in order. The gap was .152 cm (.06 inch) and therefore comparable-to or greater-than the Coanda nozzle gaps used in this study (.152 cm for the vortex and top-hat profile, .084 cm for the reference profile). It has been observed in other Rockwell studies by this author that increased BLC pressure, above that of the other primary nozzles, can delay separation to larger flap angles. This is another apparent justification for claiming that Q(0) in the N_{ST} expression should be equal to the BLC nozzle pressure if it is greater than the q of the Coanda flow at the throat. However, it is expected that if the BLC nozzle gap is made progressively smaller than the Coanda nozzle gap, a point will be reached where the BLC function is inadequate and the BLC nozzle pressure should not be used to define Q(0). Where this BLC nozzle gap size becomes critical is not known by this author. Generally, BLC area should be about 0.5 to 2% of the total A_0 for each corner and the BLC nozzle gap should be comparable to the Coanda gap.

5.0 CONCLUSIONS

1. Corner separation of the test thrust augmenting wing-type augmenter initiates at or near the augmenter diffuser exit and then rapidly progresses upstream until the whole corner from the vicinity of the augmenter throat to the exit is involved.

2. A modified form of the Stratford airfoil stall criterion successfully correlates the onset of augmenter separation in the test augmenter where the independent test variables were nozzle pressure ratio, augmenter aspect ratio, boundary layer control blower pressure ratio, and Coanda configuration. The modification consists of a change in reference pressure, P(0), and in definition of q.

3. Circular Coandas with small R/t cause earlier separation.

6.0 RECOMMENDATION

The applicability of the separation criterion detailed in this report to configurations other than the ones tested should be developed by experimentally varying augmenter parameters such as:

Diffuser/Endwall Junction Angle (Planform Sweep and Taper)

Diffuser Angle Rate of Change (Dynamic Conditions Simulating Aircraft Flight)

More Severe Reduction in A_2/A_0. This would provide a more compact ejector with increased throat secondary velocity.

It is also recommended that computer programs be used to analyze corner flow in augmenters.

7.0 REFERENCES

1. Greathouse, W. K., "Preliminary Investigation of Pumping and Thrust Characteristics of Full-size Cooling Air Ejectors at Several Exhaust-Gas Temperatures," NACA RM E54A18, 1954.

2. Throndson, L. W., "Compound Ejector Thrust Augmentation Development," ASME 73-GT-67, 1973.

3. Gauger, M., Dissertation, Technische Hochschule, Breslau, 1934.

4. "Three-Dimensional Effects on Augmenters," Rockwell International Report NR76H-36, 1976.

5. Stewart, V. R., "A Study of Scale Effects on Thrust Augmenting Ejectors," Rockwell International Report NR76H-2, 1976.

6. "Hot Wire, Hot Film Ion Anemometer Systems," Thermo-Systems, Inc., 6560375, 1975.

7. Kline, J. J., "On the Nature of Stall," J. Basic Engrg., Trans. ASME, Series D, Sept. 1959.

8. Reid, E. G., "Performance Characteristics of Plane-Wall Two-Dimensional Diffusers," NACA TN 2888, 1953.

9. Stratford, D. S., "The Predictions of Separation of the Turbulent Boundary Layer," J. Fluid Mechanics, p. 1, January 1959.

10. "Independent Research & Development Program," Vol. III, Rockwell International, Columbus Aircraft Division, 1 December 1976.

11. Gerhart, P. M. and Bober, L. J., "Comparison of Several Methods for Predicting Separation in a Compressible Turbulent Boundary Layer", NASA TM-X-3102, 1974.

8.0 ACKNOWLEDGEMENT

The author wishes to acknowledge the contribution of Dr. William Foley who supervised the separation-mode tests involving the hot-film surface sensors. He also conducted the hot-film probe surveys shown in Figure A-7. Walter Brown was the technician who performed all of the measurements.

APPENDIX A

RAW VELOCITY DATA

The following pages present hot-film survey data taken in the corner of the augmenter that was instrumented with the 13 static taps. The surveys proceed from the wall toward the augmenter centerline. The spanwise location was 1 cm from the endwall.

Figure A-1 gives the hot-film velocity surveys at the augmenter throat for the "no BLC" cases of Table I. The peak Coanda velocity, U_{max}, was used to set the value of Q(0). The velocities are near the upper limit to the usable range of the hot-film and are probably subject to larger error. This is an inherent weakness in any separation criteria which demands measurement of velocities approaching Mach number 1.

Figure A-2 is a photograph of the probes used in this experimental study. One was a Model 1264 miniature, conical, hot-film supplied by Thermo-Systems, Inc. The output of the probe is supplied to a Thermo-Systems Model 1050-2C constant temperature anemometer. For a limited number of surveys, a dual-channel probe, also shown, was used.

Figures A-3 through A-6 give the calibration of the probes for the velocity data of Figure A-7. By noting the voltage in Figure A-7 and referring to the appropriate calibration curve, the reader may obtain the corresponding velocity. Subsequent velocity data, shown in Figure A-8, was recorded in such a manner as to facilitate the reading of velocity. The velocity is shown directly on the figure, and although it is non-linear (as all hot-film probes are), the reader need not refer to a separate page for the calibration.

The velocity profiles in Figures A-7 and A-8 correspond to the eight cases of Table I. The profiles were taken at the exit, and in increments of 1.27 cm (1/2") upstream from the exit to a distance of 7.62 cm (3"). This data was initially hoped to be of use in formulating a separation criteria based upon the exit conditions, but no successful criteria was found which could use this data. The information is therefore supplied in the hope that it will be of value to other workers.

(a) Velocity Measurements for Flap Angle = .175 Radian, AR = 2.5

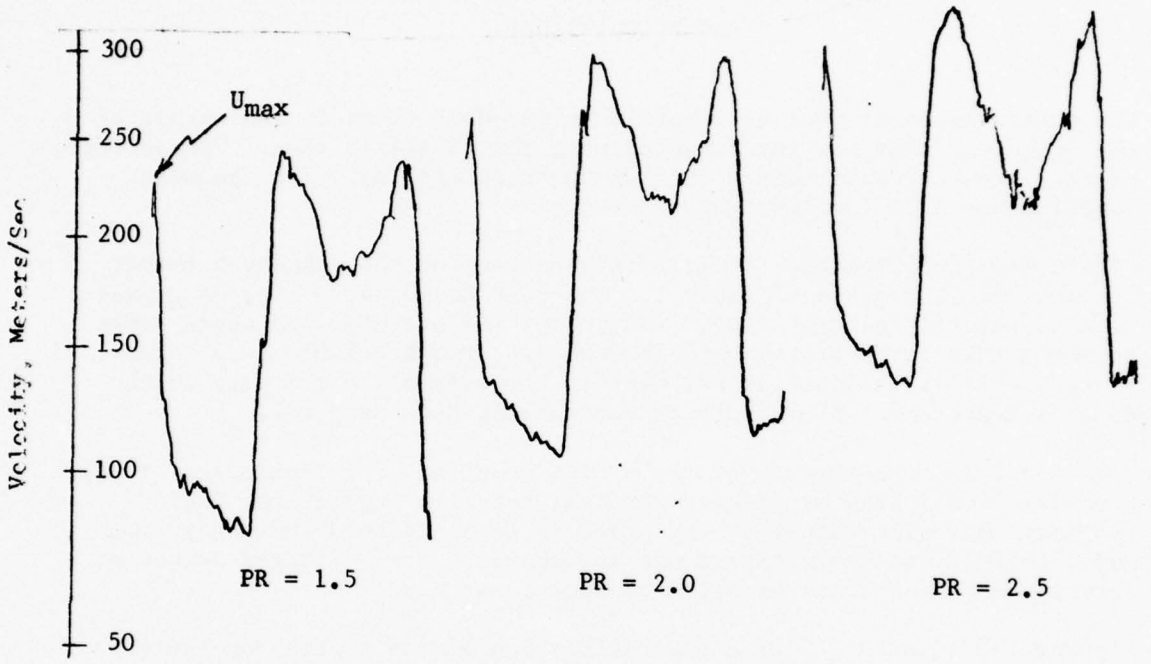

(b) Velocity Measurements for Flap Angle = .21 Radian, AR = 4.1

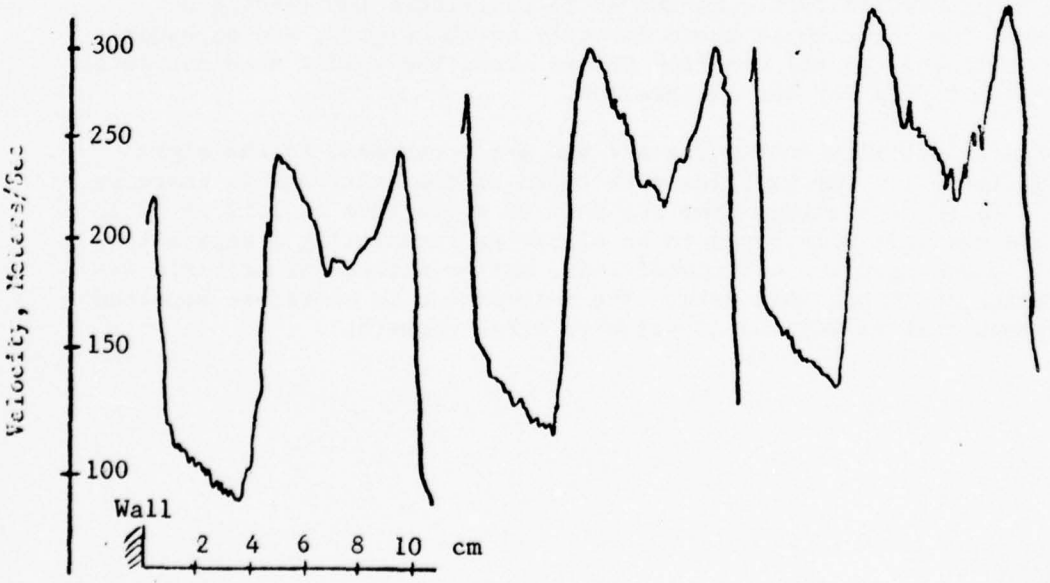

Figure A-1 . Hot Film Velocity Measurements with BLC Off. (1 cm from endwall at throat)

Figure A-2. Conical Hot Film Probe (Upper) and Dual Sensor Probe (Lower)

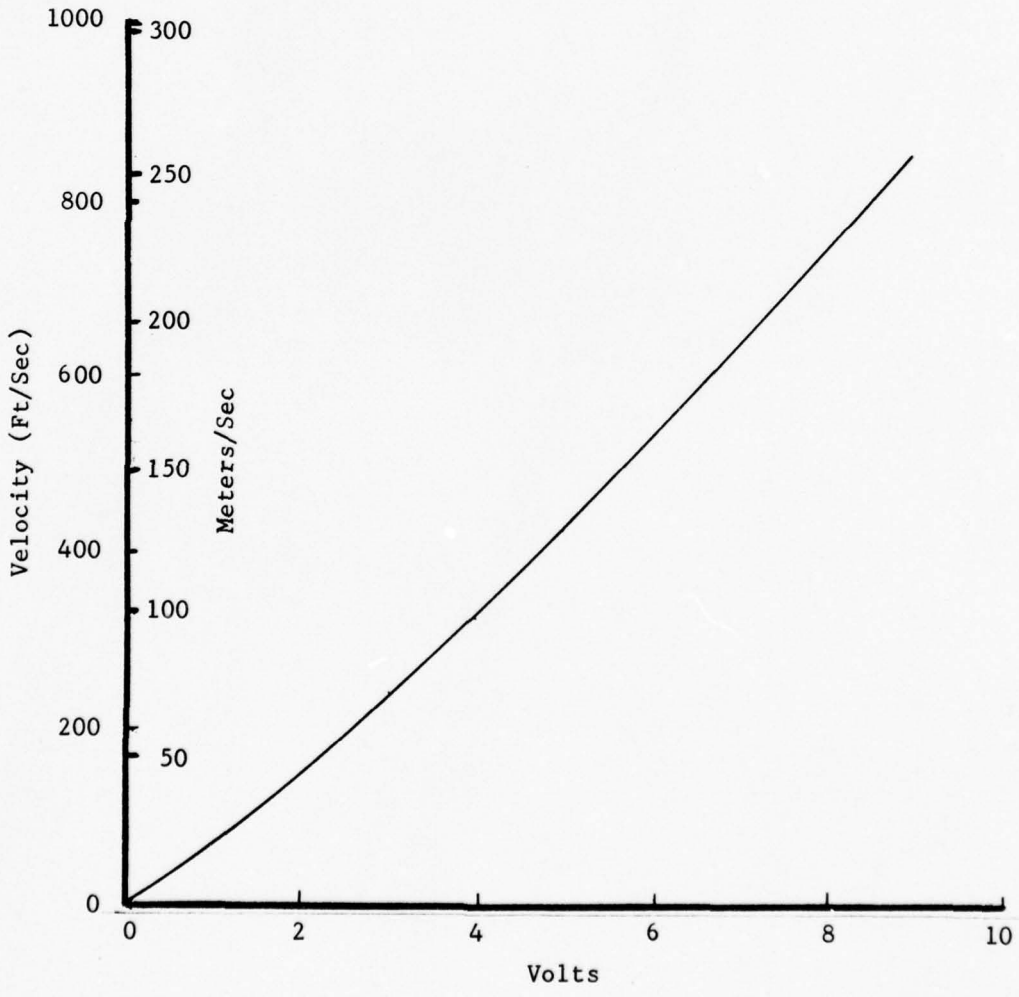

Figure A-3. Hot Film Calibration Curve "A"

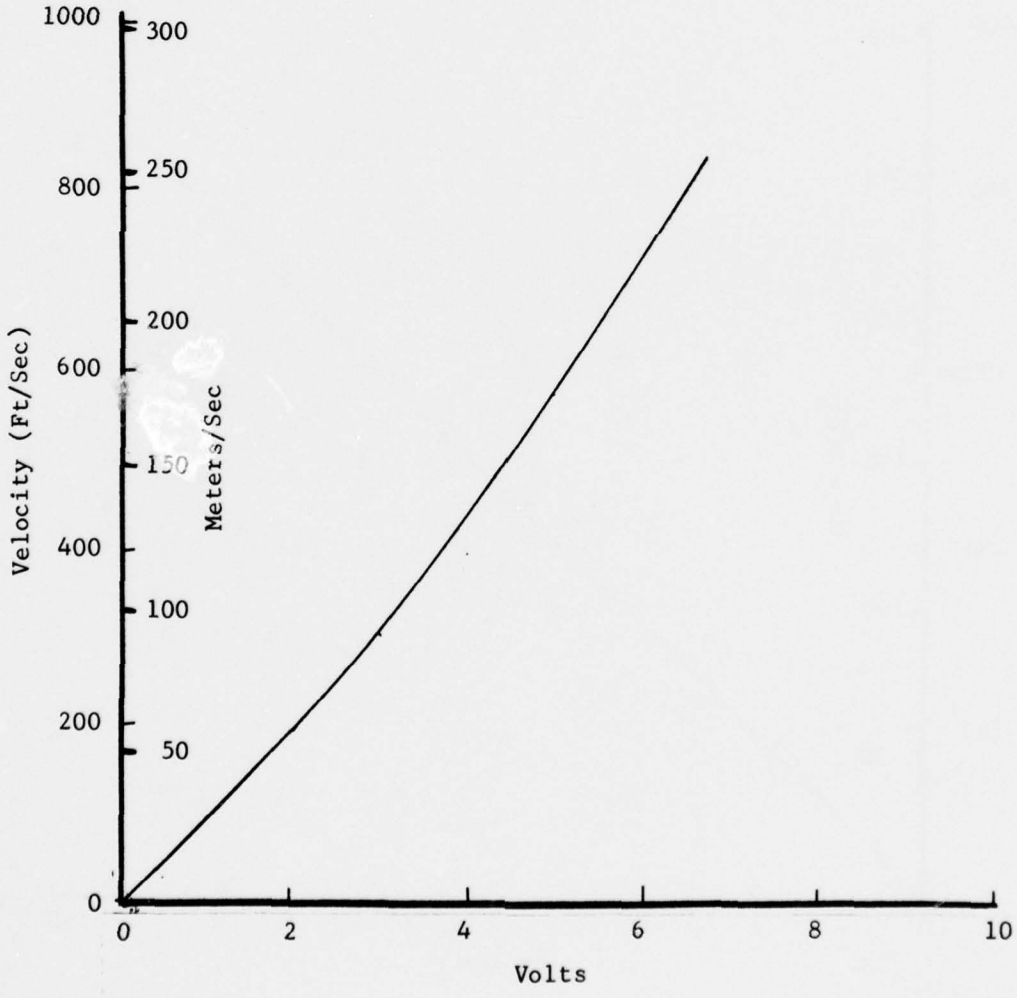

Figure A-4. Hot Film Calibration Curve "B"

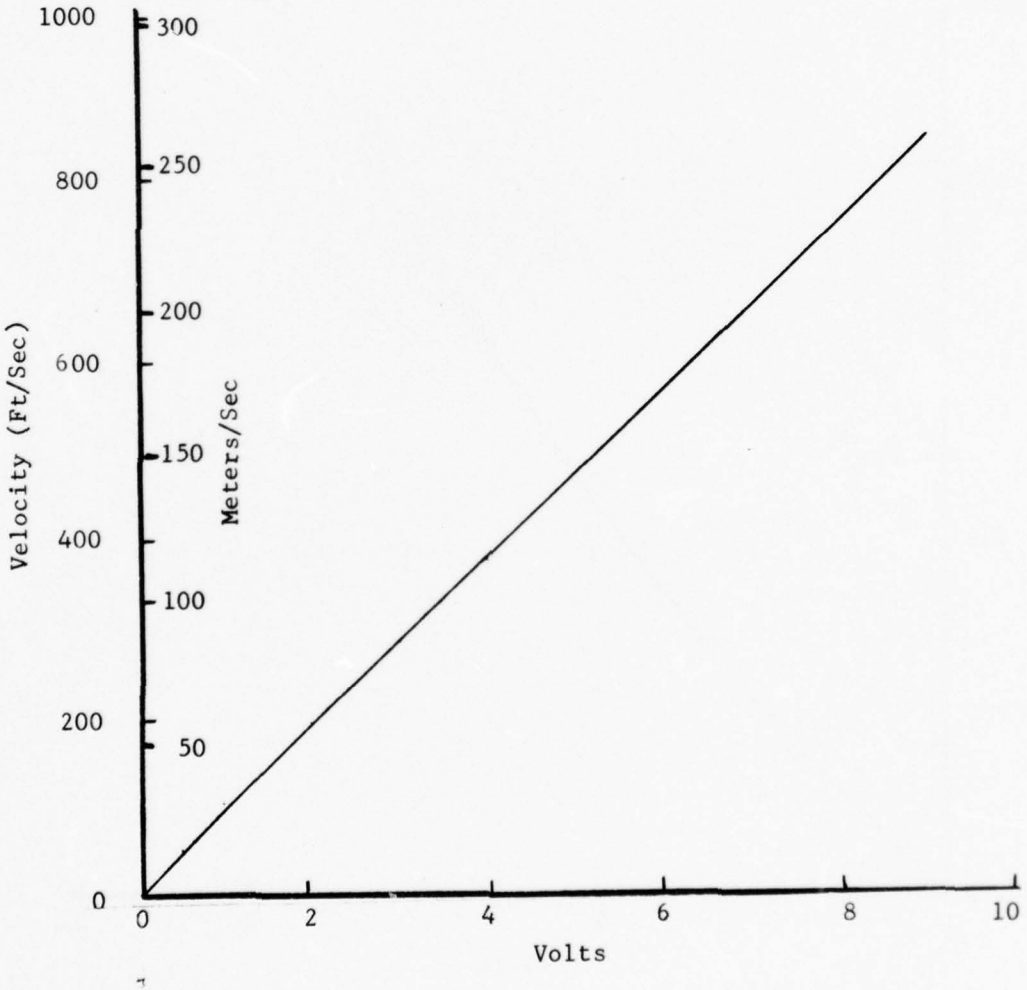

Figure A-5. Hot Film Calibration Curve "C"

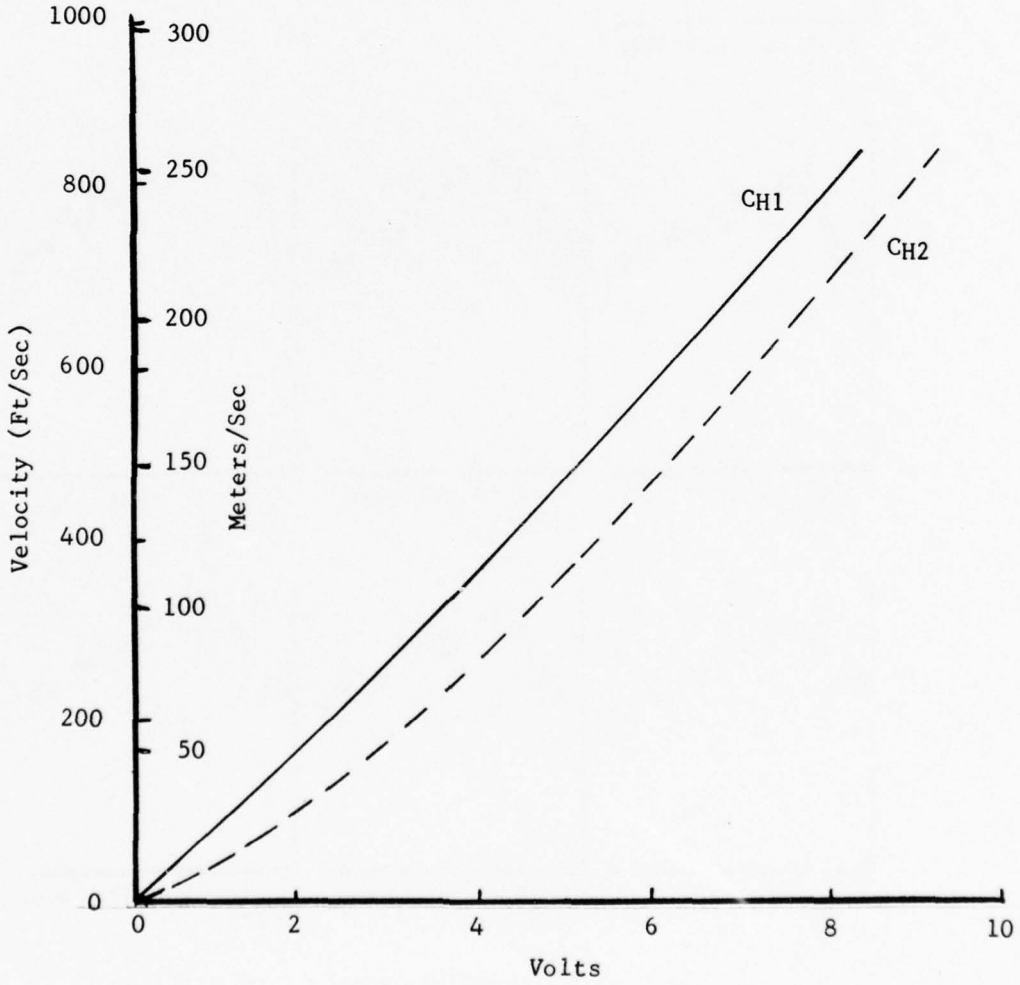

Figure A-6. Hot Film Calibration Curve "D"

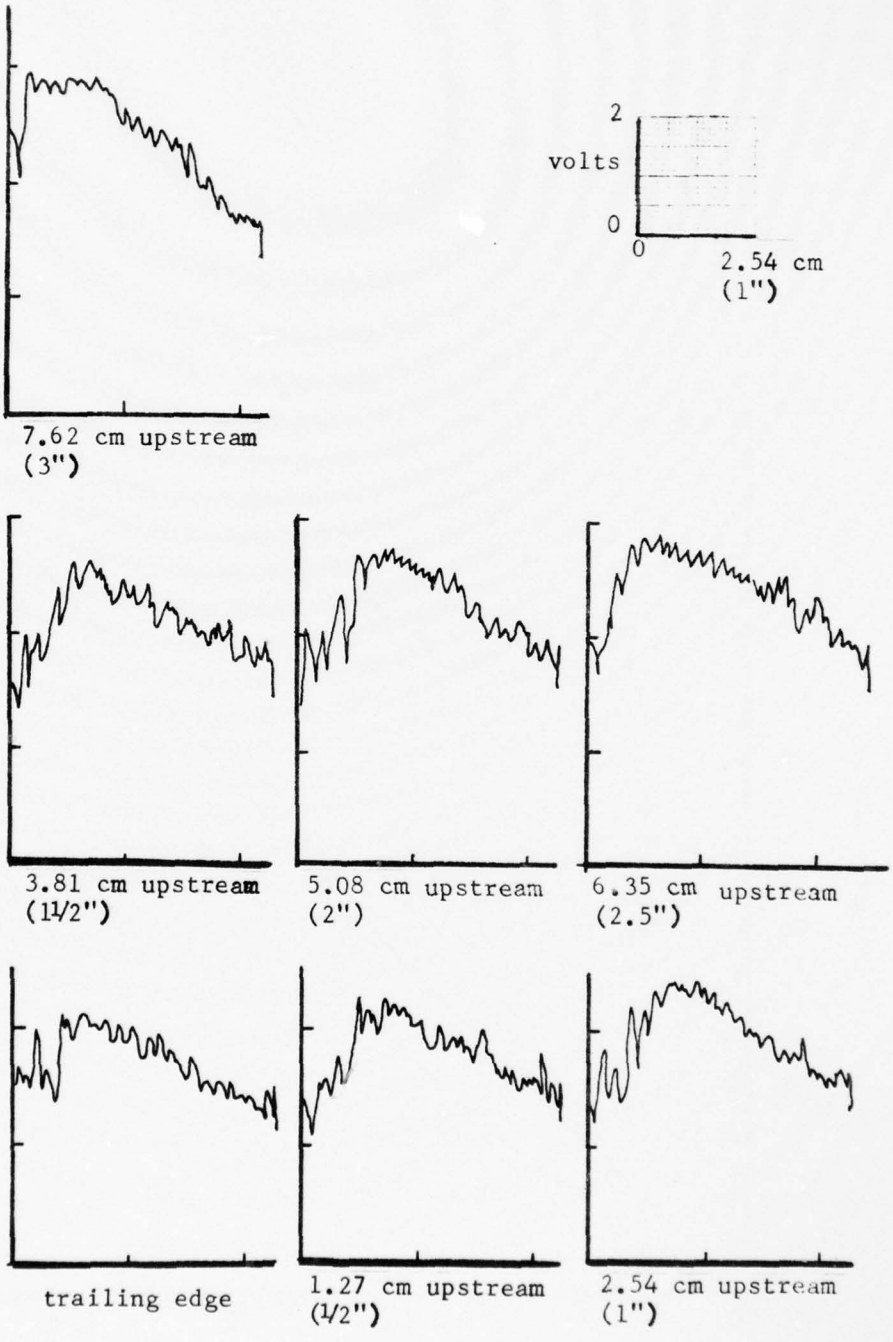

Case 1, Calibration Curve C, PR = 1.5

Figure A-7. Velocity Data

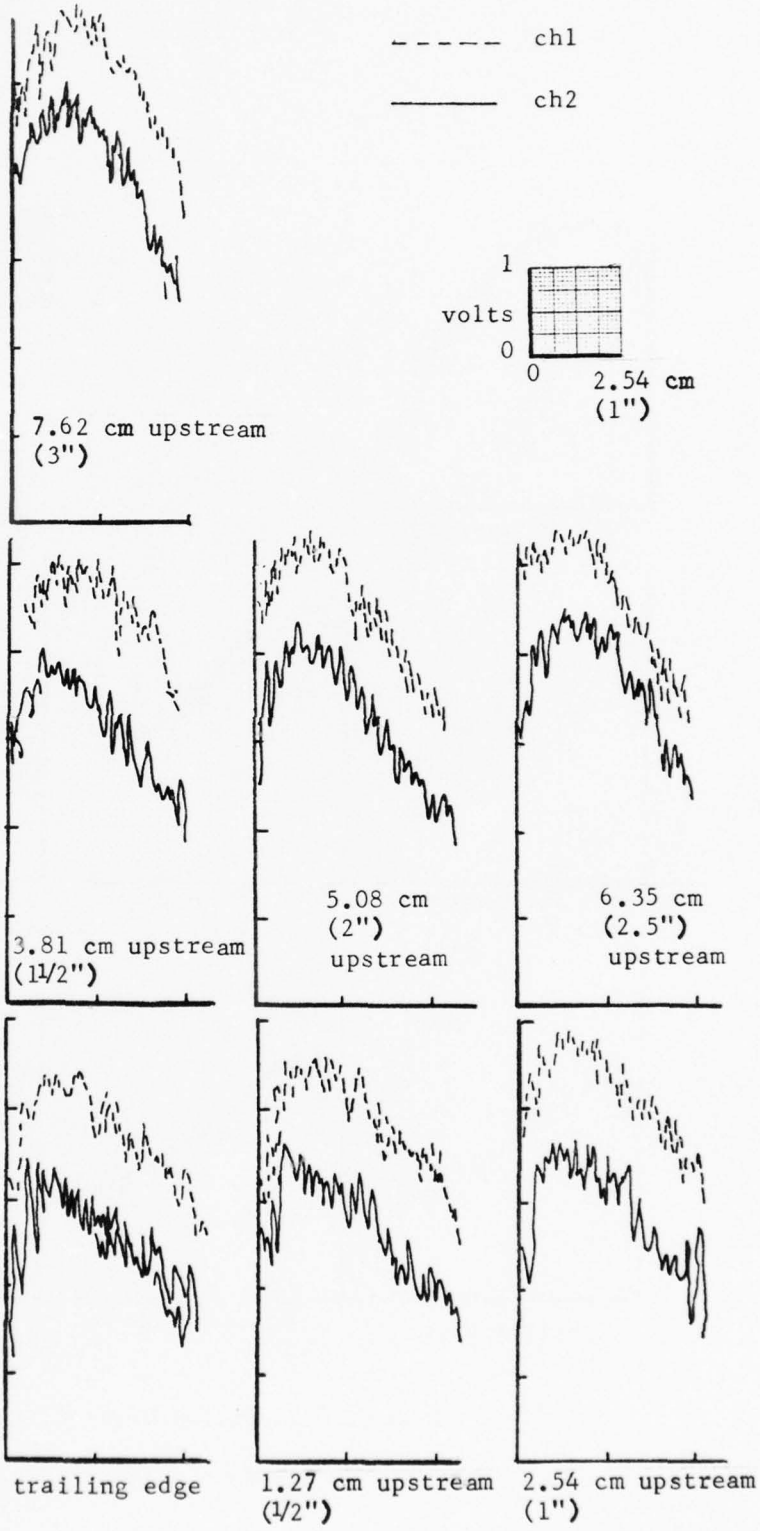

Case 1, Calibration Curve D, PR = 2.0

FORM 351-F REV 4-73

Figure A-7 (cont'd)

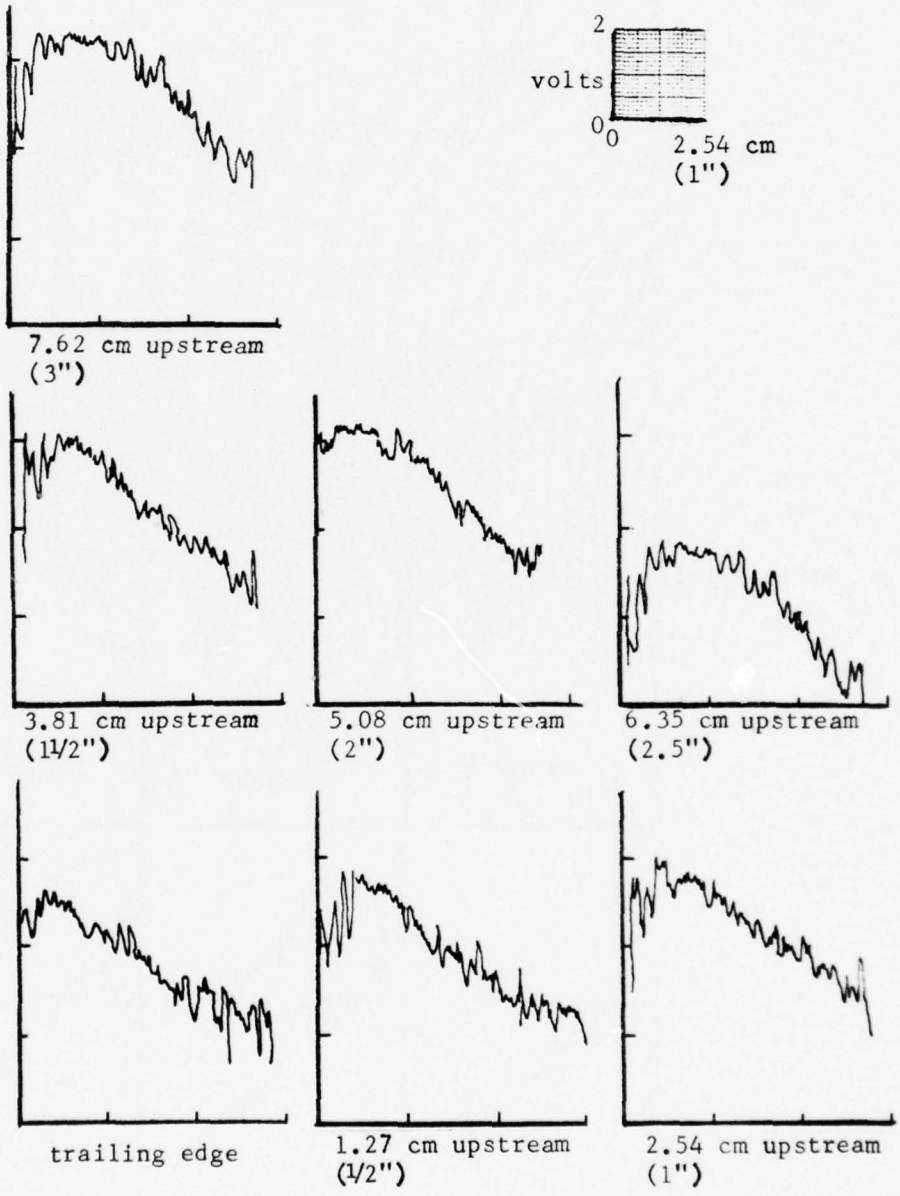

Case 1, Calibration Curve C, PR = 2.5

Figure A-7 (cont'd)

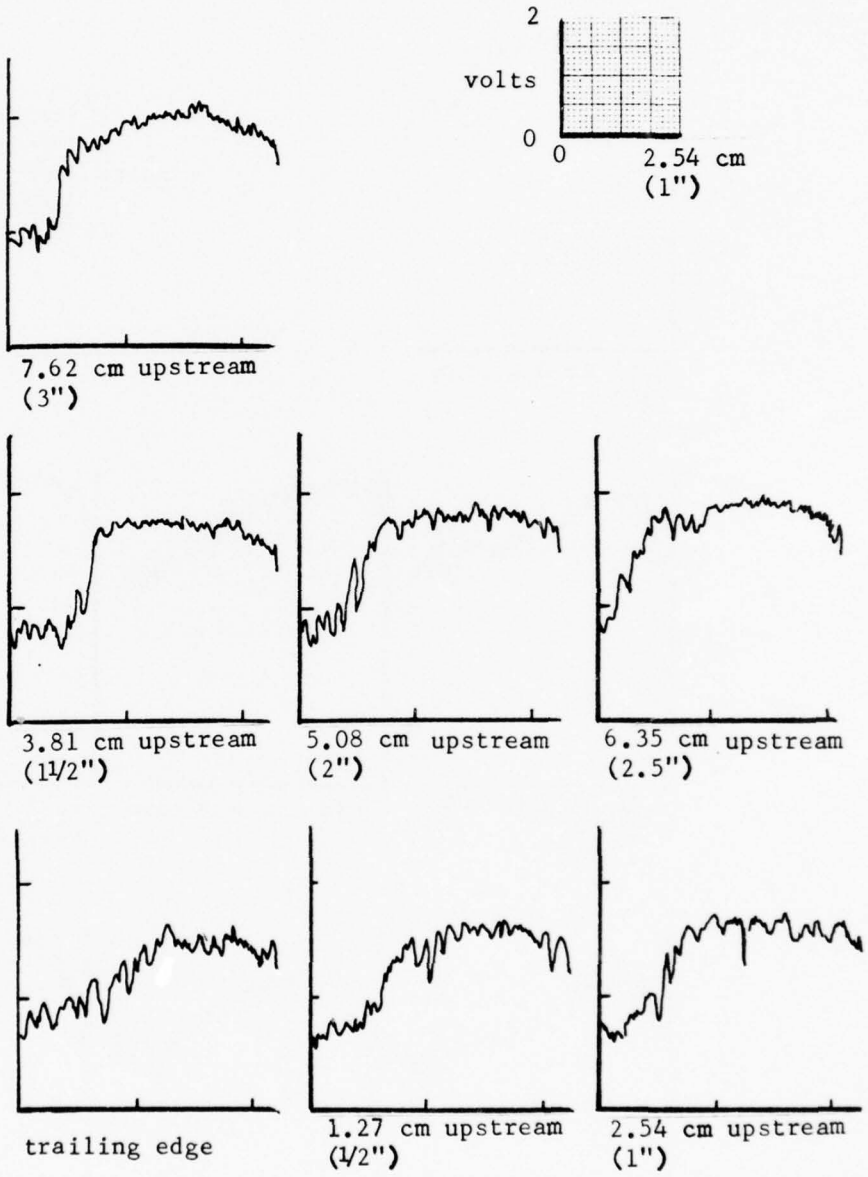

Case 2, Calibration Curve C, PR = 1.5

Figure A-7 (cont'd)

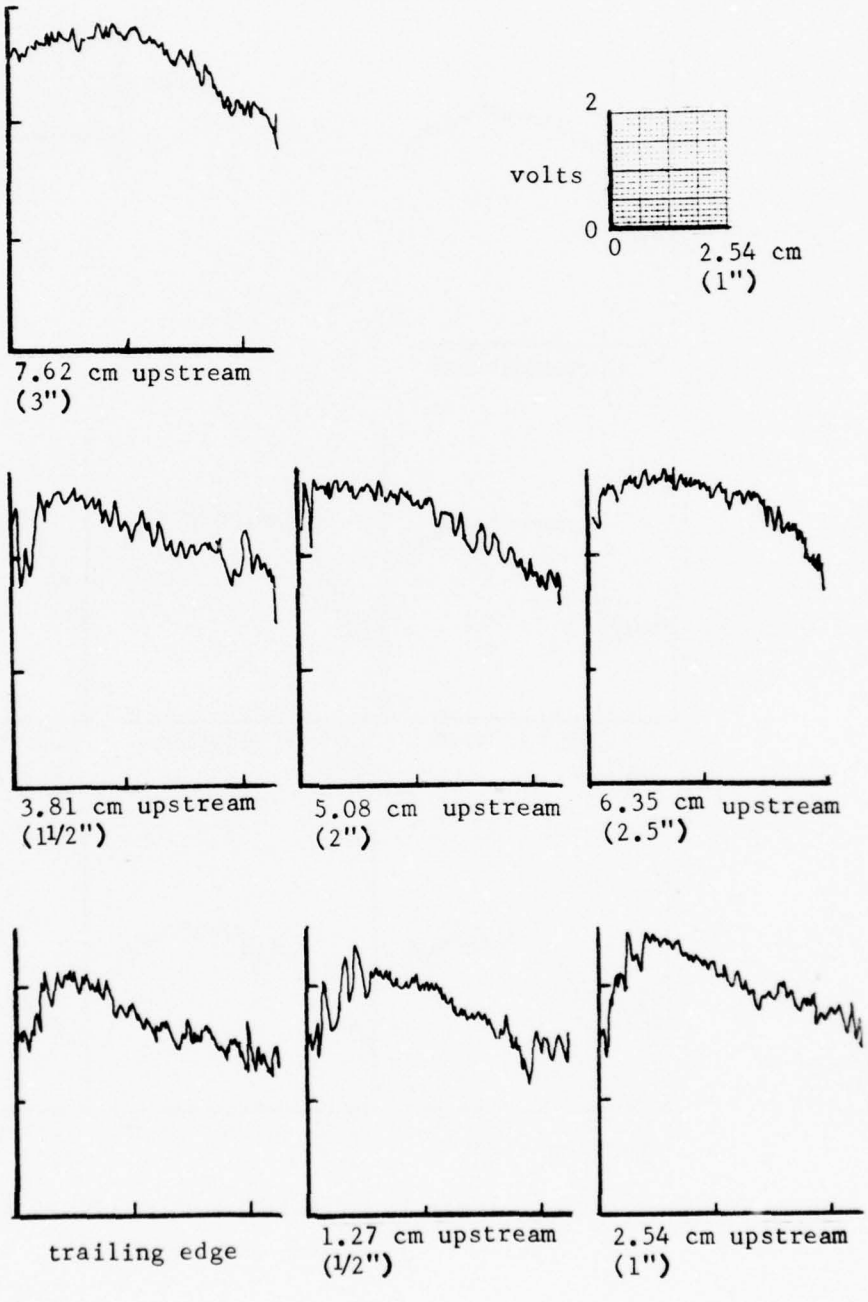

Case 2, Calibration Curve C, PR = 2.0

Figure A-7 (cont'd)

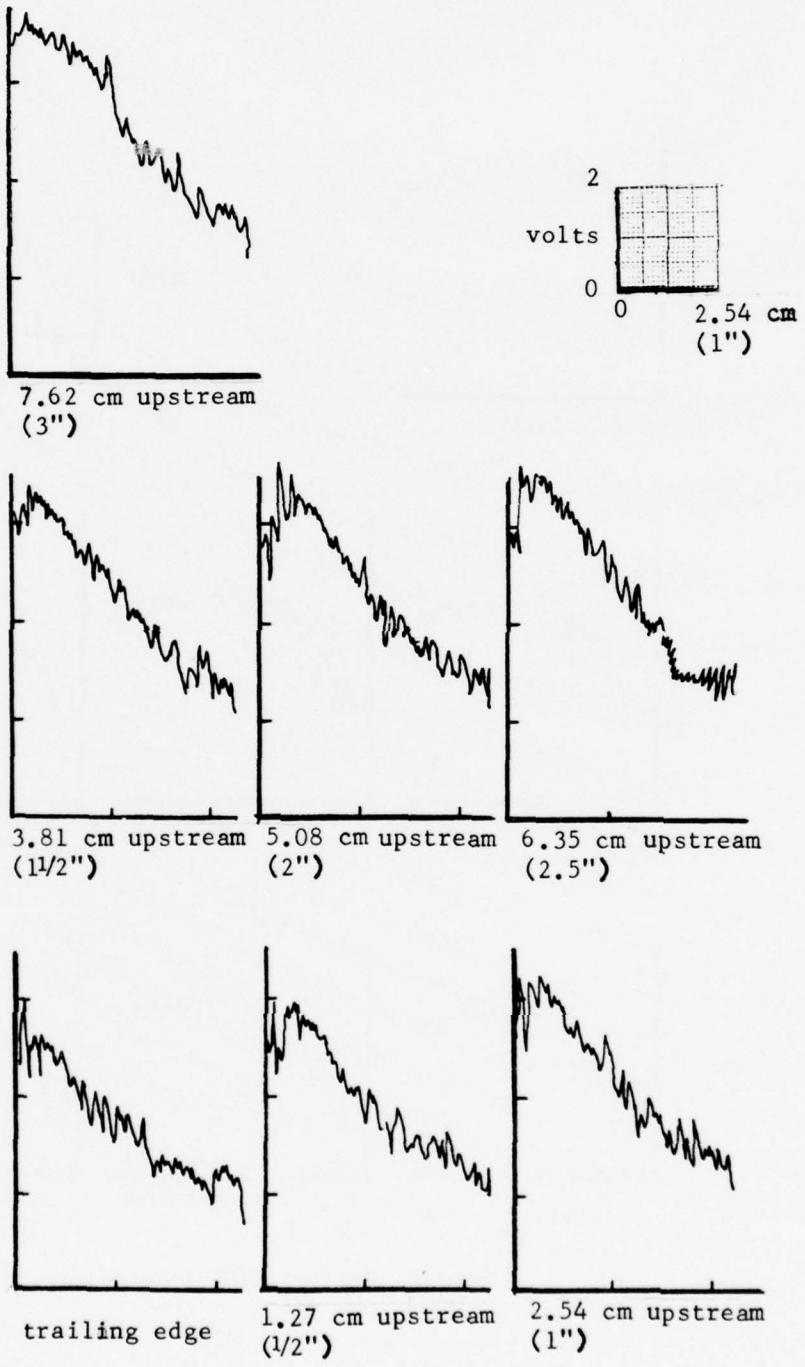

Case 2, Calibration Curve C, PR = 2.5

Figure A-7 (cont'd)

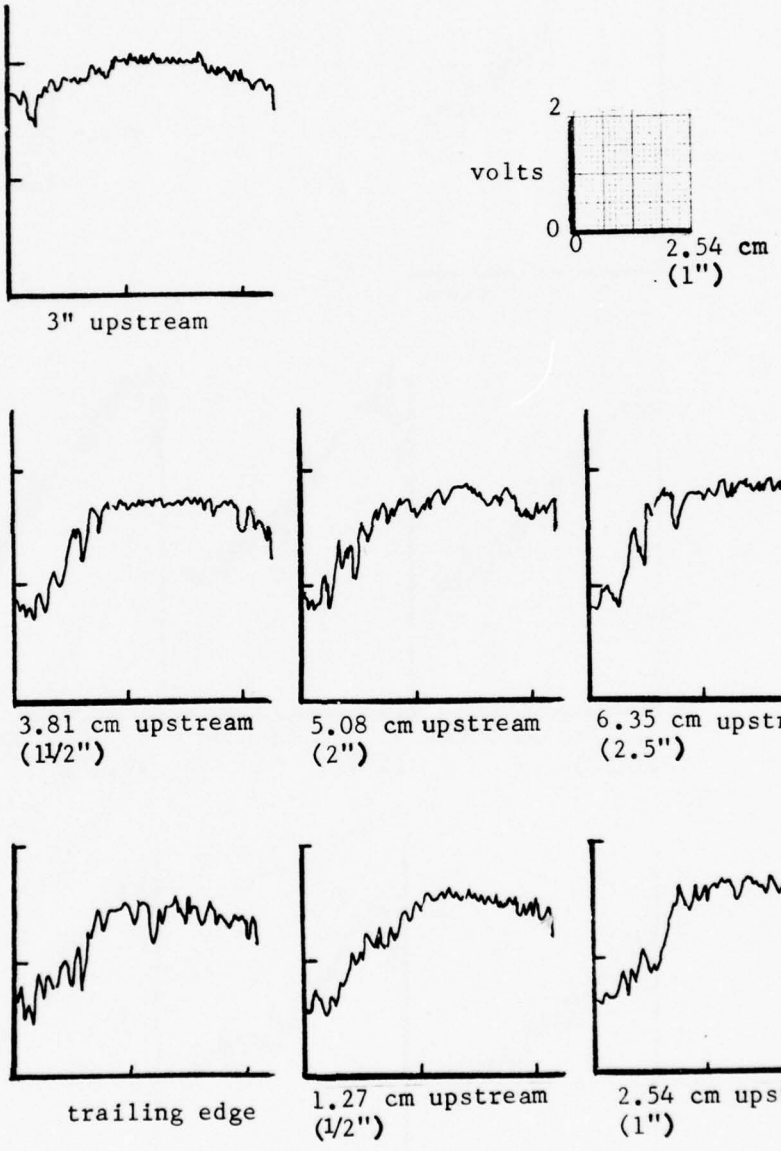

Case 3, Calibration Curve C, PR = 1.5

Figure A-7 (Cont'd)

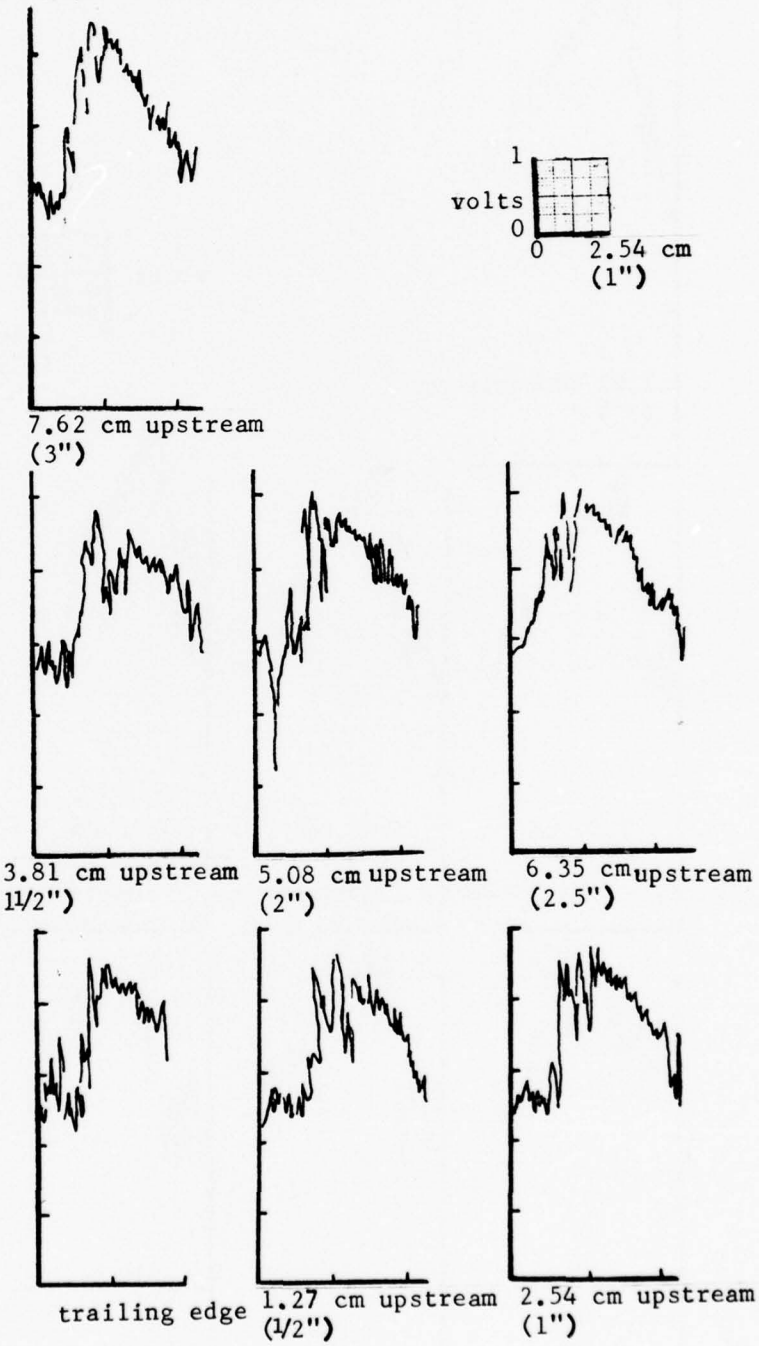

Case 3, Calibration Curve B, PR = 2.0

Figure A-7 (cont'd)

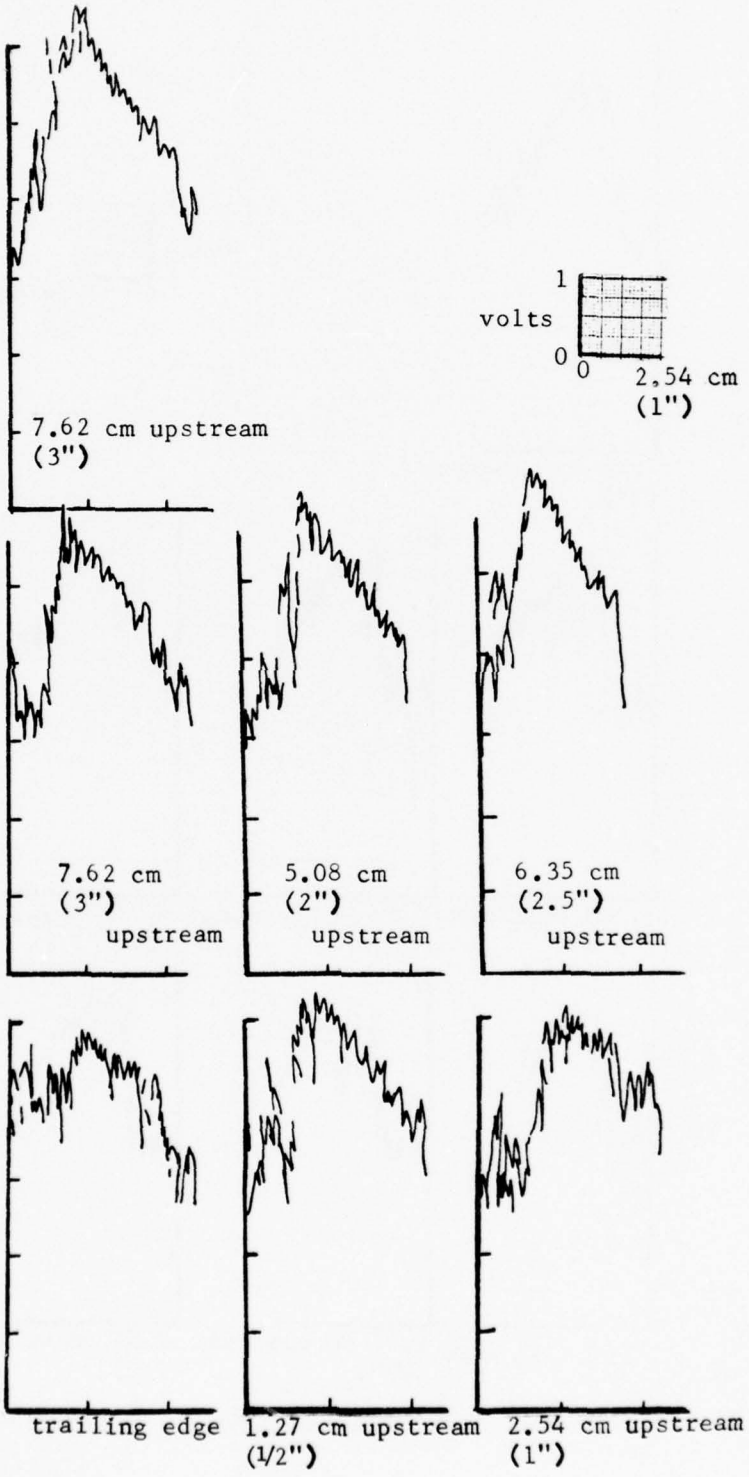

Case 3, Calibration Curve A, PR = 2.5

Figure A-7 (cont'd)

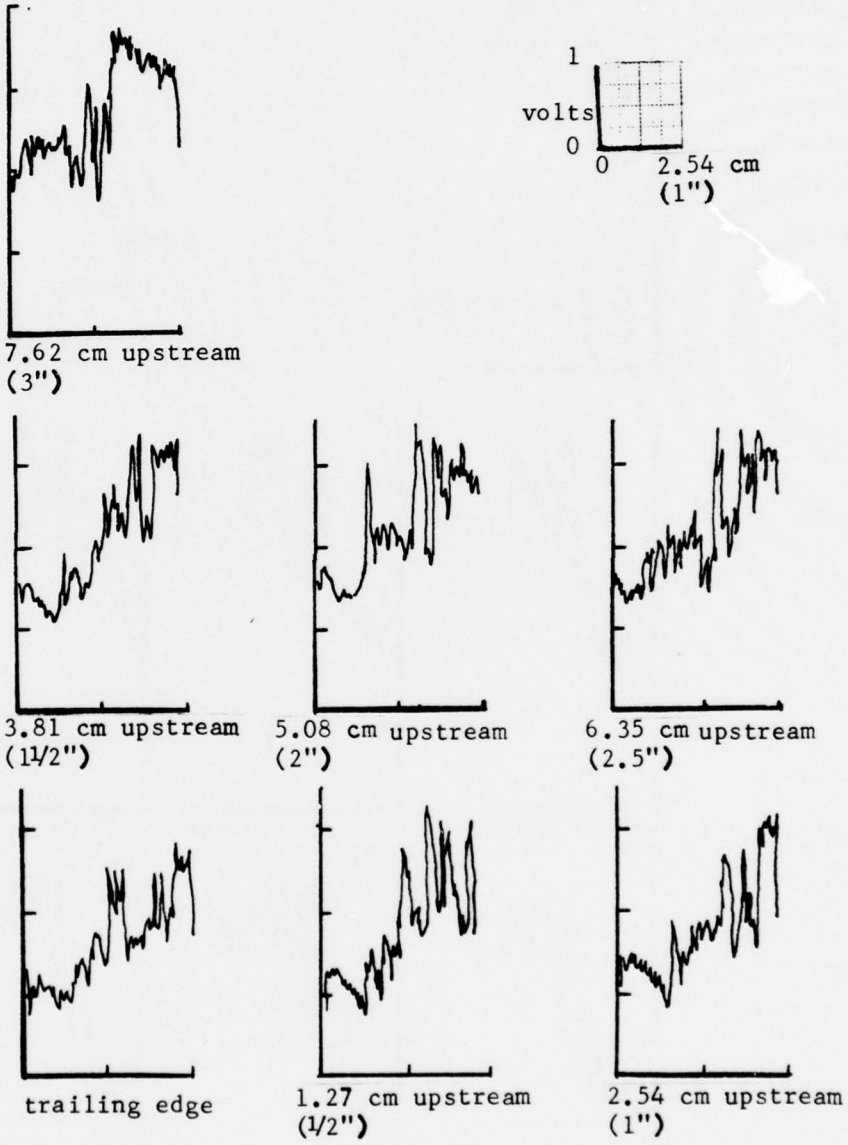

Case 4, Calibration Curve A, PR = 1.5

Figure A-7 (cont'd)

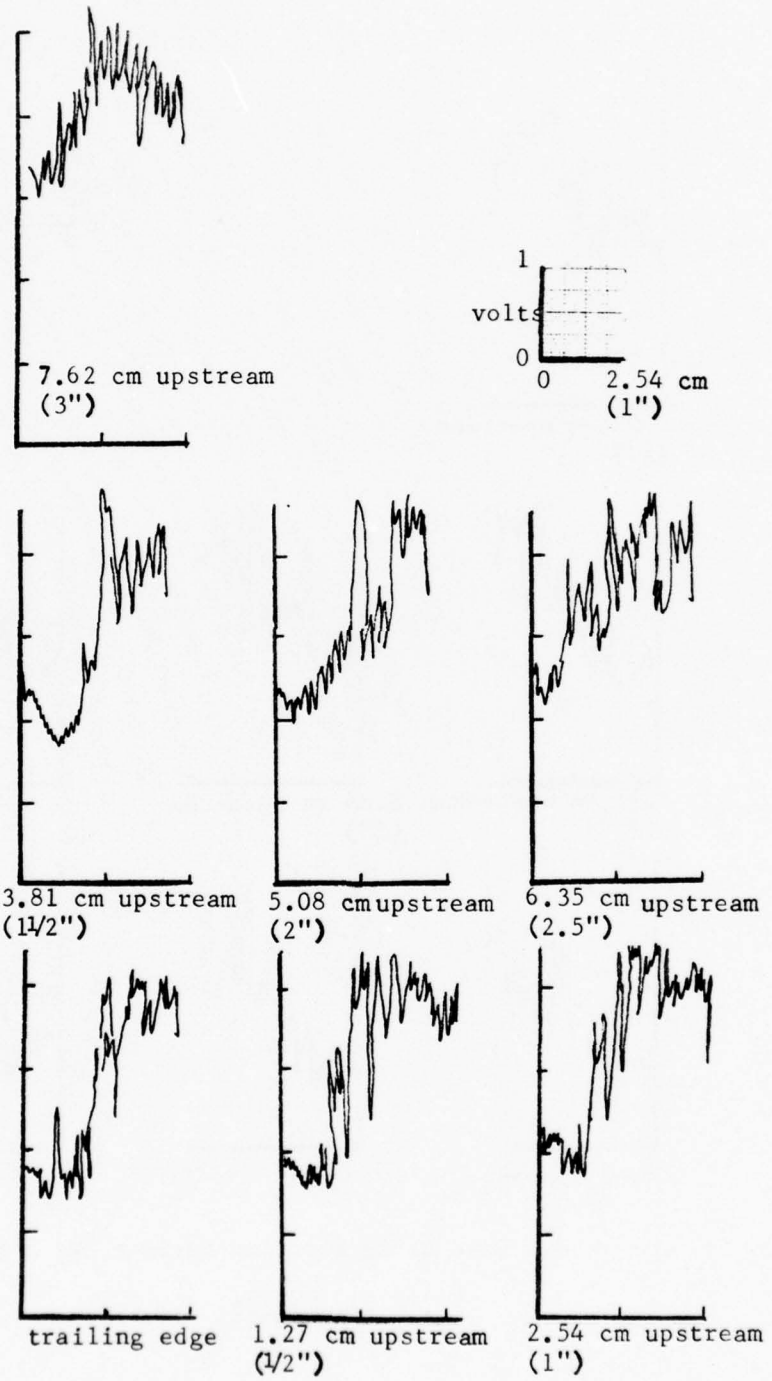

Case 4, Calibration Curve A, PR = 2.0

Figure A-7 (cont'd)

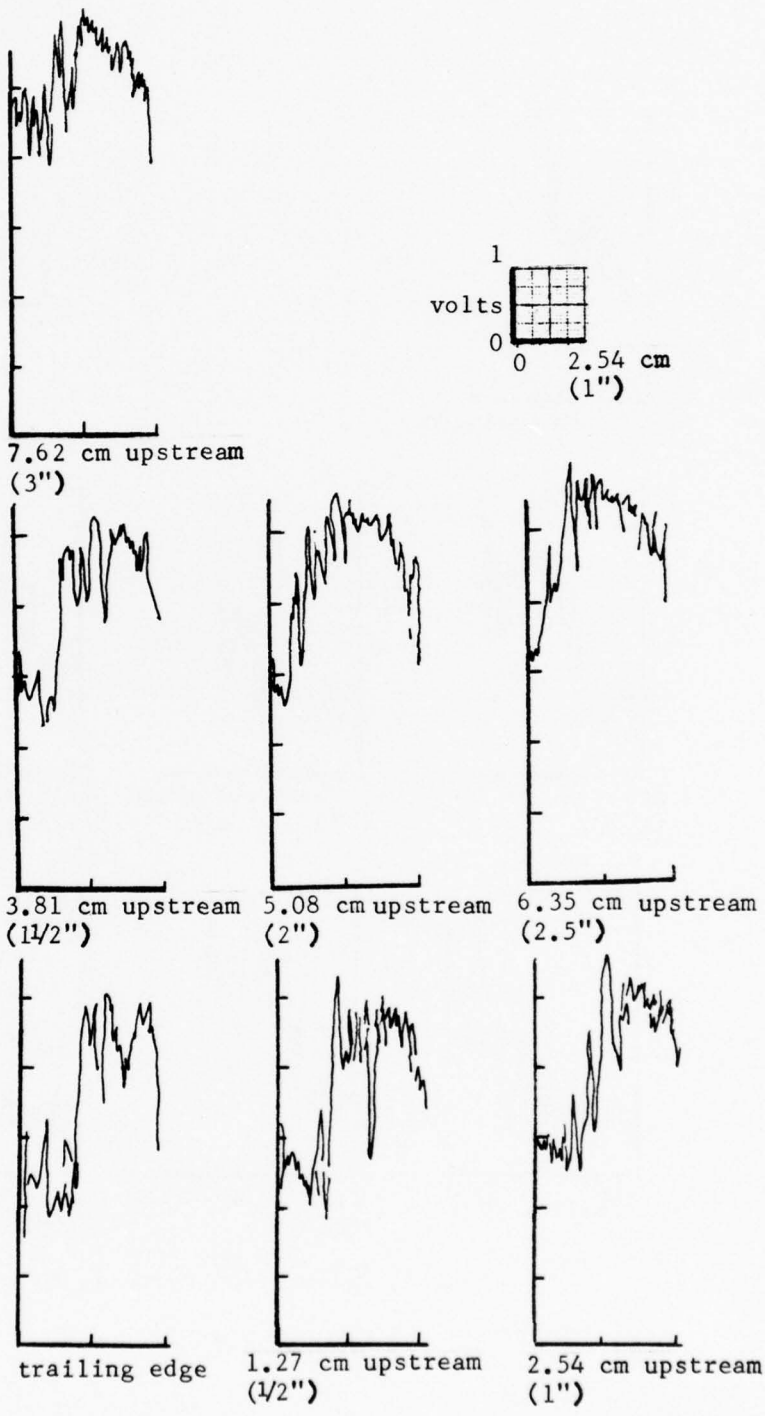

Case 4, Calibration Curve A, PR = 2.5

Figure A-7 (cont'd)

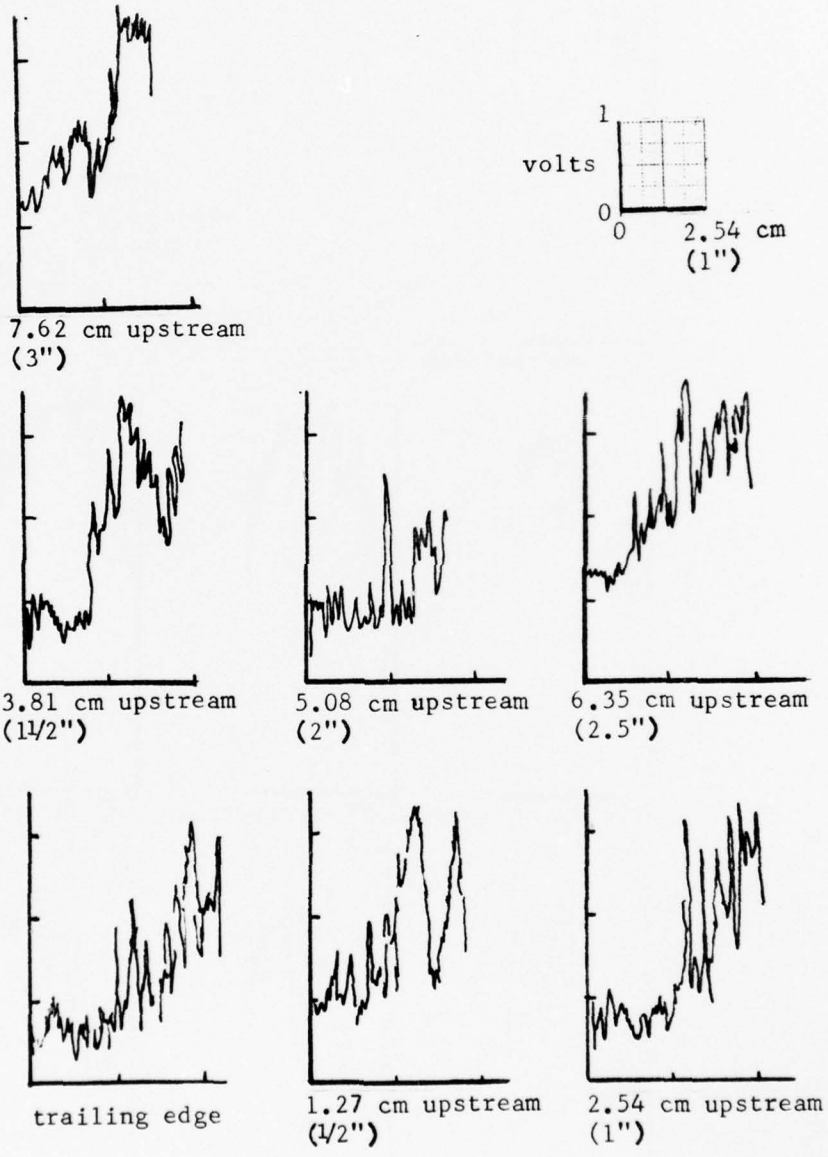

Case 5, Calibration Curve A, PR = 1.5

Figure A-7 (cont'd)

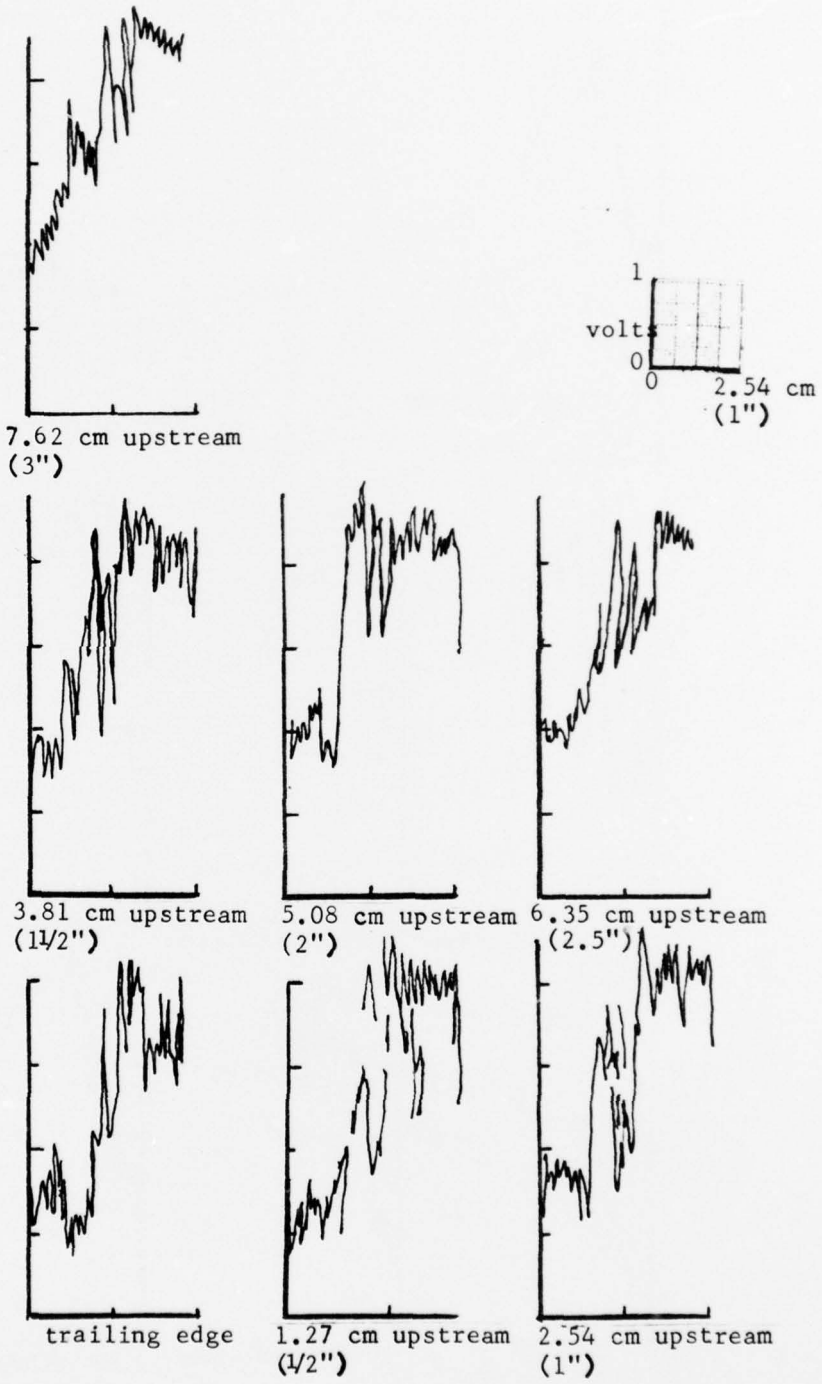

Case 5, Calibration Curve A, PR = 2.0

Figure A-7 (cont'd)

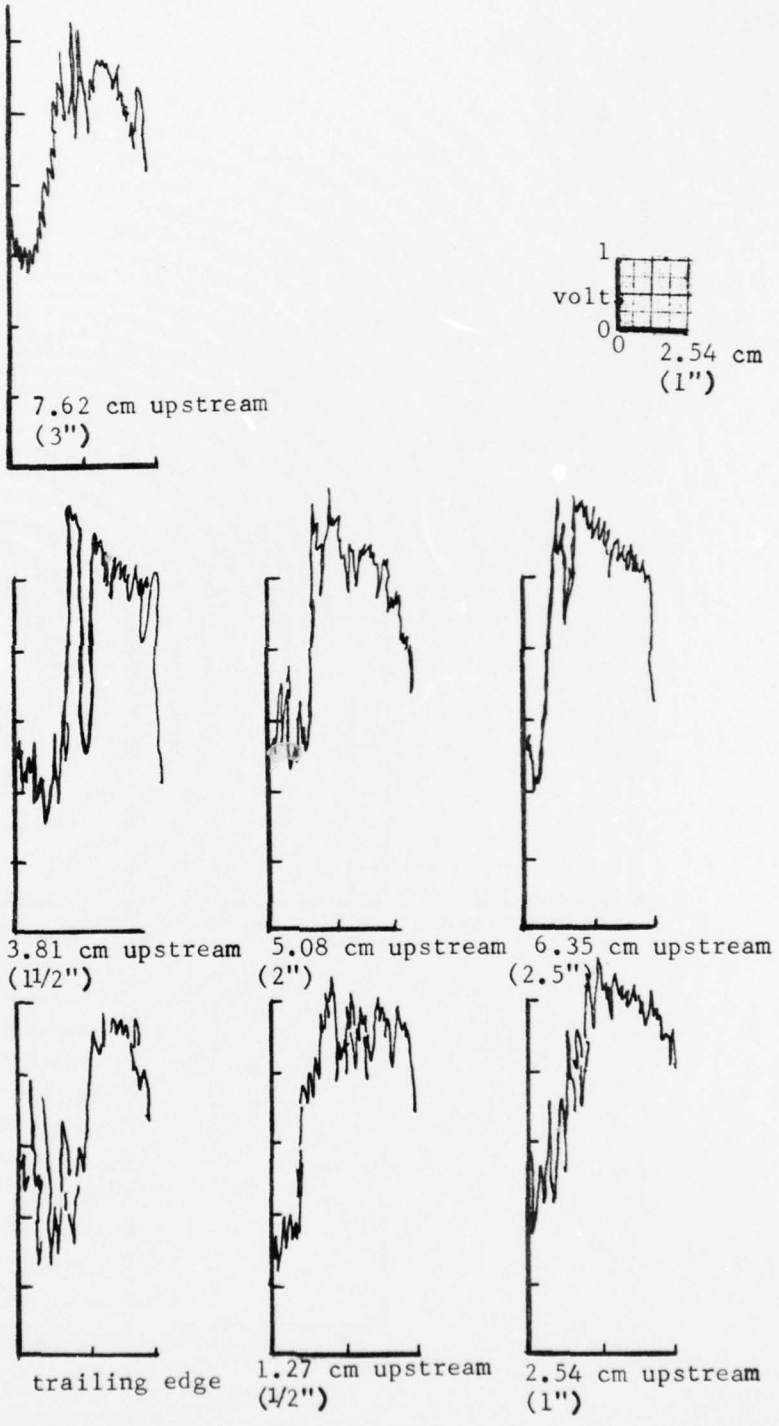

Case 5, Calibration Curve A, PR = 2.5

Figure A-7 (cont'd)

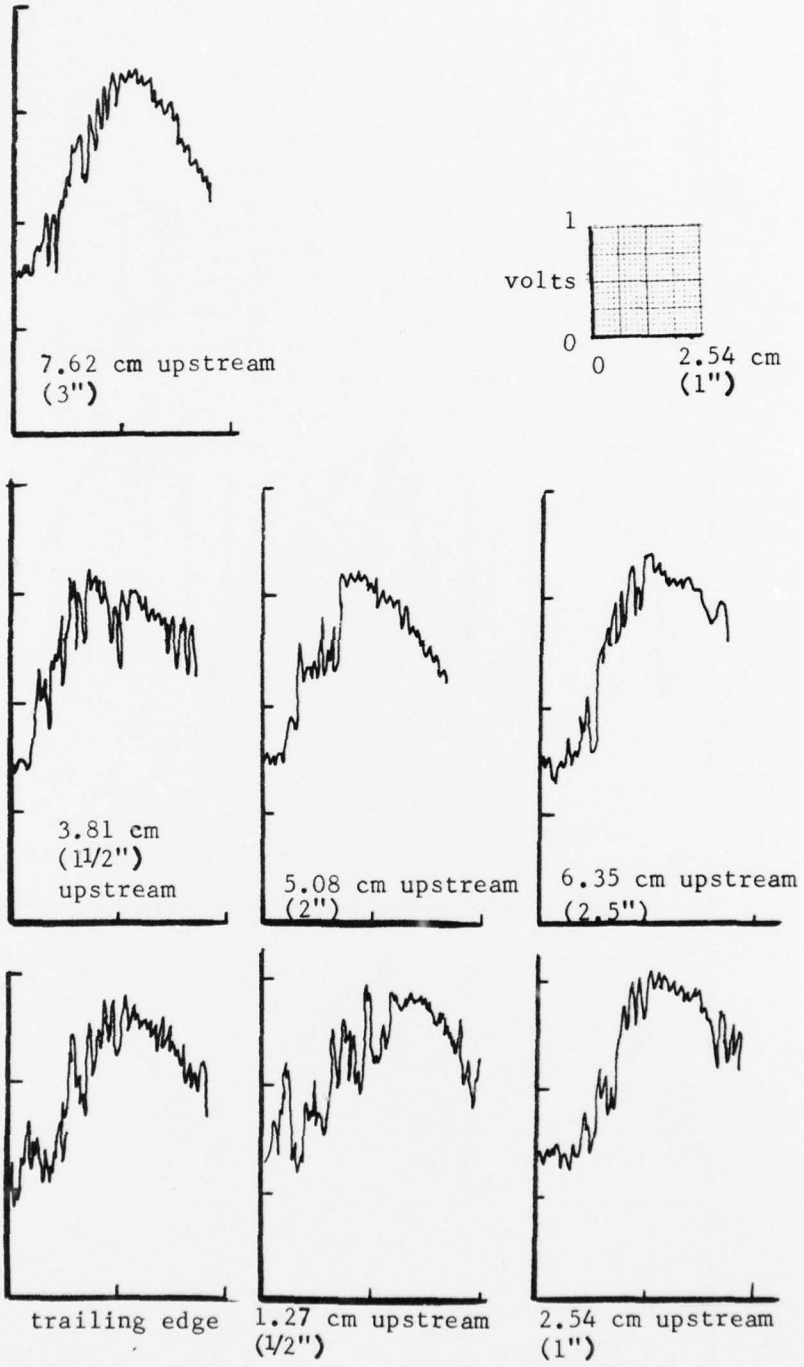

Case 6, Calibration Curve A, PR = 1.5

Figure A-7 (cont'd)

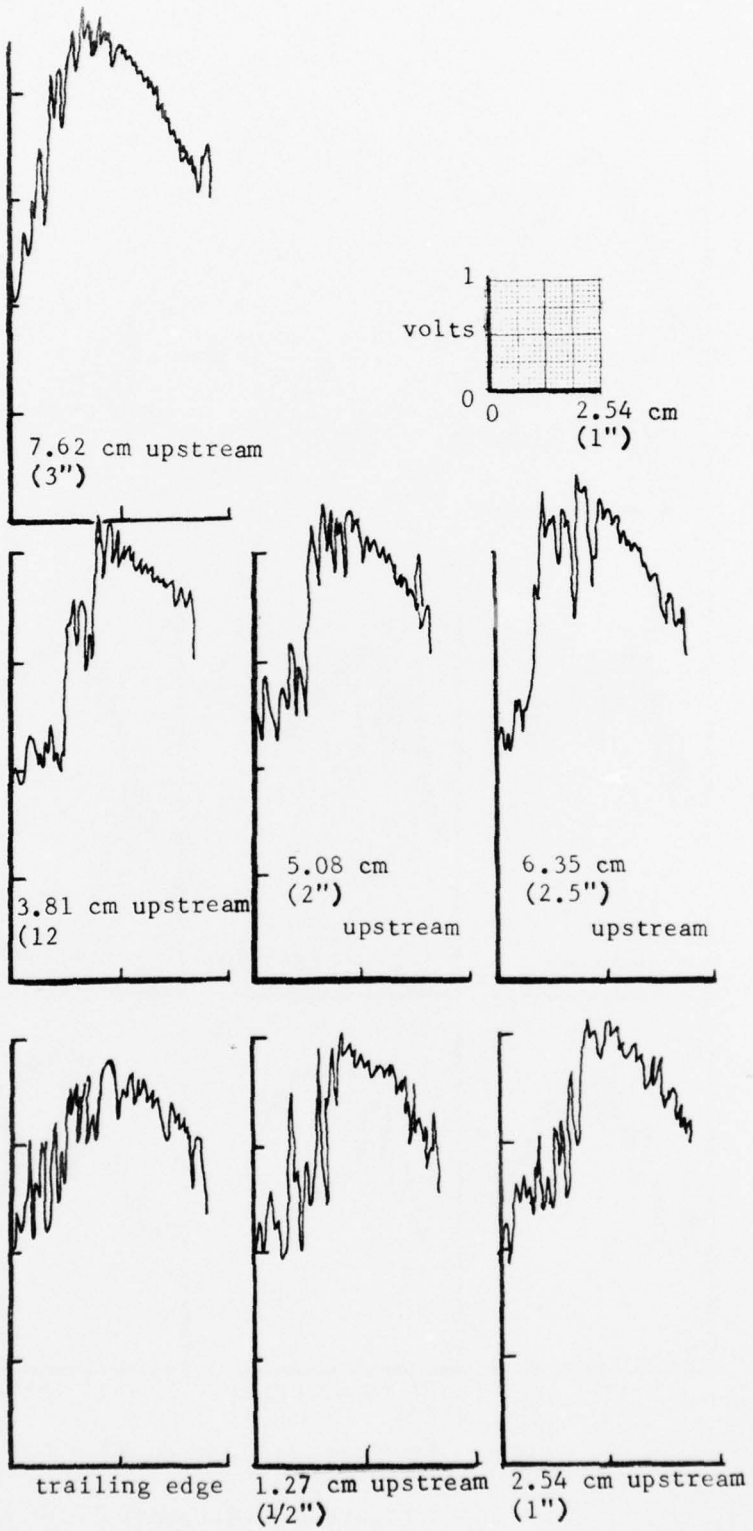

Case 6, Calibration Curve A, PR = 2.0

Figure A-7 (cont'd)

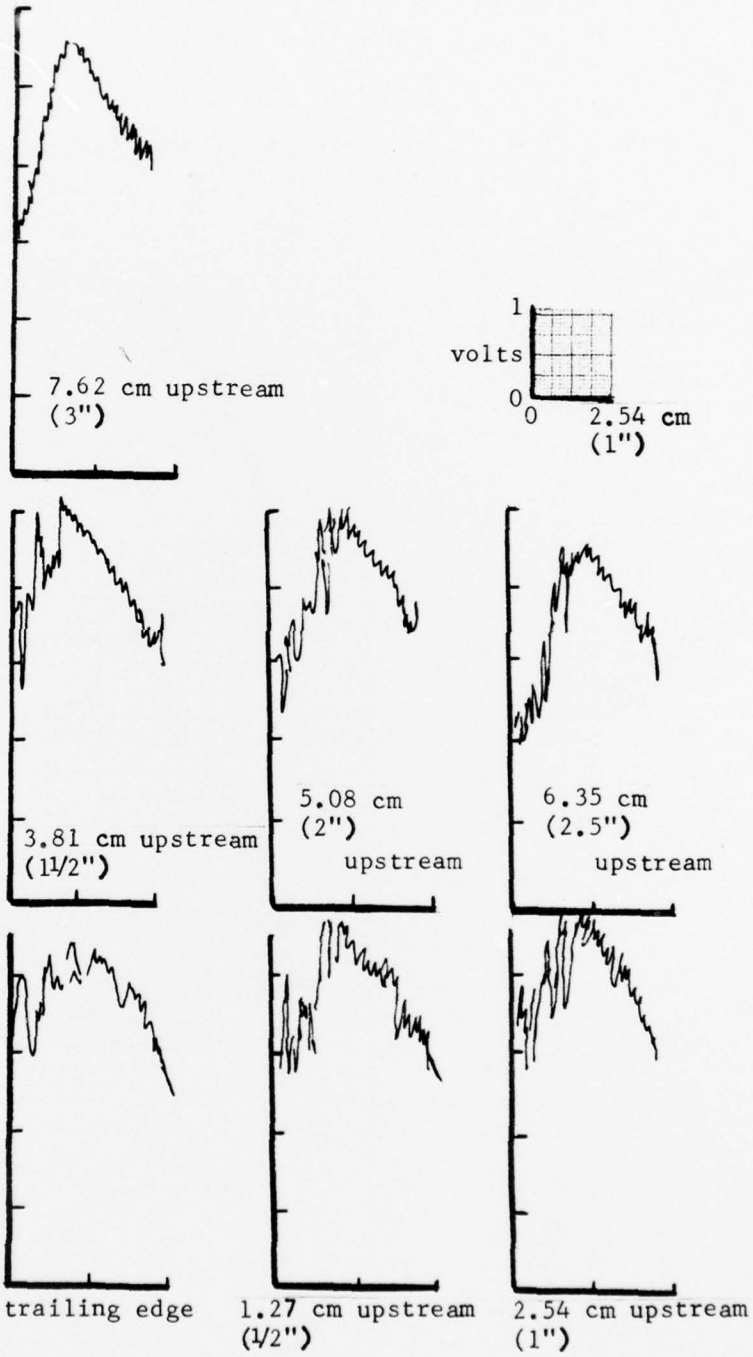

Case 6, Calibration Curve A, PR = 2.5

Figure A-7 (cont'd)

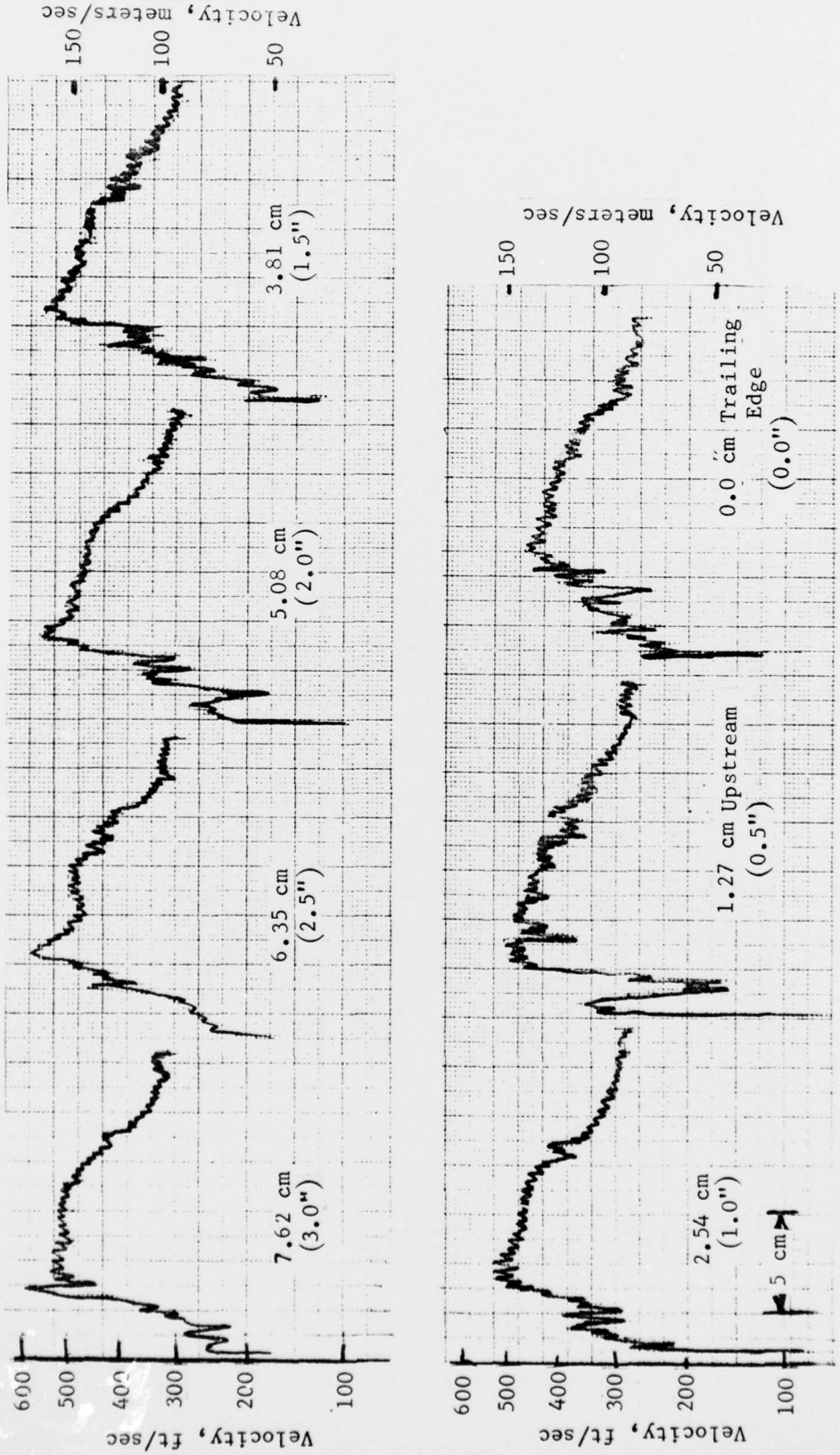

Figure A-8 . Case 7, PR = 1.5

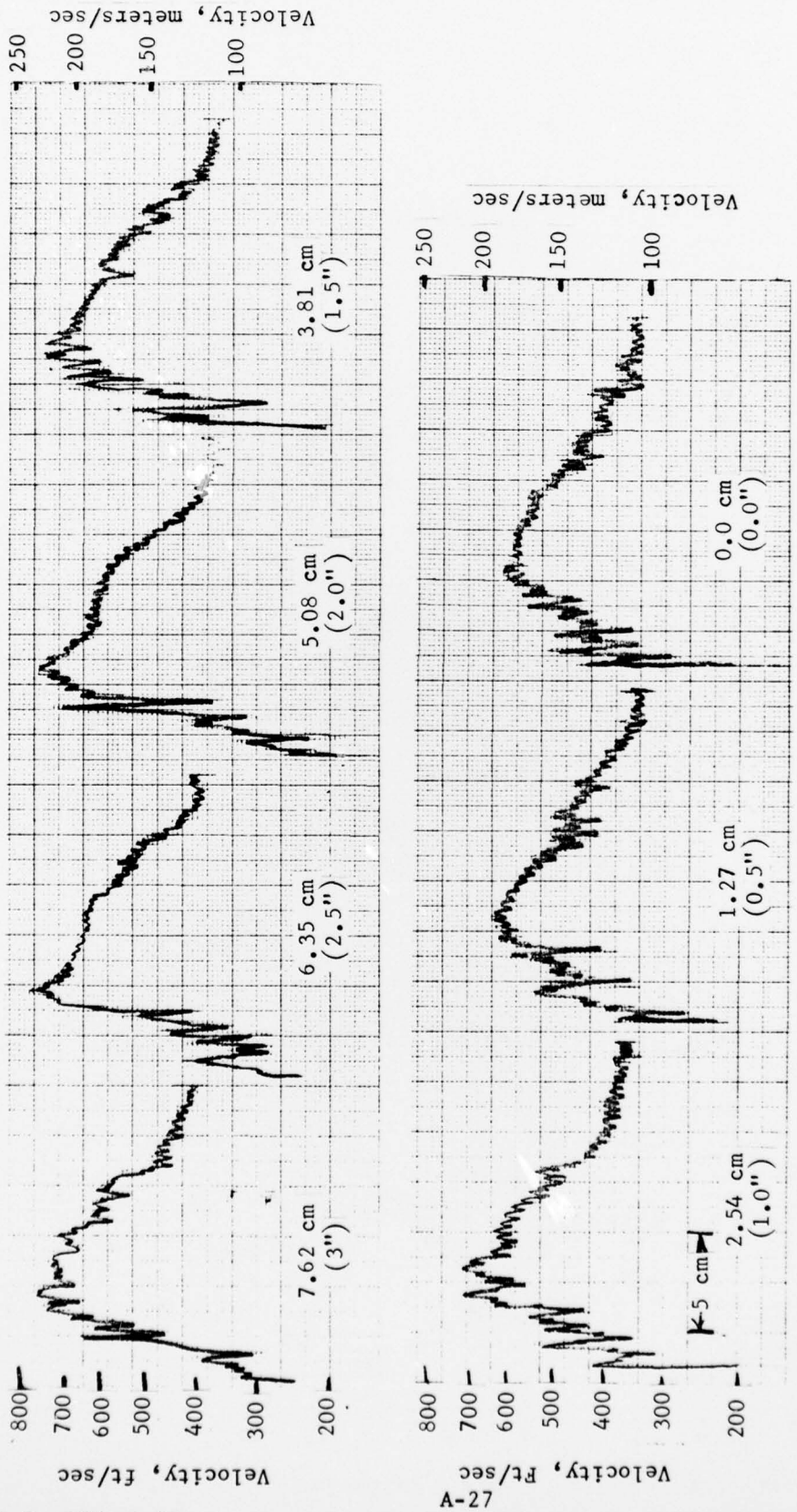

Case 7, PR = 2.0

Figure A-8. (Cont'd)

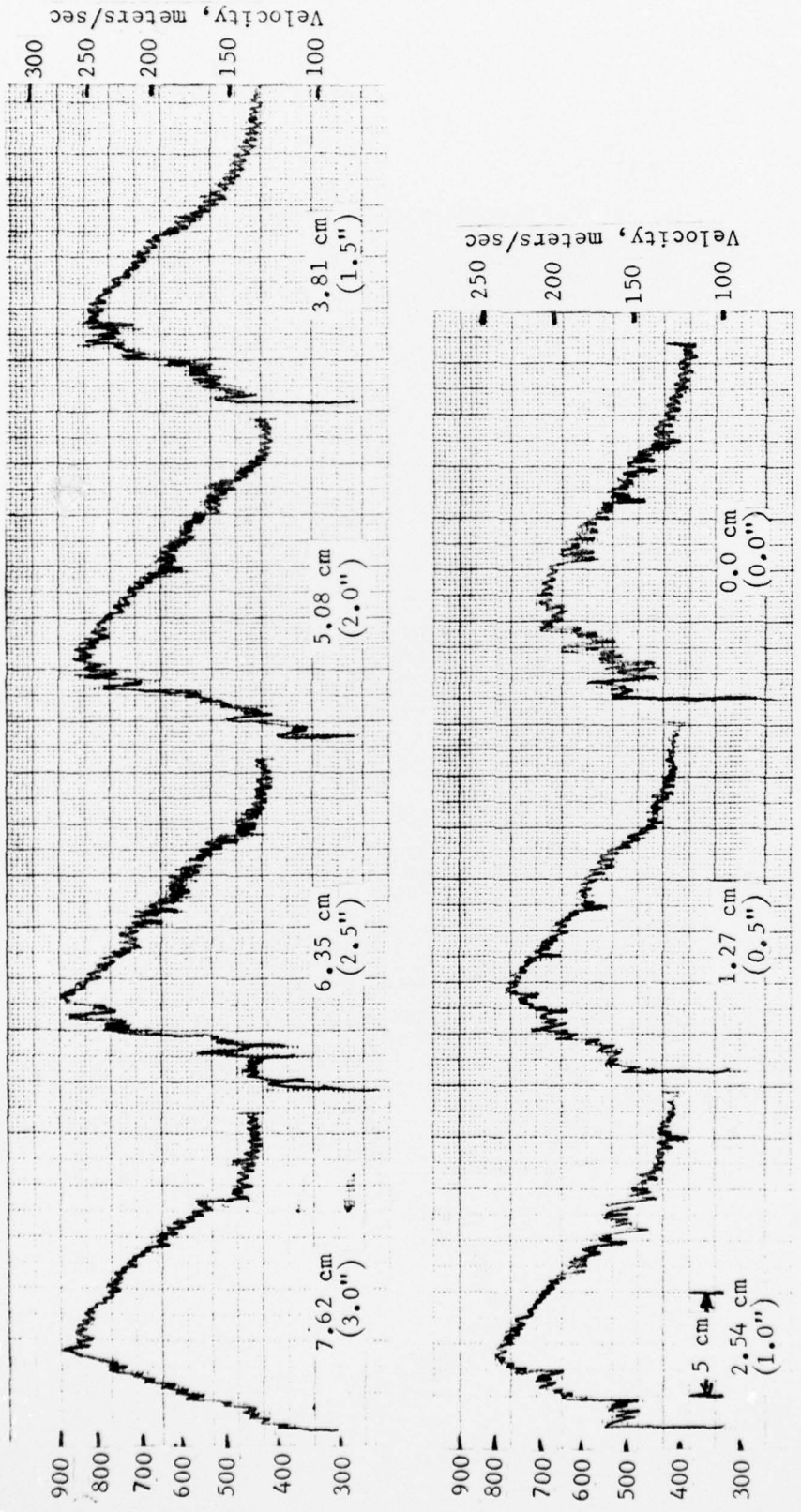

Case 7, PR = 2.5

Figure A-8. (Cont'd)

Case 8, PR = 1.5

Figure A-8. (Cont'd)

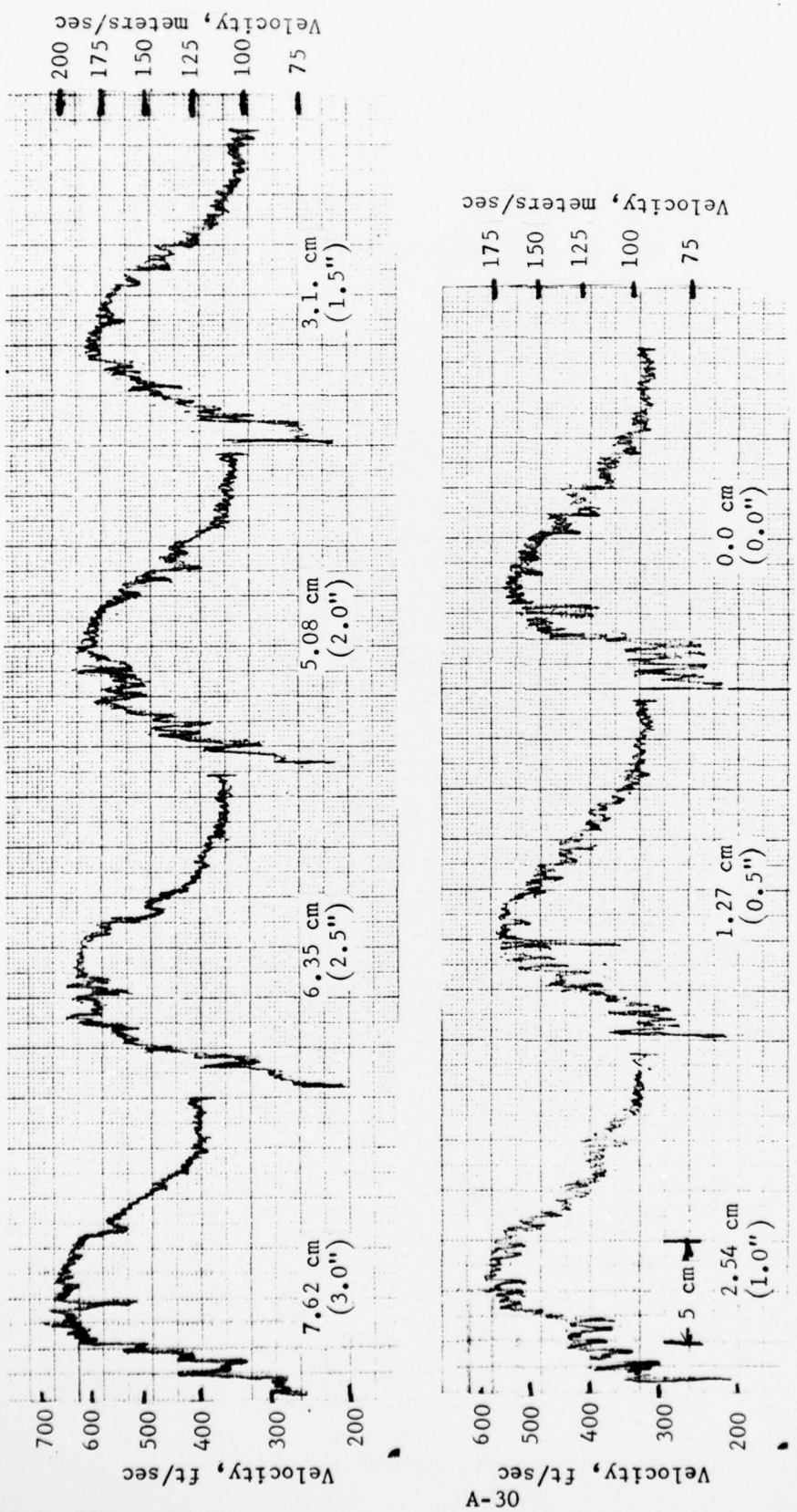

Case 8, PR = 2.06

Figure A-8. (Cont'd)

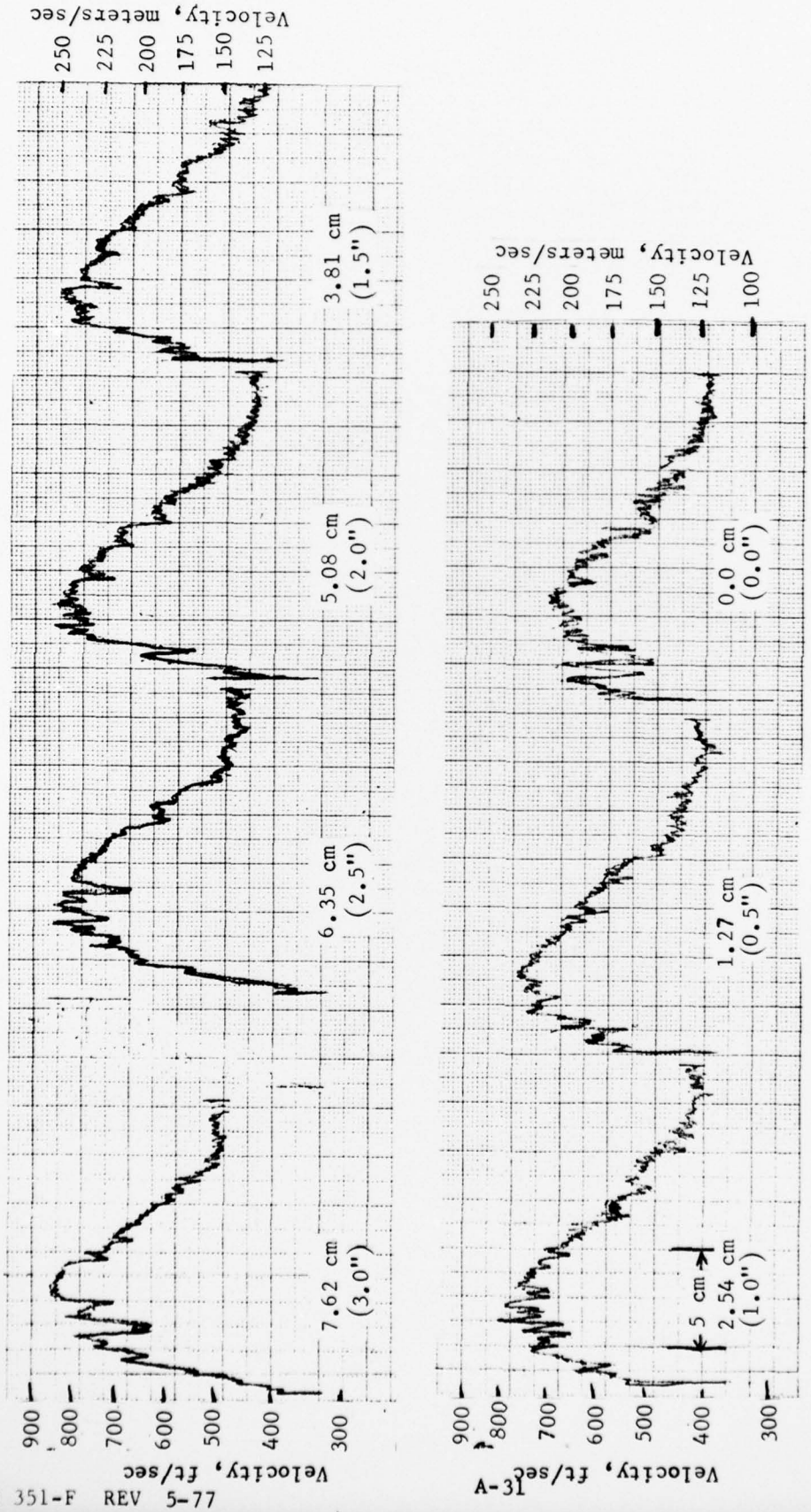

Case 8, PR = 2.5

Figure A-8. (Cont'd)

APPENDIX B

EFFECT OF BLC NOZZLE ORIENTATION

Figure B-1 shows four different BLC nozzle orientations, and their effect on the static tap readings in the corner of the west flap. The first case shows the BLC nozzle pointed 30° toward the flap. Although this causes the flow to be attached, the static readings show an oscillatory behavior due to a total pressure component in the taps. In the second case both flaps are attached and the overall level of gage pressure rises, but the oscillatory pattern is still present because of the BLC orientation. The third case is with the BLC nozzle blowing parallel to the flap and the static readings are more linear. It is this condition which achieves readings more like those of Figures 16, 17, 18 and 21. When this condition is reached, the readings are insensitive to slight orientation changes of the BLC. Notice that cases 2 and 3 produce similar slopes at the exit. This is because the last few taps are sufficiently distant from the BLC nozzles. Finally, case 4 is a separated flap showing zero slope at the exit.

This data is presented for that interested worker who may attempt additional measurements of the kind reported in this study.

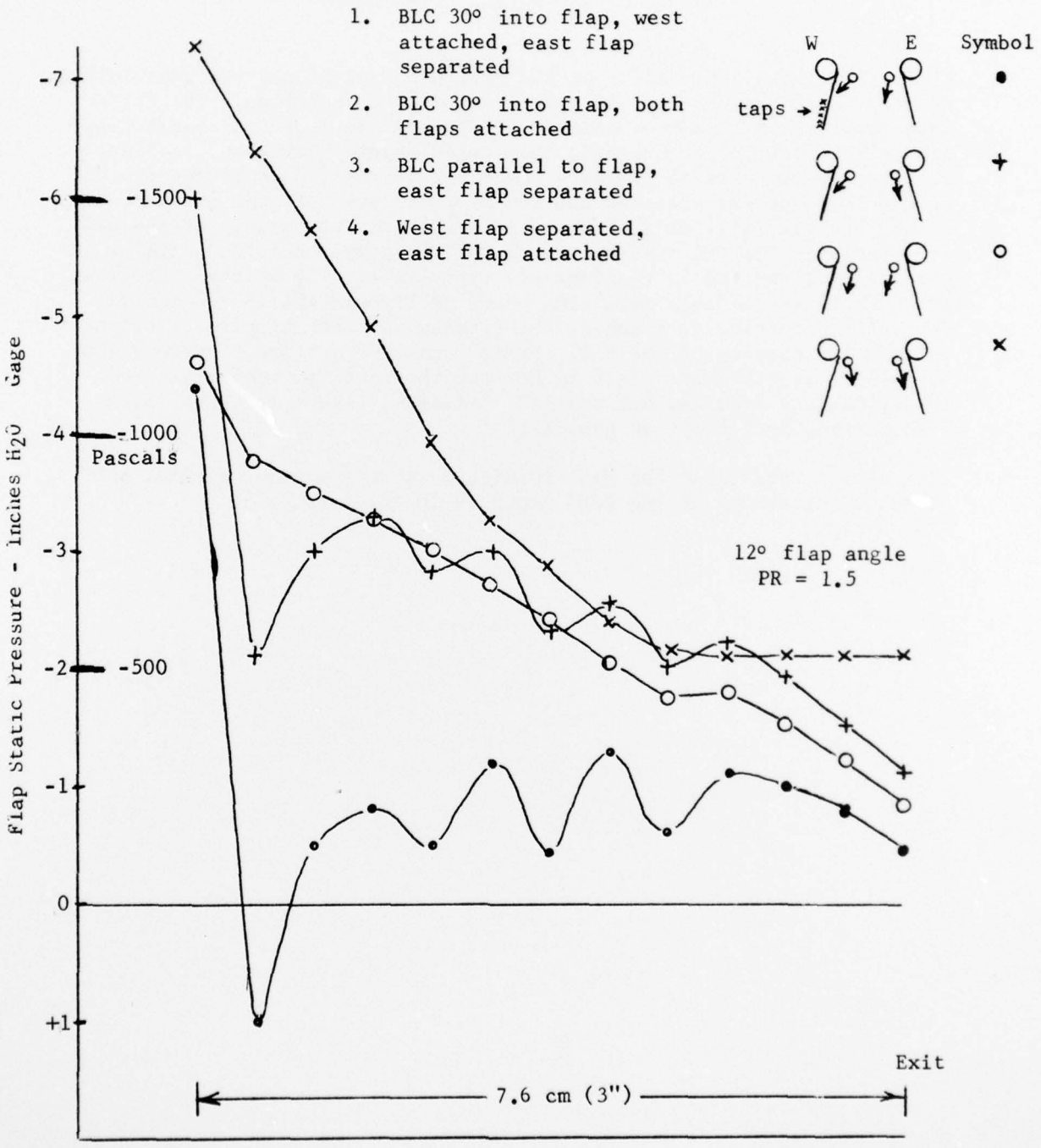

Figure B-1. Effects of BLC Nozzle Orientation on Flap Statics

DISTRIBUTION FOR FINAL REPORT NADC 76153-30

Copies	Address
7	Commander Naval Air Development Center Warminster, PA 18974 (2) Attn: Mr. C. Mazza (Code 6053) (5) Attn: Dr. K. Green (Code 6052)
3	Commander Naval Air Systems Command Jefferson Plaza Washington, D. C. 20361 Attn: Mr. R. Siewert (AIR 320D)
1	Commander Naval Weapons Center China Lake, CA 93555 Attn: Mr. B. Kowalsky (Code 3183)
1	Commander Naval Ship Research and Development Center Carderock, MD 20034 Attn: Mr. R. Murphy
1	Commander Naval Air Propulsion Test Center Trenton, NJ 98628 Attn: Mr. L. Palcza
1	Commander U. S. Naval Academy Annapolis, MD 21402 Attn: Mr. J. Sladky
1	Chief Office of Naval Research 1800 N. Quincy Street Arlington, VA 22217 Attn: Dr. R. Whitehead
1	Superintendent Naval Postgraduate School Monterey, CA 93940 Attn: Dr. M. Platzer
12	Defense Documentation Center Building #5 Cameron Station Alexandria, VA 22314
1	NASA-Ames Research Center 40 x 80 Wind Tunnel Moffett Field, CA 94035 Attn: Mr. D. Koenig (MS-247-1)
1	Director Air Force Flight Dynamics Lab. AFDL/XFM Wright-Patterson AFB Dayton, OH 45433 Attn: Dr. K. Nagaraja
1	Vought Corporation Advanced Technology Center, Inc. P. O. Box 6144 Dallas, TX 75221 Attn: Dr. C. Haight
1	General Dynamics Corporation Fort Worth, TX 76101 Attn: Mr. J. Clifton (MS-2892)
1	Rockwell International Columbus, OH 43216 Attn: Dr. P. Bevilaqua
1	Rockwell International Science Center 1049 Camino Dos Rios P. O. Box 1085 Thousand Oaks, CA 91360 Attn: Dr. N. Malmuth
1	Grumman Aerospace Corporation Bethpage, Long Island, New York 11714 Attn: Dept. 420, Plant 35
1	Flight Dynamics Research Corporation 15809 Stagg Street Van Nuys, CA 91406 Attn: Dr. M. Alperin
1	Computational Mechanics 3601A Chapman Highway Knoxville, TN 37920 Attn: Dr. J. Baker